THE PARTITIONING OF ENERGY BETWEEN GEOSTROPHIC AND AGEOSTROPHIC MODES IN A SIMPLE MODEL

by

RONALD MARK ERRICO

B.Sc. (Hons), University of Arizona, Tucson, Arizona
(1974)

SUBMITTED IN PARTIAL FULFILLMENT OF THE

REQUIREMENTS FOR THE DEGREE OF

DOCTOR OF PHILOSOPHY

AT THE

MASSACHUSETTS INSTITUTE OF TECHNOLOGY

October, 1979

Signature of Author _____

Department of Meteorology, October 1979

Certified by _____

Thesis Supervisor

Accepted by _____

Chairman, Departmental Committee on Graduate Students

THE PARTITIONING OF ENERGY BETWEEN GEOSTROPHIC AND AGEOSTROPHIC MODES IN A SIMPLE MODEL

by

RONALD MARK ERRICO

Submitted to the Department of Meteorology on 1 October, 1979
in partial fulfillment of the requirements
for the Degree of Doctor of Philosophy

ABSTRACT

We first claim that a demonstration as to why the extra-tropical tropospheric synoptic-scale wind and pressure fields are approximately geostrophic has not been offered. Previous arguments have been speculative, or have ignored possibly important processes, or have made assumptions which invalidate the demonstration. We make it clear that it is necessary to demonstrate why the prevailing time scale is the advective time scale rather than inertial time scale.

A measure of geostrophy is defined in terms of a partitioning of kinetic and available potential energy between geostrophic and ageostrophic contributions. These energies depend on linear balance conditions in a simple model. The model uses a form of the primitive equations on a f-plane in N-layers. External (but not internal) inertial-gravitational waves are excluded.

The dependence of geostrophy on various parameters is explored numerically. A very-low-order model describing many scales of motion is used for this purpose. It is demonstrated that viscosity is important in maintaining a quasi-geostrophic state. It is also demonstrated that the rate of heating is more important than the value of the mean static stability in determining the degree of geostrophy. An example of significant ageostrophic influence on a nearly quasi-geostrophic solution is presented.

Analytical results are obtained by first transforming the non-linear two-layer model. Specifically, the new non-linear prognostic equations are expressed in terms of the normal modes of the linearized two-layer model. The interactions between various modes appear explicitly. Thus the exchange between geostrophic and ageostrophic energy also becomes explicit.

The stability of simple finite-amplitude geostrophic states is explored using the transformed equations. For Rossby numbers of the unperturbed states less than one, the largest growth rates are associated with quasi-geostrophic perturbations. Perturbations dominated by ageostrophic modes also may grow exponentially. These have growth rates which are slower by a factor proportional to the Rossby number of the unperturbed state. In particular, barotropic-geostrophic modes are only weakly unstable with respect to near-resonant triad interactions with inertial-gravitational wave perturbations.

A multiple-time-scale ordering analysis is applied to the transformed equations. For sufficiently weak fields, with a sufficiently large coefficient of eddy viscosity, the importance of resonance in maintaining the largest amplitude modes is demonstrated. It is suggested that energy is not efficiently exchanged between geostrophic and ageostrophic modes because the latter are associated with relatively high natural frequencies and are dispersive. We relate this result to the maintaining of quasi-geostrophy in the atmosphere.

Thesis Supervisor: Edward N. Lorenz

Title: Professor of Meteorology

To the many people whose encouragement and support made this work possible.

ACKNOWLEDGEMENTS

I wish to begin by thanking Professor Edward N. Lorenz for his guidance and support throughout the course of this study. It was he who suggested that some important problems relating to the maintenance of quasi-geostrophy remained to be examined. I am grateful for the opportunity to have been associated with both him and Jule Charney.

My thanks to Isabelle Kole, Brad Colman, and Susan Ary for help in preparing the figures. Also thanks to Jane LeBeau, John Carlson, and Brad Colman for proof-reading the text. Liz Manzi, Patty Farrell, and Virginia Mills did a beautiful typing job under pressured circumstances. They were reliable when deadlines approached and I am expecially grateful.

During my 21 years of schooling I have had my most excellent teachers while here at M.I.T. I came here to learn dynamic meteorology, and I did so, thanks to: Jule Charney, Edward Lorenz, Steven Orszag, Eugenia Rivas, Fred Sanders, and Peter Stone. Thanks also to Jane McNabb without whose boldness in dealing with administrative hassles, all of us would have been buried in red tape long ago. I would also like to express my gratitude to Steven Solomon, Rick and Debbie Will, and Professors Norman Phillips and William Sellers for encouraging me to attend M.I.T.

My family has provided constant encouragement during all my school years. Clearly, they have been most responsible for the direction my life has taken. This is true not only regarding my work. I don't know words to express what that means to me, but I pray they understand.

I would also like to express my thanks and love to the members of the Tang Hall Bible Studies for their continuing prayers for my work, especially: Fred and Elaine Hickernell, Peter Andreae, Will Perrie, Reinhardt Viehoff, Kathleen Hill, John Congalidis, and Linda Li. They helped me to learn much more than meteorology. The experience of witnessing answers to their prayers probably more than anything else has acted to increase my faith in God's love.

At the risk of accidentally forgetting someone whom I should not overlook, I would like to thank a few friends who made my stay in Cambridge such a plèasant one: Barbara Amols, who introduced me to my office-mate Brett Mullan and to Mary Nucefora and Mike Wojcik, and through them to Cheri Pierce, Doug Stewart, Kathy Pierce, and Jane (who helped with the manuscript); Jane Hsiung; Kathy Huber who helped prepare my resumes; my apartment-mates: Charlie and Aili Smith, Alex Harris, Diane Markovitz, and Fred Hickernell, who all put up with my difficult times; Long Chiu (who helped in my 35th hour to get this manuscript completed); Jim Fullmer; and Lin Ho whose

hospitality during my last weeks is greatly appreciated. Special thanks and love are offered to Zsuzsanna Ary with whom I have shared most of my joys and sorrows while here at M.I.T.

This work has been supported by grants AF.ESD F19628-77-C-0026 and AF F1928-78-C-0032 from the United States Air Force and grants NSF-g 77 10093 ATM and NSF GARP DES 7403969 from the National Science Foundation.

TABLE OF CONTENTS

LIST OF FIGURES

Chapter 1: Introduction

1.1 The Problem

To a first approximation, large scale motions in the extratropical atmosphere are geostrophic, meaning that a near balance exists between horizontal components of the coriolis and pressure gradient forces. Departures from geostrophy are observed, being smaller in magnitude relative to the balanced portion of the motion. These departures include the presence of inertial-gravitational oscillations, divergent winds described by the quasi-geostrophic omega equation, centripetal accelerations, and frictional effects among others. A fundamental question is: Why is the atmosphere quasi-geostrophic? In particular, why is it not more or less geostrophic, assuming some quantitative measure, than it is observed to be? This is the question to be explored in this thesis.

1.2 Review of Past Explanations

Numerous writers have proposed at least partial answers to the first question. There have been studies on scale analysis, hydrodynamic instabilities, and forcing and geostrophic adjustment. Some are reviewed by Phillips (1963) and Blumen (1972). Most of these analyses are relatively simple, being linear, accounting for nonlinear effects by non-mathematical speculative arguments. Some in fact are misleading or incorrect (See the discussion on the Rossby number below).

Approximating the true wind and pressure fields by geostrophically balanced ones is common in modern meteorology. A statement as to under what conditions this procedure is valid appears in most textbooks on dynamic meteorology. Haltiner (1971; p. 50) states that if the Rossby number ε is sufficiently small, then the geostrophic approximation is valid. Holton (1972; p. 31) adds that the smallness of ε is in fact a measure of geostrophy.

These statements are based on simple scaling arguments. If ε is defined as the ratio of the acceleration to the coriolis force per unit mass then these remarks are valid. However, both Holton and Haltiner define ε as the quantity U/fL, where U is a typical velocity scale, L a length scale, and f the coriolis parameter. This, in effect, equates the acceleration and advective time scales. Assuming the time scale to be advective limits the possible significance of ageostrophic fields characterized by inertial-period oscillations.

It is correct to conclude that the atmosphere's larger spatial scales are necessarily quasi-geostrophic given the observed scales of velocity, length, etc., including that of the acceleration time scale. It is not correct to conclude from an examination of only U, L, and f that the atmosphere is quasi-geostrophic. The condition $U/fL \ll 1$ is necessary for geostrophy, but not sufficient. Scales of forcing and dissipation must be considered. This is discussed further in Chapters 3 and 8.

Charney (1955, and 1973 p. 174) explains the geostrophy of the atmosphere in terms of the scales of external forcing. The atmosphere's principal energy soruce is differential solar heating, which is

characterized by large horizontal scale (a pole-to-pole distance) and long period (infinite, with seasonal variations). Diurnal effects act only weakly on the bulk of the atmosphere's mass (Gierasch et. al., 1970). The atmosphere responds at these scales of external forcing. Large scale, long period implies a quasi-balanced state since significant unbalanced motions (not frictional induced) are generally characterized by short, inertial time periods. Charney adds that for energy to remain in the externally forced scales, the flow must be hydrodynamically stable with respect to (ageostrophic) perturbations. Also, viscous forces must be sufficiently strong to destroy any appreciable energy that may otherwise accumulate in ageostrophic motions.

Stone (1972) uses Eady's (1949) model to relate the Richardson number Ri to geostrophy. He uses an f-plane analog of a forced axi-symmetric circulation (i.e. that steady geostrophic response noted by Charney) and investigates its stability with respect to infinitesimal perturbations. This circulation is unstable. If $Ri >> 1$, then the most unstable mode is quasi-geostrophic. Whether this implies that the finite amplitude motion is quasi-geostrophic depends on the stability of this mode with respect to further perturbations.

Lorenz (1972) investigates the stability of barotropic waves with respect to other wave-like perturbations. Kim (1975) conducts a similar investigation using baroclinic waves. Both use quasi-geostrophic models. They find that both types of waves can be unstable. Duffy (1974, 1975) extends Lorenz's study to a shallow water model, and investigates the stability of barotropic waves with respect to agestrophic disturbances. This latter study is discussed further in

Chapter 7 along with new results.

The relationships between the scales of forcing and response have been investigated with simple linear models. Veronis and Stommel (1956) apply a momentum stress at the ocean's surface. Their results suggest that as long as the forcing period is larger than the inertial period, the response can be characterized as geostrophic. Pollard (1970) deals with a continuously stratified ocean. His results suggest that the duration of forcing is more important than details of the stratification in determining the response characteristics. The significance of these results can be questioned since excitations by internal processes, with response characteristics possibly very different from those of external forcing, are ignored.

Charney (1948) demonstrated that the observed scales, including the observed time scale of large weather patterns, demand that the atmosphere be quasi-geostrophic. The question as to why these particular scales are observed is not answered by any single study known to us. The many separate aspects addressed in the studies discussed must be considered together. To quote Blumen:

> The task of explaining why typical scales of geophysical fluid flows are observed is tied in with the spectrum of imposed forcing, the process of interaction between non-geostrophic and geostrophic modes of motion, and the properties of hydrodynamic instability, together with dynamical and geometrical constraints on the flow. In effect, as Lorenz (1967) has pointed out, the problem is essentially that of explaining the general circulation of these flow regimes. As a consequence, the task is a formidable one.

1.3 A Measure of Geostrophy

Before describing how our question can be investigated, it is necessary to define some measure of geostrophy. It is useful to associate some single number with a degree of geostrophy. As mentioned earlier, the Rossby number, defined in the common sense of U/fL, is not an appropriate measure. In fact, in Chapter 5, a numerical solution will be introduced that has a Rossby number, defined in this manner, on the order of its atmospheric value, but associated with a flow that ishighly ageostrophic. Another measure is needed.

One possible measure can be obtained if the total kinetic plus available potential energy E can be partitioned into that due to either geostrophic or ageostrophic motions. Then for example, the ratio R of ageostrophic to total energy is a measure of the degree of ageostrophy. R has the desirable property that it is bounded between zero and one, and we can therefore describe a particular system as being a certain percentage ageostrophic. Also, the validity of this measure is not restricted to specified allowable time scales, unlike using ε.

Rossby (1936, 1938) first described such an energy partitioning. He examined the tendency for geostrophically unbalanced fields to "adjust" towards a locally balanced state using an effectively linear model. Later he described the energetics of this solution, demonstrating that the total energy of the final balanced state is less than that of the initial state. Some energy, he reasoned, is partitioned to inertial-gravitational oscillations. Considering the energy E, this

portion of energy can be called ageostrophic energy AE, and the remaining can be called geostrophic energy GE.

One method of partitioning was suggested by Lorenz (personal communication). He specified that the following should be required:

1. $GE \geq 0$

2. $AE \geq 0$

3. $GE + AE = E$

4. $GE = 0$ if and only if the linearized potential vorticity is zero everywhere

5. $AE = 0$ if and only if both the velocity field is non-divergent and the coriolis and pressure gradient forces are in balance.

This last condition is appropriate in an f-plane model, otherwise modifications are required. In some simple one-or-two-layer models, these conditions are sufficient to uniquely determine the definitions of GE and AE. In the case of Rossby's (1936) model, the energy partitioning is exactly that obtained by Rossby (1938). Note that Lorenz did not restrict himself to a linear model, except that the potential vorticity and imbalance of forces are expressed by linear terms. While the definition of the partitioning depends on departures from a linear balance, the partitioning itself applies to a nonlinear model.

It is not clear that Lorenz's description can be extended to more than two layers or a continuous model without some method of determining an appropriate vertical structure. For a continuously stratified ocean Pollard (1970) described the vertical structure in

terms of the eigenfunctions of the linearized equation for the vertical velocity. Various, similar partitionings have been presented by a number of writers. The reader is referred to the review by Blumen (1972).

No writer has attempted to actually measure the ratio of the energy of unbalanced to balanced modes within the atmosphere. While this would be difficult if not impossible at present, it should be a relatively easy calculation for some general circulation model results. Such an analysis will likely appear in the literature shortly in connection with the initialization of primitive equation models using modal analysis (Joseph Tribbia, personal communication).

The most appropriate data at present is obtained from Chen and Wiin-Nielson (1976). They partitioned the kinetic energy into that due to either the nondivergent or irrotational part of the wind, using data from the NCAR general circulation model. For a simulated winter they obtained a value of 0.012 for the ratio of the kinetic energy of the irrotational wind field DE to the total kinetic energy KE. From results to be presented in Chapter 8, AE is about twice DE. Using a value for the available potential energy APE about four times that of KE (Piexoto and Oort (1974) obtained such a value for the atmosphere), we obtain

$$\frac{AE}{E} = \frac{2DE}{E} = \frac{2DE}{5KE} = 0.005 \qquad (1\text{-}1)$$

for the value of R.

1.4 Outline of Thesis

In this thesis, a general method of determining an energy partitioning is described. It is applied to a particular two-layer model in Chapter 2. The method utilizes a description of the motion in terms of normal linear modes. The model is hydrostatic, dry, and applied on an f-plane. Only the generation of AE by advective processes and planetary-scale heating is explored. Mountains and convective storms, both sources of sometimes significant ageostrophy, are ignored.

A limited scale analysis of the model is presented in Chapter 3 for reference in later chapters. Analytical analysis continues in Chapter 6 where the nonlinear prognostic equations are transformed into prognostic equations for the normal-modal amplitudes. The energy exchanges between geostrophic and ageostrophic modes are then described explicitly. Further analytical analysis is easier using the transformed equations. The stability of various finite amplitude solutions with respect to small pertubations is investigated in Chapter 7. Further scale analysis appears in Chapter 8.

The behavior of a numerical model is also investigated. Lorenz's (1972) very-low-order turbulence model, applied to the equations of Chapter 2, is presented in Chapter 4. It is used to generate statistics of the energy partitioning as a function of various external forcing and dissipation parameters. Five particular solutions are presented in Chapter 5. These are atmospheric-like solutions, a non-forced and inviscid solution, and an example of highly ageostrophic but low Rossby number flow. In Chapter 9 the results of experiments with

various combinations of external parameter values are presented. Conclusions and a summary follow in Chapter 10.

Chapter 2: A Method of Partitioning Energy in a Particular Model

A method for defining an energy partitioning in a model is introduced here. The method is discussed in the context of a particular model but can be generalized to some other appropriate models. The method is based on an analysis of the model's linearized normal modes. The modes can be separated into two classes on the basis of their parameter dependence and their associated eigenvalues. One class can be associated with geostrophic motion, the other with ageostrophic. If static stability is fixed in time, the different classes contribute independently to the total energy, and an energy partitioning can thereby be defined.

2.1 The Model

The choice of equations is motivated by a desire to compare geostrophic and ageostrophic energies of large-spatial scales. We therefore use a set of primitive equations. For numerical investigations, we intend to use a low-order spectral model like that presented by Lorenz (1972). For this reason, and also to facilitate defining an energy partitioning, a quadratic expression for energy is required (see Section 2.3). This can be accomplished by keeping the total mass within a vertical column constant through the use of appropriate boundary conditions. Although ageostrophic external gravity waves are thereby omitted, Veronis (1956) showed that for reasonable temperature stratification, the energy in the ageostrophic external mode is smaller than the ageostrophic internal

by an order of magnitude. This results from the "reduction of gravity" for the latter (i.e. through buoyancy effects). Applying the equations on a mid-latitude f-plane allows use of Lorenz's (1972) model with very little modification. Equatorial regions, where large ageostrophy can be expected, are excluded.

2.1.1 Continuous Form of Equations

Using usually defined symbols, listed in appendix 1, the primitive equations are:

$$\frac{\partial \underset{\sim}{V}}{\partial t} = -\left(\underset{\sim}{V}\cdot\nabla\right)\underset{\sim}{V} - \omega\frac{\partial \underset{\sim}{V}}{\partial p} - \nabla\phi - f\underset{\sim}{k}\times\underset{\sim}{V} \qquad (2\text{-}1)$$

$$\frac{\partial \theta}{\partial t} = -\underset{\sim}{V}\cdot\nabla\theta - \omega\frac{\partial \theta}{\partial p} \qquad (2\text{-}2)$$

$$\frac{\partial \omega}{\partial p} = -\nabla\cdot\underset{\sim}{V} \qquad (2\text{-}3)$$

$$\frac{\partial \phi}{\partial p} = -\left(p^{\kappa-1}/p_s^{\kappa}\right)R\theta \qquad (2\text{-}4)$$

The boundary conditions imposed are motivated by a desire to apply these equations to a spectral numerical model. In the horizontal all fields are periodic, e.g. for θ ,

$$\theta(x,y,p,t) = \theta(x+D,y,p,t) = \theta(x,y+D,p,t) \qquad (2\text{-}5)$$

for all x,y,p,t , where D is a large distance to be specified. In the vertical,

$$\omega\left(p_T\right) = 0 \quad ; \qquad \omega\left(p_s\right) = 0 \tag{2-6}$$

where subscripts T and S denote the top and surface values respectively. Eq. 2-6 makes the kinetic energy a quadratic quantity, although it eliminates external gravity wave modes.

Both V and θ are to be specified independently as initial conditions with the restrictions that

$$0 = \int_{p_T}^{p_s} \nabla \cdot \underset{\sim}{V} \, dp \tag{2-7}$$

which follows from (2-3) and (2-6), and also

$$\phi_s p_s - \phi_T p_T =$$

$$\int_{p_T}^{p_s} \left\{ \nabla^{-2}\left[f \nabla \times \underset{\sim}{V} - \nabla \cdot \left(\left(\underset{\sim}{V} \cdot \nabla \right) \underset{\sim}{V} + \omega \frac{\partial \underset{\sim}{V}}{\partial p} \right) \right] - \left(\frac{p}{p_s} \right)^{\kappa} R\theta \right\} dp \tag{2-8}$$

This latter is derived from (2.7) and (2.1). If ϕ_s and ϕ_T are constrained to satisfy (2-8), then (2-7) remains true at all times if satisfied initially.

Rather than using the equations as presented, we transform them into equations for vorticity ζ , streamfunction ψ ,

divergence δ , and velocity potential χ , each defined as

$$\zeta = \underset{\sim}{k} \cdot \nabla \times \underset{\sim}{V} \quad ; \quad \nabla^2 \psi = \zeta$$

$$\delta = \nabla \cdot \underset{\sim}{V} \quad ; \quad \nabla^2 \chi = \delta \tag{2-9}$$

The (vector) momentum equation (2-1) is now replaced by

$$\frac{\partial \zeta}{\partial t} = r_\zeta - f\delta \tag{2-10}$$

$$\frac{\partial \delta}{\partial t} = r_\delta + f\zeta - \nabla^2 \phi \tag{2-11}$$

where r_ζ and r_δ represent the nonlinear terms

$$r_\zeta = - J(\psi, \zeta) - \nabla \cdot \zeta \nabla \chi - \nabla \cdot \delta \nabla \psi + J(\chi, \delta) + \frac{\partial}{\partial p}\left[J(\chi, \omega) - \nabla \cdot \omega \nabla \psi \right] \tag{2-12}$$

$$r_\delta = \nabla \cdot \zeta \nabla \psi - J(\psi, \delta) - J(\chi, \zeta) - \nabla \cdot \delta \nabla \chi - \nabla^2 \left[\tfrac{1}{2} \nabla \psi \cdot \nabla \psi + J(\psi, \chi) + \tfrac{1}{2} \nabla \chi \cdot \nabla \chi \right] - \frac{\partial}{\partial p}\left[J(\psi, \omega) + \nabla \cdot \omega \nabla \chi \right] \tag{2-13}$$

We also separate the θ field into two components, an isobaric-mean field

$$\bar{\theta}(p,t) = \frac{1}{D^2}\int_0^D\int_0^D \theta(x,y,p,t)\, dy\, dx \tag{2-14}$$

and a remainder field

$$\theta'(x,y,p,t) = \theta(x,y,p,t) - \bar{\theta}(p,t) \tag{2-15}$$

Hereafter we shall simply designate this θ' field as θ (i.e. the prime notation will be dropped when there is no confusion). $\bar{\theta}$ enters the equations dynamically through the isobaric-mean static stability

$$\sigma(p) = -\frac{\partial\bar{\theta}}{\partial p} \tag{2-16}$$

The prognostic equations for θ and $\bar{\theta}$ are

$$\frac{\partial\theta}{\partial t} = r_\theta + \sigma\omega \tag{2-17}$$

$$\frac{\partial\bar{\theta}}{\partial t} = -\frac{\partial}{\partial p}\overline{\theta\omega} \tag{2-18}$$

where the overbar ($\bar{}$) denotes an isobaric-mean operator, as used for $\bar{\theta}$ (for example) above. The function r_θ represents the nonlinear

terms

$$r_\theta = -J(\psi,\theta) - \nabla\cdot\theta\nabla\chi - \frac{\partial}{\partial p}\theta\omega \qquad (2\text{-}19)$$

In terms of θ, the hydrostatic relation is

$$\frac{\partial\phi}{\partial p} = -p^{k-1}p_s^{-k}R\theta \qquad (2\text{-}20)$$

like (2-4), except here ϕ is actually $\phi - \bar{\phi}$; i.e. the mean geopotential field, which doesn't enter into the dynamic equations (since $\nabla\phi = 0$), has been subtracted out.

Finally, we non-dimensionalize the equations, scaling t^{-1} by f, θ by some T_o, p by p_s, ω by $p_s f$, x and y by $L = (RT_o/f^2)^{1/2}$, ϕ by RT_o. The equations become

$$\frac{\partial\zeta}{\partial t} = r_\zeta - \delta \qquad (2\text{-}21)$$

$$\frac{\partial\delta}{\partial t} = r_\delta + \zeta - \nabla^2\phi \qquad (2\text{-}22)$$

$$\frac{\partial\theta}{\partial t} = r_\theta + \sigma\omega \qquad (2\text{-}23)$$

$$\frac{\partial\bar{\theta}}{\partial t} = -\frac{\partial}{\partial p}\overline{\theta\omega} \qquad (2\text{-}24)$$

$$\frac{\partial\phi}{\partial p} = -p^{k-1}\theta \qquad (2\text{-}25)$$

$$\frac{\partial\omega}{\partial p} = -\delta \qquad (2\text{-}26)$$

where the r's are given by (2-12), (2-13), (2-19), non-dimensionalized appropriately. From this point on, all equations and variables are dimensionless, unless otherwise noted.

2.1.2 Layered model

At this point, use of the equations continuous in the vertical shall be dropped, except for an analysis in Chapter 3. Instead, we make use of a layered model in the vertical. Specifically we use the grid shown in Fig. 2.1. This grid significantly simplifies the modal analysis to follow, especially in the two-layer case. The applying of $\bar{\theta}$ and θ to alternate levels is not as peculiar as it seems since $\bar{\theta}$ enters the dynamic equations only in the form $\sigma = -\partial\bar{\theta}/\partial p$. In the remainder of the chapter $\bar{\theta}$ will be time independent, for reasons to be presented in Sections 2.3 and 3.1. Hereafter an overbar $(\bar{\ })$ will denote a time mean value.

With this vertical grid, the odd-layered prognostic equations are:

$$\frac{\partial \zeta}{\partial t}_{2n-1} = r_{\zeta 2n-1} - \delta_{2n-1} \tag{2-27}$$

$$\frac{\partial \delta}{\partial t}_{2n-1} = r_{\delta 2n-1} + \zeta_{2n-1} - \nabla^2 \phi_{2n-1} \tag{2-28}$$

The subscript denotes a level with $n = 1,2,\ldots N$ for a model with ζ defined in N independent levels (to be called an N-layer model). The remaining equations are defined for $n = 1,2,\ldots,N-1$

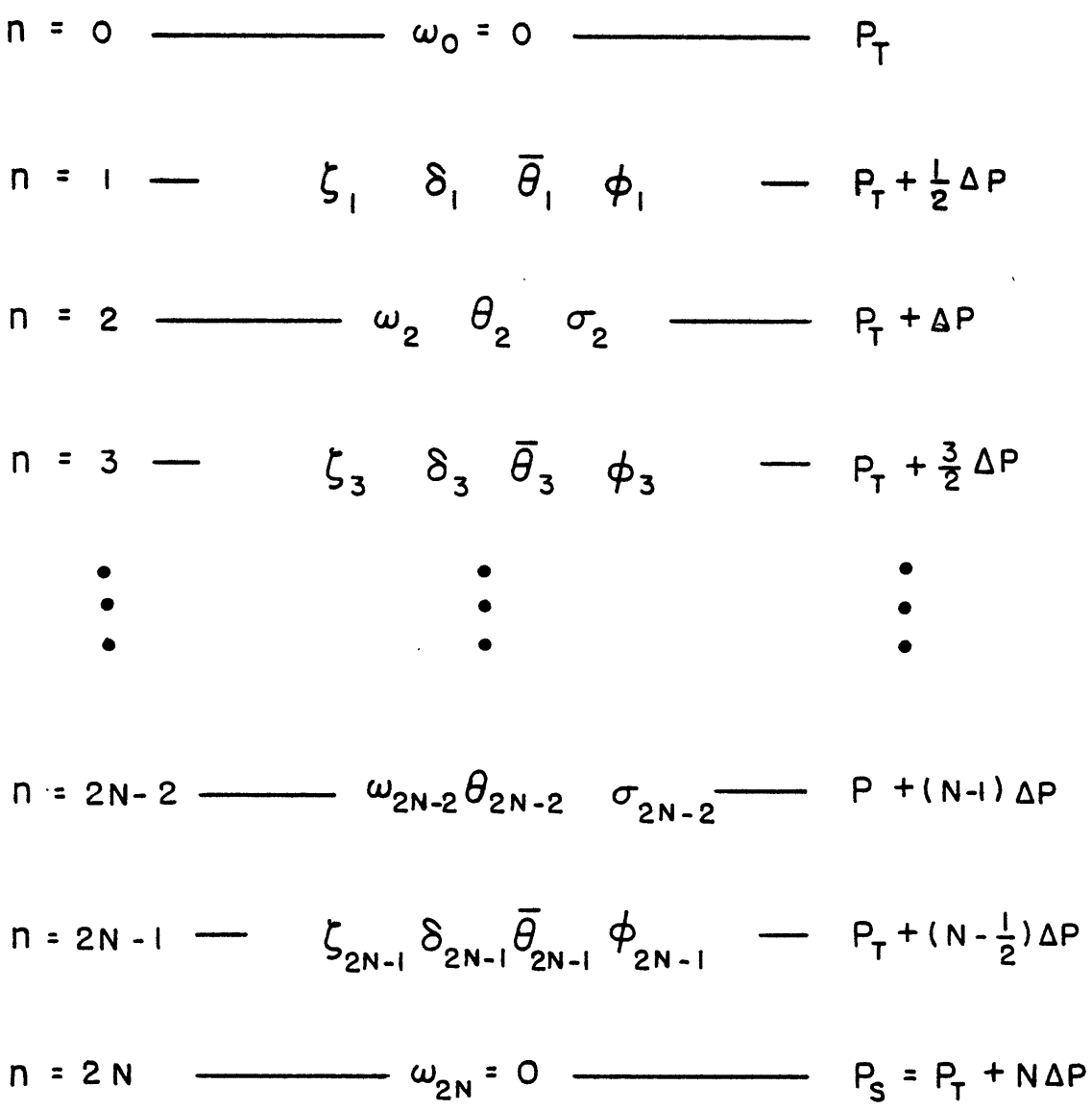
n = 0
$\omega_0 = 0$
P_T
n = 1
ζ_1 δ_1 $\bar{\theta}_1$ ϕ_1
$P_T + \frac{1}{2}\Delta P$
n = 2
ω_2 θ_2 σ_2
$P_T + \Delta P$
n = 3
ζ_3 δ_3 $\bar{\theta}_3$ ϕ_3
$P_T + \frac{3}{2}\Delta P$
n = 2N-2
ω_{2N-2} θ_{2N-2} σ_{2N-2}
$P + (N-1)\Delta P$
n = 2N-1
ζ_{2N-1} δ_{2N-1} $\bar{\theta}_{2N-1}$ ϕ_{2N-1}
$P_T + (N - \frac{1}{2})\Delta P$
n = 2N
$\omega_{2N} = 0$
$P_S = P_T + N\Delta P$

Figure 2.1

$$\frac{\partial \theta}{\partial t}_{2n} = r_{\theta 2n} + \sigma_{2n}\,\omega_{2n} \tag{2-29}$$

$$\omega_{2n} = \omega_{2n-2} - \delta_{2n-1} \tag{2-30}$$

$$\phi_{2n-1} = \phi_{2n+1} + \alpha_{2n}\,\theta_{2n} \tag{2-31}$$

where a factor of $(\Delta p)^{-1}$ has been absorbed in ω, and

$$\sigma_{2n} = \frac{1}{N}\left(\bar{\theta}_{2n-1} - \bar{\theta}_{2n+1}\right) \tag{2-32}$$

$$\alpha_{2n} = \frac{1}{\kappa}\left(p^{\kappa}_{2n+1} - p^{\kappa}_{2n-1}\right) \tag{2-33}$$

The latter arises when the hydrostatic equation is integrated between levels $2n-1$ and $2n+1$ with constant θ_{2n}. ϕ_{2N-1} is given by (2-41).

The functions r are:

$$\begin{aligned} r_{\zeta\,2n-1} = &\left[-J(\psi,\zeta) - \nabla\cdot\zeta\nabla\chi - \nabla\cdot\delta\nabla\psi + J(\chi,\delta)\right]_{2n-1} \\ &+ \left[J(I\chi,\omega) - \nabla\cdot\omega\nabla I\psi\right]_{2n} - \left[J(I\chi,\omega) - \nabla\cdot\omega\nabla I\psi\right]_{2n-2} \end{aligned} \tag{2-34}$$

$$\begin{aligned} r_{\delta\,2n-1} = &\left[\nabla\cdot\zeta\nabla\psi - J(\psi,\delta) - J(\chi,\zeta) - \nabla\cdot\delta\nabla\chi\right]_{2n-1} \\ &-\nabla^2\left[\tfrac{1}{2}\nabla\psi\cdot\nabla\psi + J(\psi,\chi) + \tfrac{1}{2}\nabla\chi\cdot\nabla\chi\right]_{2n-1} \\ &-\left[J(I\psi,\omega) + \nabla\cdot\omega\nabla I\chi\right]_{2n} + \left[J(I\psi,\omega) + \nabla\cdot\omega\nabla I\chi\right]_{2n-2} \end{aligned} \tag{2-35}$$

$$r_{\theta 2n} = -\left[J(I\psi,\theta) + \nabla\cdot\theta\nabla I\chi\right]_{2n} - \left[I\theta\, I\omega\right]_{2n+1} + \left[I\theta\, I\omega\right]_{2n-1} \tag{2-36}$$

A subscript outside brackets indicates that variables inside are all to be taken at the same level; i.e. $[A+B]_n$ denotes A_n+B_n. The letter I before a variable indicates an interpolated value; e.g. $I\psi_n = \frac{1}{2}(\psi_{n+1} + \psi_{n-1})$. The stream function and velocity potential are evaluated by inverting

$$\nabla^2\psi_n = \zeta_n \tag{2-37}$$

$$\nabla^2\chi_n = \delta_n \tag{2-38}$$

Eq's (2-27) through (2-38) are to be solved with the grid representations of conditions (2-6), (2-7) and (2-8). These are

$$0 = \omega_0 = \omega_{2N} \tag{2-39}$$

$$0 = \sum_{n=1}^{N} \delta_{2n-1} \tag{2-40}$$

$$\phi_{2N-1} = \frac{1}{N}\sum_{n=1}^{N} \nabla^{-2}\left(r_{\delta 2n-1} + \zeta_{2n-1}\right) - \frac{1}{N}\sum_{n=1}^{N-1} n\alpha_{2n}\theta_{2n} \tag{2-41}$$

to be satisfied at all x,y,t.

2.1.3 Spectral Equations

Finally, we write the equations in spectral form. The spectra are discrete by the choice of horizontal boundary conditions. Each of the variables ζ_n, δ_n, θ_n, ψ_n, χ_n, ϕ_n and ω_n are expanded in a double Fouier series, e.g. for ζ_n

$$\zeta_n(x,y) = \sum_{\underset{\sim}{K}} \zeta_{n,\underset{\sim}{K}} \exp\left(i \underset{\sim}{K} \cdot \underset{\sim}{r}\right) \tag{2-42}$$

where

$$\underset{\sim}{r} = x\hat{i} + y\hat{j} \tag{2-43}$$

The vector $\underset{\sim}{K}$ thus has components which are integral multiples of $2\pi/D$, where D is now dimensionless. The physical necessity for ζ_n to be real requires

$$\zeta_{n,\underset{\sim}{K}} = \zeta^*_{n,-\underset{\sim}{K}} \tag{2-44}$$

where an asterisk denotes complex conjugate. Substitution of expressions like (2-42) and (2-44) for the remaining variables into partial differential equations (2-25) through (2-39) yields a system of ordinary differential equations for the Fouier coefficients $\zeta_{n,\underset{\sim}{K}}$, etc.

Horizontal scales are explicitly described by $\underset{\sim}{K}$, and the horizontal differential operators become algebraic. In particular $-\nabla^2$ becomes $K^2 = \underset{\sim}{K} \cdot \underset{\sim}{K}$. For each wave vector $\underset{\sim}{K}$, the prognostic spectral equations are

$$\frac{\partial \zeta}{\partial t}_{2n-1,\underset{\sim}{K}} = r_{\zeta\, 2n-1,\underset{\sim}{K}} - \delta_{2n-1,\underset{\sim}{K}} \qquad n = 1, \ldots, N \tag{2-45}$$

$$\frac{\partial \delta}{\partial t}_{2n-1,\underset{\sim}{K}} = \sum_{m=1}^{N} C_{n,m}\left(\zeta_{2m-1,\underset{\sim}{K}} + r_{\zeta\, 2m-1,\underset{\sim}{K}}\right) + K^2 \sum_{m=1}^{N-1} d_{n,m}\,\alpha_{2m}\,\theta_{2m,\underset{\sim}{K}} \tag{2-46}$$

$$n = 1, \ldots, N$$

$$\frac{\partial \theta}{\partial t}_{2n,\underset{\sim}{K}} = r_{\theta\, 2n,\underset{\sim}{K}} - \sigma_{2n} \sum_{m=1}^{n} \delta_{2m-1,\underset{\sim}{K}} \qquad n = 1, \ldots, N-1 \tag{2-47}$$

with

$$C_{n,m} = \begin{cases} 1 - 1/N & n = m \\ -1/N & n \neq m \end{cases} \tag{2-48}$$

$$d_{n,m} = \begin{cases} 1 - m/N & n \leq m \\ -m/N & n > m \end{cases} \tag{2-49}$$

The diagnostic equations have been eliminated. The r's are now sums of quadratic terms with scale-dependent coefficients. Since only the 2-layer model is used after Chapter 3, only the simpler 2-layer expres-

sions appear below

$$r_{\zeta\,2n-1,\underset{\sim}{K}} = \sum_{\underset{\sim}{L},\underset{\sim}{M}} \Big\{ \tfrac{1}{2}\, \underset{\sim}{L}\times\underset{\sim}{M}\left(L^{-2}-M^{-2}\right)\left(\delta^{*}_{\underset{\sim}{L}}\delta^{*}_{\underset{\sim}{M}} - \zeta^{*}_{\underset{\sim}{L}}\zeta^{*}_{\underset{\sim}{M}}\right)_{2n-1}$$

$$-\left(2+\underset{\sim}{L}\cdot\underset{\sim}{M}\left(L^{-2}+M^{-2}\right)\right)\left(\zeta^{*}_{\underset{\sim}{L}}\delta^{*}_{\underset{\sim}{M}}\right)_{2n-1} \qquad (2\text{-}50)$$

$$+\left(1+\underset{\sim}{L}\cdot\underset{\sim}{M}\,L^{-2}\right)\left(\zeta^{*}_{1,\underset{\sim}{L}}+\zeta^{*}_{3,\underset{\sim}{L}}\right)\delta^{*}_{2n-1,\underset{\sim}{M}}\Big\}$$

$$r_{\delta 1,\underset{\sim}{K}} - r_{\delta 3,\underset{\sim}{K}} = \sum_{\underset{\sim}{L},\underset{\sim}{M}} \Big\{ \left(1+\tfrac{1}{2}\underset{\sim}{L}\cdot\underset{\sim}{M}\,L^{-2}M^{-2}\left(L^{2}+M^{2}-K^{2}\right)\right)$$

$$\left(\left(\zeta^{*}_{\underset{\sim}{L}}\,\zeta^{*}_{\underset{\sim}{M}}\right)_{1}-\left(\zeta^{*}_{\underset{\sim}{L}}\,\zeta^{*}_{\underset{\sim}{M}}\right)_{3}\right)$$

$$-\underset{\sim}{L}\times\underset{\sim}{M}\;L^{-2}M^{-1}\left(L^{2}+M^{2}+K^{2}\right)\left(\zeta^{*}_{1,\underset{\sim}{L}}-\zeta^{*}_{3,\underset{\sim}{L}}\right)\delta^{*}_{1,\underset{\sim}{M}} \qquad (2\text{-}51)$$

$$+2\;\underset{\sim}{L}\times\underset{\sim}{M}\;L^{-2}\;\left(\zeta^{*}_{1\,\underset{\sim}{L}}+\zeta^{*}_{3,\underset{\sim}{L}}\right)\delta^{*}_{1,\underset{\sim}{M}}\Big\}$$

$$r_{\theta\,2,\underset{\sim}{K}} = -\sum_{\underset{\sim}{L},\underset{\sim}{M}} \underset{\sim}{L}\times\underset{\sim}{M}\;L^{-2}\left(\zeta^{*}_{1,\underset{\sim}{L}}+\zeta^{*}_{3,\underset{\sim}{L}}\right)\theta^{*}_{2,\underset{\sim}{M}} \qquad (2\text{-}52)$$

The summations $\sum$ are only over those pairs $\underset{\sim}{L}$ and $\underset{\sim}{M}$ which satisfy $\underset{\sim}{K}+\underset{\sim}{L}+\underset{\sim}{M}=0$.

2.2 Normal Modes

One method of partitioning energy into geostrophic and ageostrophic contributions is in terms of normal linearized modes. These modes are defined by linearizing the prognostic equations about a state $\underset{\sim}{V} = 0$, $\theta = \bar{\theta}(p)$, with no forcing or dissipation terms. Such a linearization is identical with ignoring the nonlinear and parameterized terms. The linear equations describe an eigenvalue problem which separates into distinct problems for each $\underset{\sim}{K}$. This method will be further described in the context of the model just introduced.

For each $\underset{\sim}{K}$, the N-layer linear equations can be written as

$$\frac{d}{dt} \underset{\sim}{X}_{\underset{\sim}{K}} = A_K \underset{\sim}{X}_{\underset{\sim}{K}} \tag{2-53}$$

where

$$\underset{\sim}{X}_{\underset{\sim}{K}} = \left(\zeta_{1,\underset{\sim}{K}}, \cdots, \zeta_{2N-1,\underset{\sim}{K}}, \delta_{1,\underset{\sim}{K}}, \cdots, \delta_{2N-1,\underset{\sim}{K}}, \theta_{2,\underset{\sim}{K}}, \cdots, \theta_{2N-2,\underset{\sim}{K}} \right)^T \tag{2-54}$$

Superscript T denotes a transpose. A_K is a (3N-1) x (3N-1) matrix which depends only on N, σ_n, α_n, and $K = (\underset{\sim}{K} \cdot \underset{\sim}{K})^{1/2}$. It is presented below for the case N=2.

The solutions to (2-53) can be written as

$$\underset{\sim}{X}_{\underset{\sim}{K}}(t) = C_K \, e^{D_K (t-t_0)} \underset{\sim}{Y}_{\underset{\sim}{K}}(t_0) \tag{2-55}$$

where D_K is a diagonal matrix of 3N-1 eigenvalues λ_{iK}, C_K is the matrix whose columns are the corresponding eigenvectors $\underset{\sim}{c}_{iK}$ and $\underset{\sim}{Y}_K$ is a vector of eigenvector amplitudes which depend on initial conditions at time t_o. Henceforward we shall refer to the eigenvectors as modes. The λ_{iK} and $\underset{\sim}{c}_{iK}$ satisfy

$$\left(A_K - \lambda_{iK} I\right) \underset{\sim}{c}_{iK} = 0 \tag{2-56}$$

where I is the identity matrix. The model amplitudes satisfy

$$\underset{\sim}{Y}_K(t_o) = C_K^{-1} \underset{\sim}{X}_K(t_o) \tag{2-57}$$

In general, as long as $\sigma_n > 0$ for all n, there are N-1 distinct pairs of conjugate imaginary eigenvalues with moduli greater than 1, and N+1 zero eigenvalues. The former describe ageostrophic, inertial-gravity wave solutions. The $\underset{\sim}{c}_{iK}$ corresponding to the zero eigenvalues are not uniquely determined, although the vector space spanned by them is determined. Two of these steady modes can be chosen to be barotropic, and the remainder baroclinic.

In particular, for the two layer model:

$$\underset{\sim}{X}_K = \left(\zeta_{1K}, \zeta_{3K}, \delta_{1K}, \delta_{3K}, \theta_{2K}\right)^T \tag{2-58}$$

$$A_K = \begin{pmatrix} 0 & 0 & -1/2 & 1/2 & 0 \\ 0 & 0 & 1/2 & -1/2 & 0 \\ 1/2 & -1/2 & 0 & 0 & 1/2\,\alpha_2 K^2 \\ -1/2 & 1/2 & 0 & 0 & -1/2\,\alpha_2 K^2 \\ 0 & 0 & -\sigma_2/2 & \sigma_2/2 & 0 \end{pmatrix} \tag{2-59}$$

$$C_K = \omega_K^{-2} \begin{pmatrix} 0 & \omega_K^2 & \omega_K^2 - 1 & 1 & 1 \\ 0 & \omega_K^2 & 1-\omega_K^2 & -1 & -1 \\ \omega_K^2 & 0 & 0 & -i\omega_K & i\omega_K \\ \omega_K^2 & 0 & 0 & i\omega_K & -i\omega_K \\ 0 & 0 & -\sigma_2 & \sigma_2 & \sigma_2 \end{pmatrix} \tag{2-60}$$

$$C_K^{-1} = \frac{1}{2} \begin{pmatrix} 0 & 0 & 1 & 1 & 0 \\ 1 & 1 & 0 & 0 & 0 \\ 1 & -1 & 0 & 0 & -2\sigma_2^{-1} \\ \frac{1}{2} & -\frac{1}{2} & \frac{1}{2} i\omega_K & -\frac{1}{2} i\omega_K & \frac{1}{2}\alpha_2 K^2 \\ \frac{1}{2} & -\frac{1}{2} & -\frac{1}{2} i\omega_K & \frac{1}{2} i\omega_K & \frac{1}{2}\alpha_2 K^2 \end{pmatrix} \tag{2-61}$$

$$D_K = \text{diag}\ (\ 0\ ,\ \ 0\ ,\ \ 0\ ,\ i\omega_K\ ,\ -i\omega_K\ ) \tag{2-62}$$

where

$$\omega_K = 1 + K^2\mu^{-2} \tag{2-63}$$

is the natural frequency for inertial-gravitational waves in this model (The notation ω_K is distinguishable from the pressure tendency, denoted by $\omega_{\underset{\sim}{K}}$, because the latter depends on the vector scale.), and $\mu^{-1} = \left(\frac{1}{2}\alpha_1\sigma_1\right)^{1/2}$ defines the ratio of the baroclinic to barotropic radii of deformation (for $T_o \sim$ dimensional $\bar{\theta}$).

The components of $\underset{\sim}{Y}_{\underset{\sim}{K}}$ for the two-layer model will be denoted as

$$\underset{\sim}{Y}_{\underset{\sim}{K}} = \left(\ d_{\underset{\sim}{K}}\ ,\ b_{\underset{\sim}{K}}\ ,\ g_{\underset{\sim}{K}}\ ,\ a_{1\underset{\sim}{K}}\ ,\ a_{2\underset{\sim}{K}}\ \right)^T \tag{2-64}$$

Respectively, these components are the amplitudes of: the barotropic divergence mode, the barotropic geostrophic mode, the baroclinic geostrophic mode, and a pair of ageostrophic modes. These five are given by:

$$d_{\underset{\sim}{K}} = \frac{1}{2}\left(\delta_{1\underset{\sim}{K}} + \delta_{3\underset{\sim}{K}}\right) = 0 \tag{2-65}$$

$$b_{\underset{\sim}{K}} = \frac{1}{2}\left(\zeta_{1\underset{\sim}{K}} + \zeta_{3\underset{\sim}{K}}\right) \tag{2-66}$$

$$g_{\underset{\sim}{K}} = \frac{1}{2}\left(\zeta_{1\underset{\sim}{K}} - \zeta_{3\underset{\sim}{K}} - 2\theta_{2\underset{\sim}{K}}\sigma_2^{-1}\right) \tag{2-67}$$

$$a_{1\underset{\sim}{K}} = \frac{1}{2}\left(\frac{1}{2}\left(\zeta_{1\underset{\sim}{K}} - \zeta_{3\underset{\sim}{K}}\right) + \frac{1}{2}\alpha_2 K^2\theta_{2\underset{\sim}{K}} + i\frac{1}{2}\omega_K\left(\delta_{1\underset{\sim}{K}} - \delta_{3\underset{\sim}{K}}\right)\right) \tag{2-68}$$

$$a_{2\underset{\sim}{K}} = \frac{1}{2}\left(\frac{1}{2}\left(\zeta_{1\underset{\sim}{K}} - \zeta_{3\underset{\sim}{K}}\right) + \frac{1}{2}\alpha_2 K^2\theta_{2\underset{\sim}{K}} - i\frac{1}{2}\omega_K\left(\delta_{1\underset{\sim}{K}} - \delta_{3\underset{\sim}{K}}\right)\right) \tag{2-69}$$

The second equality in (2-65) follows from (2-40). In the linearized problem, $a_{1\underset{\sim}{K}}$ and $a_{2\underset{\sim}{K}}$ are the amplitudes of inertial-gravitational waves with oppositely directed phase velocities $\pm\ \omega_K\ \underset{\sim}{K}\ K^{-2}$. If $a_{1\underset{\sim}{K}}$ and $a_{2\underset{\sim}{K}} = 0$, then $b_{\underset{\sim}{K}}$ and $g_{\underset{\sim}{K}}$ describe the vertical mean and shear respectively of the geostrophic potential vorticity of scale $\underset{\sim}{K}$.

The $Y_{\underset{\sim}{K}}$ defined in (2-57) are time independent. Retaining the nonlinear terms in (2-45) through (2-52), the general solution can no longer be written in the form (2-55) unless $Y_{\underset{\sim}{K}}$ is allowed to vary in time. However, ignoring (2-55), and replacing (2-57) with

$$Y_{\underset{\sim}{K}}(t) = C_K^{-1}\ X_{\underset{\sim}{K}}(t) \tag{2-70}$$

does provide an alternate description of the general solution to the nonlinear system. That is, rather than describing the evolution of the fluid in terms of $X_{\underset{\sim}{K}}(t)$, we can just as well describe it in terms

of $\underset{\sim}{Y}_{\underset{\sim}{K}}(t)$. At any particular initial time t_o , (2-70) with $\underset{\sim}{Y}_{\underset{\sim}{K}}(t) = e^{D_K(t-t_o)}\, \underset{\sim}{Y}_{\underset{\sim}{K}}(t_o)$ describes the solution to the linear system (2-53).

While the components of the $\underset{\sim}{Y}_{\underset{\sim}{K}}$ defined by either (2-70) or (2-57) have identical $\zeta_{n,\underset{\sim}{K}}$, $\delta_{n,\underset{\sim}{K}}$, and $\theta_{n,\underset{\sim}{K}}$ dependencies, their meanings are altered. For example, for the two-layer case, the ageostrophic modal amplitudes are given by (2-68) and (2-69) although in the nonlinear system they do not necessarily represent inertial-gravitational oscillations with time dependence $e^{\pm i \omega_K t}$. Even so, these modes are still characterized by ageostrophy, since their amplitudes depend on geostrophically non-balanced fields. They can be called ageostrophic, irrespective of their time dependence.

2.3 Energetics

The nonlinear equations (2-45) through (2-52) conserve a form of total energy E . The fields at each (vector) scale $\underset{\sim}{K}$ contribute independently to the total energy. We can therefore write

$$E = \sum_{\underset{\sim}{K}} \mathcal{E}_{\underset{\sim}{K}} \tag{2-71}$$

$$\mathcal{E}_{\underset{\sim}{K}} = \frac{1}{2N}\left[\sum_{n=1}^{N} K^{-2}\left(\zeta_{2n-1,\underset{\sim}{K}}\, \zeta^{*}_{2n-1,\underset{\sim}{K}} + \delta_{2n-1,\underset{\sim}{K}}\, \delta^{*}_{2n-1,\underset{\sim}{K}}\right) + \sum_{n=1}^{N-1} \frac{\alpha_{2n}}{\sigma_{2n}}\, \theta_{2n,\underset{\sim}{K}}\, \theta^{*}_{2n,\underset{\sim}{K}}\right] \tag{2-72}$$

The first summation determines the kinetic energy, separable into components due to either the vorticity or divergence fields. The latter summation determines the available potential energy. The energy described is non-dimensional, with the dimensional energy per unit mass given by the product ERT_o . In terms of (2-54), (2-72) can be written as

$$\underset{\sim}{\mathcal{E}}_K = \underset{\sim}{X}_K^{T*} \; E_K \; \underset{\sim}{X}_K \tag{2-73}$$

where E_K is the diagonal matrix with first 2N elements $\frac{1}{2N} K^{-2}$ and with remaining N-1 elements $\frac{1}{2N} \alpha_{2N} \sigma_{2n}^{-1}$.

The energy $\underset{\sim}{\mathcal{E}}_K$ can also be written in terms of $\underset{\sim}{Y}_K$. Combining (2-70) with (2-73) yields

$$\underset{\sim}{\mathcal{E}}_K = \underset{\sim}{Y}_K^{T*} \; E_K' \; \underset{\sim}{Y}_K \tag{2-74}$$

where

$$E_K' = C_K^{T*} \; E_K \; C_K \tag{2-75}$$

As long as the order of the components of $\underset{\sim}{Y}_K$ can be assigned such that E_K' is block diagonal then different groups of modes contribute inde-

pendently to the energy. That is the case here as long as the static stability is time independent. If the static stability is time dependent then the definition of APE must be as defined by Lorenz (1960). E then is not strictly quadratic, and the energy can not be partitioned among the modes as described here. With the static stability time independent, the energy, although not necessarily partitionable between individual modes, can be partitioned between groups of modes having distinct eigenvalues.

For the case N=2 ,

$$E'_K = \mathrm{diag}\left(\tfrac{1}{2}\omega_K^4 K^{-2}, \tfrac{1}{2}K^{-2}, \tfrac{1}{4}\alpha_2\sigma_2\omega_K^{-2}, \omega_K^{-2}K^{-2}, \omega_K^{-2}K^{-2}\right) \qquad (2\text{-}76)$$

The energy contributed by the geostrophic modes can be further partitioned into that due to either the barotropic mode or the baroclinic mode. Denoting $G\mathcal{E}_{\underset{\sim}{K}}$ the geostrophic energy contributed by scale $\underset{\sim}{K}$, $B\mathcal{E}_{\underset{\sim}{K}}$ the barotropic contribution, $\Theta\mathcal{E}_{\underset{\sim}{K}}$ the baroclinic contribution, and BE the total barotropic energy, then

$$G\mathcal{E}_{\underset{\sim}{K}} = B\mathcal{E}_K + \Theta\mathcal{E}_K \qquad (2\text{-}77)$$

$$B\mathcal{E}_{\underset{\sim}{K}} = \tfrac{1}{2}K^{-2}b^*_{\underset{\sim}{K}}b_{\underset{\sim}{K}} = \tfrac{1}{8}K^{-2}\left|\zeta_{1\underset{\sim}{K}} + \zeta_{3\underset{\sim}{K}}\right|^2 \qquad (2\text{-}78)$$

$$\theta \mathcal{E}_{\underset{\sim}{K}} = \frac{a_2 \sigma_2}{4\omega_K^2} g^*_{\underset{\sim}{K}} g_{\underset{\sim}{K}} = \frac{\alpha_2 \sigma_2}{4\omega_K^2} \left| \frac{1}{2}(\zeta_{1,\underset{\sim}{K}} - \zeta_{3,\underset{\sim}{K}}) - \theta_{2,\underset{\sim}{K}} \sigma_2^{-1} \right|^2 \quad (2\text{-}79)$$

$$GE = \sum_{\underset{\sim}{K}} G\mathcal{E}_{\underset{\sim}{K}} \quad (2\text{-}80)$$

$$BE = \sum_{\underset{\sim}{K}} B\mathcal{E}_{\underset{\sim}{K}} \quad (2\text{-}81)$$

The ageostrophic energy $A\mathcal{E}_{\underset{\sim}{K}}$ contributed by scale $\underset{\sim}{K}$ is given by

$$A\mathcal{E}_{\underset{\sim}{K}} = \omega_K^{-2} K^{-2} \left[a^*_{1,\underset{\sim}{K}} a_{1\underset{\sim}{K}} + a^*_{2\underset{\sim}{K}} a_{2\underset{\sim}{K}} \right]$$

$$= \frac{1}{8K^2\omega_K^2} \left[\left| \zeta_{1\underset{\sim}{K}} - \zeta_{3\underset{\sim}{K}} + \alpha_2 K^2 \theta_{2,\underset{\sim}{K}} \right|^2 + \omega_K^2 \left| \delta_{1\underset{\sim}{K}} - \delta_{3\underset{\sim}{K}} \right|^2 \right] \quad (2\text{-}82)$$

$$AE = \sum_{\underset{\sim}{K}} A\mathcal{E}_{\underset{\sim}{K}} \quad (2\text{-}83)$$

$A\mathcal{E}_K$ depends on an imbalance between the coriolis and pressure gradient forces, and on the divergent wind field. The barotripic divergence mode contributes no energy since its amplitude is always zero. The energy partitioning described by (2-77) through (2-83) is identical to the results obtained from applying Lorenz's conditions, described in Chapter 1, to this two layer model.

2.4 Forcing and Dissipation Parameterization

In conjunction with the simplicity of the two-layer numerical model used (Chapter 4), only simple parameterizations of forcing and dissipation are incorporated. These are similar to those used by Charney (1959) and Phillips (1956).

We distinguish vertically and horizontally acting eddy viscosity coefficients ν_V and ν_H respectively and denote $\nu = \nu_v (\Delta p)^{-2}$ The dissipation functions for the $\zeta_{1,\underset{\sim}{K}}$ and $\zeta_{3,\underset{\sim}{K}}$ prognostic equations are

$$F_{\zeta 1 \underset{\sim}{K}} = - \nu_H K^2 \zeta_{1\underset{\sim}{K}} + \nu \left(\zeta_{3\underset{\sim}{K}} - \zeta_{1\underset{\sim}{K}} \right) \quad (2\text{-}84)$$

$$F_{\zeta 3 \underset{\sim}{K}} = - \nu_H K^2 \zeta_{3\underset{\sim}{K}} - \nu \left(2\zeta_{3\underset{\sim}{K}} - \zeta_{1\underset{\sim}{K}} \right) \quad (2\text{-}85)$$

respectively. These are to be added to the right-hand side of (2-50) for the appropriate level. Analogous expressions with δ replacing ζ are to be added to the right-hand side of (2-51). Eq (2-85) is similar to Charney's (1959) parameterization with his $k = 2k_i$. The dissipation functions act to exchange energy between levels as well as to dissipate energy.

The forcing and dissipation function to be added to the right-hand side of (2-53) is given by

$$F_{\theta 2 \underset{\sim}{K}} = -k_H K^2 \theta_{2,\underset{\sim}{K}} + \tau_{rad}^{-1}\left(\theta_{rad\,\underset{\sim}{K}} - \theta_{2,\underset{\sim}{K}}\right) \quad (2\text{-}86)$$

K_H is a horizontally acting eddy diffusion coefficient. Radiative heating is parameterized by the Newtonian cooling function given by the last term in (2-86), where τ_{rad} is a radiative relaxation time, and $\theta_{rad,K}$ is a scale dependent radiative equilibrium temperature. Appropriate atmospheric-like values for the external parameters $\theta_{rad,K}$, τ_{rad}, K_H, ν_H, and ν are presented in Chapter 5.

Chapter 3: Ordering Analysis 1

We have previously scaled (2-10) through (2-20) to non-dimensionalize them. This is not to mean that the various variables and terms are of the same magnitude as the scaling parameters. We apply ordering concepts here in order to reiterate some familiar results and for later reference. One result concerns the relationship between the Rossby number and the degree of geostrophy. The other result is a description of the ageostrophic fields under quasi-geostrophic conditions. From the latter, an alternative measure of ageostrophy is defined.

3.1 Ordering by Rossby Number

We identify an ordering parameter ε. For our problem we define it as some time-and-mass-averaged function of ζ/f; e.g. $\varepsilon = \overline{(\zeta/f)^2}^{\frac{1}{2}}$. It is therefore a kind of Rossby number. For a winter hemisphere, $\varepsilon \approx 0.1$.

We define any variable γ as n^{th} order in ε if the magnitude of γ in some time-and-mass-weighted-mean, non-negative definite sense (e.g. $\overline{\gamma^2}^{\frac{1}{2}}$) decreases as fast as ε^n as $\varepsilon \to 0$. That is, we denote $O(\gamma) \sim \varepsilon^n$ if, for example, $\lim \overline{\gamma^2}^{\frac{1}{2}} / \varepsilon^n$ is both bounded and non-zero as $\varepsilon \to 0$. We also associate T_o with the time-mean value of $\overline{\theta}(p_T) - \overline{\theta}(p_S)$.

It is not necessarily possible to determine the order of a function of variables from the order of the variables themselves. For example, if the function is a sum of various terms it may be that cancellation tends to occur so that the sum is much smaller than any individual term. In some cases it is however possible to determine an

upper bound for the function (i.e. least order) given the order of its arguments. As an example, if $O(\gamma_1) = O(\gamma_2) = \varepsilon$, then $O(\gamma_1+\gamma_2) \leq \varepsilon$.

For some time scales, variations of some variables are the same order as the variables themselves. Two such time scales are suggested by the linear analysis of Chapter 2. One is the inertial time scale of order 1, and the other is the advective time scale of order ε^{-1}. For now we examine only those solutions for which ζ, δ, and θ have the same time scale τ, but allow $\overline{\theta}$ to have a different time scale τ_1.

We use the dimensionless equations and assume throughout that $O(\delta) \lesssim O(\zeta) \sim \varepsilon$ so that divergence may be prominent but not dominant. The order of the nonlinear terms in the vorticity and divergence equations therefore satisfy $O(r_\zeta) \lesssim \varepsilon^2$ and $O(r_\delta) \lesssim \varepsilon^2$ since they are sums of quadratic terms. As a result of the T_O assignment, $O(\overline{\theta}) \gtrsim 1$ and $O(\sigma) \sim 1$. Attention is focused on large scales such that (nondimensional) $O(\nabla^2\theta) \;/\; O(\theta) \lesssim 1$. This ratio cannot be much smaller than $O(1)$ because of the finite size of the horizontal domain. The bulk of the atmosphere's energy is in motions of such scales. The diagnostic equations (2.25) and (2.26) readily yield $O(\omega) = O(\delta)$ and $O(\phi) = O(\theta)$. The prognostic equations appear with the least order of the various terms appearing below:

$$\underset{\tau^{-1}\,\varepsilon}{\frac{\partial \zeta}{\partial t}} = \underset{\varepsilon^2}{r_\zeta} - \underset{O(\delta)}{\delta} \qquad (3\text{-}1)$$

$$\underset{\tau^{-1}\;O(\delta)}{\frac{\partial \delta}{\partial t}} = \underset{\varepsilon^2}{r_\delta} + \underset{\varepsilon}{\zeta} - \underset{O(\nabla^2\theta)}{\nabla^2\phi} \qquad (3\text{-}2)$$

$$\frac{\partial \theta}{\partial t} = r_\theta + \sigma\omega \qquad (3\text{-}3)$$

$$\tau^{-1}\, o(\theta) \qquad \varepsilon\, o(\theta) \qquad o(\delta)$$

$$\frac{\partial \bar{\theta}}{\partial t} = \frac{\partial}{\partial p}\,\overline{\theta\omega} \qquad (3\text{-}4)$$

$$\tau_1^{-1}\, o(\bar{\theta}) \qquad o(\theta)\, o(\delta)$$

Applying a dominant balance argument (Bender and Orszag, 1978) at those horizontal scales where $O(\nabla^2\theta) \sim O(\theta)$, solutions characterized by each time scale are possible. The scaling $\tau = 1$ implies $O(\theta) = O(\delta) = \varepsilon$, yielding inertial gravitational waves to lowest order. The other solution is described by $\tau = \varepsilon^{-1}$, $O(\theta) = \varepsilon$, $O(\delta) = \varepsilon^2$. This is the quasi-geostrophic solution. If there exists a horizontal scale such that $O(\nabla^2\theta) \sim \varepsilon\, O(\theta)$, each time scale is again possible. Given $\tau \sim 1$, $O(\theta) = O(\delta)$ is again implied, but now the θ field only has second order effects on the inertial field. The solution through first order is characterized by inertial waves advecting an inert (i.e. on the inertial time scale, the waves are unaffected) θ field. The scaling $\tau \sim \varepsilon^{-1}$ implies quasi-geostrophy with $O(\theta) \sim 1$.

Examination of (3-4) indicates that for the time and space scales investigated, $\tau_1^{-1} \lesssim \varepsilon^2$. This implies that $\bar{\theta}$ changes little over the long advective time scale. Since $\bar{\theta}$ has been scaled by the vertical mean static stability, this also implies that σ is also relatively constant over an advective time period.

This simple scale analysis of the non-forced inviscid equations does not demonstrate that $\varepsilon << 1$ implies solutions are quasi-geostrophic.

It does suggest that $\varepsilon \ll 1$ is a necessary condition for quasi-geostrophy, otherwise lowest order balances are no longer necessarily linear (i.e. geostrophic). The scaling also suggests that consideration of the forcing and dissipation with details of the advective process are necessary to explain why the atmosphere is quasi-geostrophic. The relationship between Rossby number, dissipation, and energy partitioning is further discussed in Chapter 5 and following.

3.2 Quasi-Geostrophic Imbalances

Eqs. (2.21), (2-22), (2-23), (2-25) and (2-26), with time independent σ can be combined to yield a single equation relating time and space variations of ω to the nonlinear terms:

$$\mathcal{L}(\omega) = -\frac{\partial}{\partial p} r_\zeta - \frac{\partial}{\partial p}\frac{\partial}{\partial t} r_\delta - p^{\kappa-1}\nabla^2 r_\theta \qquad (3\text{-}5)$$

where $\mathcal{L}$ is the linear operator

$$\mathcal{L} = \frac{\partial^4}{\partial t^2 \partial p^2} + \frac{\partial^2}{\partial p^2} - p^{\kappa-1}\sigma\nabla^2 \qquad (3\text{-}6)$$

ω also appears implicitly on the right-hand side of (3-5) as given by (2-12), (2-13), and (2-19). The homogeneous problem

$$\mathcal{L}(\omega) = 0$$

will not be discussed here. An equation similar to (3-7) has been

discussed in detail by Pollard (1970) who was interested in ageostrophic modes in a stratified ocean. With the boundary conditions described in Chapter 2, (3-7) describes a Stürm-Liuville problem whose solution has two classes of eigenvalues, similar to those of the two-layer model.

For quasi-geostrophic solutions,

$$\left(\frac{\partial^2}{\partial p^2} - p^{\kappa-1}\sigma\nabla^2\right)\omega \sim -\frac{\partial r_\zeta'}{\partial p} - p^{\kappa-1}\nabla^2 r_\theta' + O(\varepsilon^3) \quad (3\text{-}7)$$

The r_ζ' and r_θ' are second-order quasi-geostrophic approximations to r_ζ and r_θ. The nonlinear terms depending on ω or δ are of least order ε^3 for this scaling, and thus are excluded from r_ζ' and r_θ'. Eq. 3-7 with $O(\varepsilon^3)$ ignored is a form of the well-known quasi-geostrophic omega equation.

Even if the ζ, δ, and θ fields are geostrophic to first order, there can be order ε^2 variations of ζ, δ, and θ with a time scale of 1. If so, then (3-7) is to be replaced by

$$\mathcal{L}(\omega) = -\frac{\partial}{\partial p} r_\zeta' - p^{\kappa-1}\nabla^2 r_\theta' + O(\varepsilon^3) \quad (3\text{-}8)$$

Denoting ω_g as that ω which satisfies (3-7), and ω' as the quantity $\omega-\omega_g$, (3-8) can be written as

$$\mathcal{L}(\omega') = O(\varepsilon^3) \quad (3\text{-}9)$$

The homogeneous equation for ω' is the same as that described

for (3-5). Thus, if ω departs much from its quasi-geostrophic value (i.e. if $O(\omega') \gtrsim O(\omega_g) \sim \varepsilon^2$), then such departures describe inertial-gravitational waves superimposed on a quasi-geostrophic ω_g field, to lowest order. If $O(\omega') < O(\omega)$, then ω' need not have an inertial time scale to lowest order.

Examination of the $\partial\delta/\partial t$ equation indicates that for the orders discussed, oscillations in $\omega-\omega_g$ are accompanied by ascillations in $\frac{\partial \zeta}{\partial p} + p^{\kappa-1}\nabla^2\theta + \frac{\partial r_2'}{\partial p}$, with a phase difference of $\pi/2$. The function r_2' is the quasi-geostrophic approximation to r_2. The equation

$$\frac{\partial \zeta}{\partial p} + p^{\kappa-1}\nabla^2\theta + \frac{\partial r_2}{\partial p} = 0 \tag{3-10}$$

describes a nonlinear balance condition.

When $\varepsilon << 1$ it seems appropriate to describe a quasi-geostrophic departure in terms of ω' rather than ω. Any non-zero δ or ω describes a departure from geostrophic balance. But a geostrophic field undergoing differential advection will not remain geostrophic. An ω_g is necessary to maintain an approximate balance. The balance is only approximate because of this non-zero divergent wind field.

We therefore define a quasi-geostrophic imbalance pseudo-energy QE for the two layer model

$$QE = \sum_{\underset{\sim}{K}} QE_{\underset{\sim}{K}} \tag{3-11}$$

$$QE_{\underset{\sim}{K}} = \frac{1}{\beta K^2 \omega_K}\left[\left(r_{S1\underset{\sim}{K}} + \zeta_{1\underset{\sim}{K}} - r_{S3\underset{\sim}{K}} - \zeta_{3\underset{\sim}{K}} - \alpha_2 K^2 \theta_{2\underset{\sim}{K}}\right)^2 + \left(\delta_{1\underset{\sim}{K}} + \delta_{3\underset{\sim}{K}} + \frac{r_{S1\underset{\sim}{K}} - r_{S3\underset{\sim}{K}} + \alpha_2 K^2 r_{2\theta\underset{\sim}{K}}}{\omega_K^2}\right)^2\right] \tag{3-12}$$

The first and second squared expressions are two-layer finite difference analogs of the left hand side of (3-10) and the quantity $\omega-\omega_g$ respectively. QE is not a true energy because it is not quadratic in the variables ζ, δ, θ. Neither can an energy partitioning be found, for if we attempt to define a balance pseudo-energy G'E by the remainder E-QE, then G'E is not positive definite. Although it lacks the desirable properties of a true form of energy, we do consider QE to be informative when $\varepsilon << 1$. We define

$$R_Q = \frac{QE}{E} \tag{3-13}$$

as an alternative measure of ageostrophy.

The term inside brackets [ ] in (3-12) can be interpreted in another way. If $a_{1\underset{\sim}{K}}$ is replaced by $(i\omega_K)^{-1}\, da_{1\underset{\sim}{K}}/dt$ and $a_{2\underset{\sim}{K}}$ by $(-i\omega_K)^{-1}\, da_{2\underset{\sim}{K}}/dt$ in the definition of $A\underset{\sim}{\xi}_K$ given by (2-82), the result is a new $A\underset{\sim}{\xi}_K$ defined as $Q\underset{\sim}{\xi}_K$. As AE depends on departures from geostrophic balance, QE depends on the time rate of change of such departures. We can define the quantity

$$\hat{\omega} = \left(\overline{QE} \,/\, \overline{AE}\right)^{1/2} \tag{3-14}$$

which is a root-mean-square frequency describing the ageostrophic fields. If $\hat{\omega} << 1$, then the time scale is advective and the ageostrophic fields are approximately quasi-geostrophic. If $\hat{\omega} \sim 1$ then either the ageostrophic modes describe inertial gravitational waves to lowest order, or $\varepsilon \sim 1$ so that the advective and inertial time scales are not distinct.

The power spectra of various modes as determined using the numerical model of Chapter 4 appear in Chapter 8. Further analysis for $\varepsilon \to 0$ is presented there also. Multiple time scales and the form of the functions r are then explicitly considered.

Chapter 4: Low-Order Numerical Model

Using the two-layer model we would like to examine how the forcing and dissipation, in conjunction with advective processes, act to determine various statistics of the energy partitioning. The nonlinear terms in the model do not represent a small effect, and make analytical analysis difficult. For this reason we desire to solve (2-45) etc. numerically in order to investigate several solutions with various values of forcing and dissipation parameters.

Both the geostrophic energy containing planetary scales and the subsynoptic scales, which may contribute most of the ageostrophic energy, need to be described. If all possible (vector) scales within this range are to be described explicitly, on the order of 100,000 coupled ordinary differential equations need to be solved. Each equation may require that tens of thousands of products and sums be calculated. The determination of time-mean statistics of the solutions requires numerical integration over a long time period. Also, time steps must be small enough to resolve the inertial-gravitational waves. To obtain a variety of solutions therefore requires a prohibitive amount of computation time.

To make numerical computation feasible the equations are applied to a low-order model representing many scales of motion. We replace the large set of Fourier coefficients and associated equations by a much smaller set, with each remaining equation having a much smaller number of products and sums to compute. The detailed spatial description that the complete set of coefficients provide is thereby sacrificed.

With a few modifications, however, certain statistics (e.g. time-mean values) of the partitioned energy spectra in this low-order model are expected to approximate those of the complete set of equations.

Lorenz (1972) describes a method for creating a low-order model representing many scales. For simplicity we use what he calls a very-low-order model. The validity of assumptions he uses to modify the interaction coefficients and the model's suitability for studying atmospheric-like problems have not yet been demonstrated. We use the model in any case because of both our own interest in it and its computational suitability. Finer details of the statistics are not to be suggestive of those of the complete set of equations, much less those of the atmosphere. Even so, the results are expected to be informative.

To construct the very-low-order model, the horizontal (vector) scales are first separated into half-octave bands. A particular vector $\underset{\sim}{K}$ is in a band m if

$$\left(\tfrac{1}{2}\right)^{m-\frac{1}{2}} \leq K^2 < \left(\tfrac{1}{2}\right)^{m-\frac{1}{2}} \qquad (4\text{-}1)$$

Then one vector in each band, plus its 90, 180, and 360 degree rotations about the origin, are chosen. Specifically, we choose the same vectors as Lorenz. Only those equations and terms in (2-45) etc. which depend on these few chosen $\underset{\sim}{K}$ are retained. All equations are then modified to account for the reduced number of terms so that the effects of the omitted terms are retained in a parameterized form. This is done by introducing multiplicative factors before all summations

as described by Lorenz.

Further simplification results when the initial conditions and forcing are restricted to be invariant with respect to a ninety-degree rotation. Effectively the model then consists of one time dependent variable for each of ζ_1, ζ_3, δ_1, δ_3, and θ_2 for each band m. These variables are then multiplied by a band dependent factor $2r_m^{\frac{1}{2}}$. The factor r_m is the ratio of the number of vectors in band m for the complete set to that for the low-order set. For the m^{th} band these modified prognostic variables are denoted $X_{1,m}$, $X_{2,m}$, $Y_{1,m}$, $Y_{2,m}$, T_m respectively. Since $\delta_1 = -\delta_3$ by (2-40) we write $Y_m = Y_{1,m} = -Y_{2,m}$. We denote the band containing the non-dimensional length scale $|\underset{\sim}{K}|^{-1} = 1$ as band m=0 (larger scales then have a negative index). Finally, we approximate K_m^2 by 2^m wherever it appears in the equations.

The low-order model prognostic equations are

$$\begin{aligned}
\frac{d}{dt} X_{n,m} = {} & 2c\sqrt{7}\left[2(X_{n,m-2}X_{n,m-1} - Y_{m-2}Y_{m-1}) - 3(X_{n,m-1}X_{n,m+1}\right. \\
& \left. - Y_{m-1}Y_{m+1}) + X_{n,m+1}X_{m+2} - Y_{m+1}Y_{m+2}\right] \\
& + 2c(-1)^n\left[22X_{n,m-2}Y_{m-1} + 22X_{n,m-1}Y_{m-2} + X_{n,m-1}Y_{m+1}\right. \\
& \left. + X_{n,m+1}Y_{m-1} + X_{n,m+1}Y_{m+2} + X_{n,m+2}Y_{m+1}\right] \\
& - c(-1)^n\left[12\bar{X}_{m-2}Y_{m-1} + 10\bar{X}_{m-1}Y_{m-2} - 4\bar{X}_{m-1}Y_{m+1}\right. \\
& \left. + 5\bar{X}_{m+1}Y_{m-1} - 2\bar{X}_{m+1}Y_{m+2} + 3\bar{X}_{m+2}Y_{m+1}\right] \\
& + (-1)^n Y_m + (-1)^n\nu\left[X_{1,m} - X_{2,m}\right] - \nu_H 2^m X_{n,m} - \delta_{n,2}\nu X_{2,m} \qquad (4\text{-}2)
\end{aligned}$$

$$\frac{d}{dt} Y_m = c\left[14\left(X_{1,m-2} X_{1,m-1} - X_{2,m-2} X_{2,m-1}\right) + 7\left(X_{1,m-1} X_{1,m+1} - X_{2,m-1} X_{2,m+1}\right) + 3.5\left(X_{1,m+1} X_{1,m+2} - X_{2,m+1} X_{2,m+2}\right)\right]$$
$$+ 2c\sqrt{7}\left[-2\, Y_{m-2} \bar{X}_{m-1} + 3\, Y_{m-1} \bar{X}_{m-2} - Y_{m-1} \bar{X}_{m+1} - 0.5\, Y_{m+1} \bar{X}_{m-1} + 0.75\, Y_{m+1} \bar{X}_{m+2} - 0.25\, Y_{m+2} \bar{X}_{m+1}\right]$$
$$+ 0.5\left[X_{1,m} - X_{2,m} + 2^m \alpha_2 T_m\right]$$
$$- \left[1.5\nu + 2^m \nu_H\right] Y_m \qquad (4\text{-}3)$$

$$\frac{d}{dt} T_m = c\sqrt{7}\left[4\, \bar{X}_{m-2} T_{m-1} - 2\, \bar{X}_{m-1} T_{m-2} - 4\, \bar{X}_{m-1} T_{m+1} + \bar{X}_{m+1} T_{m-1} + 2\, \bar{X}_{m+1} T_{m+2} - \bar{X}_{m+2} T_{m+1}\right]$$
$$- \sigma_2 Y_m - \tau_{rad}^{-1}\left(T_m - \tilde{T}_m\right) - k_H 2^m T_m \qquad (4\text{-}4)$$

where

$$\bar{X}_m = X_{1,m} + X_{2,m} \qquad (4\text{-}5)$$

$\delta_{n,2}$ is the Kronecker delta. $c = 0.1$, which corresponds to a value of $c_o = 0.53$ in Lorenz's notation. This parameter depends on how the individual nonlinear terms in the summations of (2-50), etc. are assumed to be correlated (c.f. Lorenz, 1972). The relationship between $\tilde{T}_m$ and θ_{rad} $\underset{\sim}{K}$ is discussed in chapter 5. The integers m are restricted to be between m_f and m_l with m_f and m_l defined below, and all m dependent variables zero for $m < m_f$ and $m > m_l$.

The various spectral values are now replaced by quantities per half-octave band m.

$$D\mathcal{E}_m = 2^{-m-1} Y_m^2 \tag{4-6}$$

$$K\mathcal{E}_m = 2^{-m-2} \left(X_{1,m}^2 + X_{2,m}^2 + 2 Y_m^2 \right) \tag{4-7}$$

$$AP\mathcal{E}_m = \frac{\alpha_2}{4\sigma_2} T_m^2 \tag{4-8}$$

$$\mathcal{E}_m = K\mathcal{E}_m + AP\mathcal{E}_m \tag{4-9}$$

$$B\mathcal{E}_m = 2^{-m-3} \left(X_{1,m} + X_{2,m} \right)^2 \tag{4-10}$$

$$\Theta\mathcal{E}_m = \frac{1}{16} \sigma_2 \alpha_2 \omega_m^{-2} \left(X_{1,m} - X_{2,m} - 2 T_m \sigma_2^{-1} \right)^2 \tag{4-11}$$

$$G\mathcal{E}_m = B\mathcal{E}_m + \Theta\mathcal{E}_m \tag{4-12}$$

$$A\mathcal{E}_m = \mathcal{E}_m - G\mathcal{E}_m \tag{4-13}$$

$$Q\mathcal{E}_m = 2^{-m-3}\omega_m^{-4}\left[\left(\frac{d}{dt}X_{1,m} - \frac{d}{dt}X_{2,m} + \alpha_2 2^m \frac{d}{dt}T_m\right)^2 + 4\omega_m^2\left(\frac{d}{dt}Y_m\right)^2\right] \tag{4-14}$$

$$V\mathcal{E}_m = \frac{1}{4}\left(X_{1,m}^2 + X_{2,m}^2\right) \tag{4-15}$$

where $V\mathcal{E}_m$ is the enstrophy contributed by band m, and

$$\omega_m = 1 + 2^m \mu^{-2} \tag{4-16}$$

The space average quantities are sums of the corresponding spectral-band quantities over all indices m, e.g.

$$E = \sum_{m_f}^{m_l} \mathcal{E}_m \tag{4-17}$$

In all experiments forcing is at a single band m_F with a time independent amplitude $\tilde{T}_{m_F}$. For $m \neq m_F$, $\tilde{T}_m = 0$. Initial conditions are obtained from the forced and dissipative steady-state solution with the horizontal eddy viscosity terms neglected since they are negligible for the parameter values used. This solution is

$$T_{m_F} = \tilde{T}_{m_F}\left(1 - \nu\tau_{rad}\left(\omega_{m_F}^2 - 1\right)\right) \tag{4-18}$$

$$Y_{m_F} = \nu\alpha_2 2^{m_F - 1} T_{m_F} \tag{4-19}$$

$$X_{1,m_F} = -\alpha_2 2^{m_F} T_{m_F} \tag{4-20}$$

$$X_{2,m_F} = 0 \tag{4-21}$$

To create interaction with other bands it is necessary to add a small initial pertubation in a band that interacts with m_F. Therefore we also initialize

$$X_{1,m_f+1} = 0.01 \; X_{1,m_f} \tag{4-22}$$

All other prognostic variables are zero initially.

Eqs. (4-2) for both n = 1 and n = 2, (4-3), and (4-4) are numerically integrated using Lorenz's (1971) alternating N-cycle scheme with N = 4. The time step chosen is nearly one-half its critical value for stability. Decreasing the time step results in no significant change in the statistics we examine (Integrating for a longer simulated time is more urgent). Band m_f describes the largest planetary scales. Band m_1 describes the smallest retained scales, and is carefully chosen so that increasing m_1 results in no significant change in the relevant statistics. All results are reported in dimensional units for which we use R = 287 m^2 k^{-1} sec^{-2}, T_o = 290 K, and f = (3 hours)$^{-1}$. These values yield a length scale L = 2890 km. A table of dimensional values of $|\underset{\sim}{K}_m|$ and the inertial period t_m corresponding to a frequency ω_m (with μ^{-2} = .02) appear along with r_m in Table 4.1.

The statistics of the low-order model solutions will be very unlike those obtained using the complete set of equations under certain conditions. These conditions will be discussed when certain properties of the complete equations or numerical results are presented. They will also be summarized in the conclusion. The low-order equations do conserve E in the non-forced invisid case.

Table 4.1 Description of the very-low-order model bands.

$|K_m|^{-1}$, r_m, and t_m are respectively: a typical length scale for band m (in km); the ratio of the total number of vectors in a band to the number retained, and the natural period of inertial-gravitational waves at scale $|K_m|$ (in min.). Dimensional values obtained using L = 2880 km, $\mu^2 = 50$, and f = (3 hours)$^{-1}$.

m	$\|K\|_m^{-1}$	$r_m^{1/2}$	t_m
-2	5760.	1.00	1128.
-1	4070.	1.00	1125.
0	2880.	1.73	1120.
1	2040.	2.45	1109.
2	1440.	3.61	1088.
3	1020.	4.90	1050.
4	720.	7.21	984.
5	509.	9.90	883.
6	360.	14.2	749.
7	255.	20.0	599.
8	180.	28.4	457.
9	127.	40.0	337.
10	90.	56.6	244.
11	64.	80.0	175.
12	45.	113.	124.
13	32.	160.	87.5
14	23.	226.	62.
15	16.	320.	43.8

Chapter 5: Numerical Results 1

The first four numerical experiments are designed to introduce the behavior of the numerical model and some simple relationships between the Rossby number, dissipation parameters, and the energy partitioning between geostrophic and ageostrophic modes. The ninety-degree rotation invariance and periodic boundary conditions, among other restrictions, make it impossible to describe physically real systems with this model. However this simple model may in fact describe the essential features of what we wish to investigate, namely interaction between different scales and linear modes.

5.1 Atmospheric-Like Forcing and Dissipation

The numerical model is not expected to reproduce the statistical behavior of the atmosphere as a whole, or even that of only a restricted region like the mid-latitude troposphere. Yet, an accounting of those aspects it does reproduce is an appropriate introduction to the model. Experiments 1 and 2 are presented for this purpose.

Even with detailed general circulation models, the most appropriate values for the eddy viscosity and some other parameters may be uncertain by a factor of two or more. For the very-low-order model, not only is the choice of parameters difficult to make, but it is even unclear with what real physical domain the model can best be compared. Rather than attempt to choose another domain, which cannot be justified in any case, the model statistics of experiments 1 and 2 are arbitrarily compared with those of a northern hemisphere January.

Non-dimensional values of all parameters for Experiment 1 appear in Table 5.1. These particular values are denoted by a subscript '$_o$' in later chapters. Dimensional eddy viscosity coefficients $\nu_V = 0.1\ mb^2 s^{-1}$ and $\nu_H = 5 \times 10^8\ cm^2 s^{-1}$ are representative of those used in many large-scale models. We also fix $K_H = \nu_H$ which is also common. Values of $p_s = 1000$ mb, $p_T = 200$ mb, $\kappa = 0.287$, and $\bar{\theta}$ (400mb) - $\bar{\theta}$ (800 mb) = 20K yield $\alpha_2 = .59$, $\sigma_2 = 0.069$, and $\mu^{-2} = 0.02$. $\tau_{rad} = 3.3 \times 10^5$s.

As detailed in chapter 9, model results are very sensitive to the forcing amplitude $\tilde{T}_{m_F}$. The value of $\tilde{T}_{m_F}$ used in Experiment 1 is equal to θ_{rad}, given by $\frac{1}{2}\left(\frac{1}{2}\right)^{\kappa}\left(\Delta T_{rad}\right)$ with $\Delta T_{rad} = 90$ K. With a complete set of $\underset{\sim}{K}$, forcing only one scale $\underset{\sim}{K}_F$ would be appropriate, and for this reason we ignore a factor of 2 $r_{m_F}^{1/2}$ which otherwise appears in determining $\tilde{T}_{mF}$ from $\theta_{rad}\underset{\sim}{K}_F$ if all the $\underset{\sim}{K}$ in band m_F are forced similarly. The value of $\tilde{T}_{m_F}$ is reduced by a factor $2^{1/2}$ in experiment 2. Other values are discussed in Chapter 9. The forcing scale $m_F = 0$ corresponds to a pole-to-pole wavelength.

Time mean values of E, KE, DE, APE, ΘE, BE, AE, QE, VE, R, R_Q, and $\hat{\omega}$ for Experiments 1 and 2 appear in Table 5.1. Using atmospheric data, Peixoto and Oort (1974) give values of KE $\approx$ 173 $m^2 s^{-1}$ and APE $\approx$ 663 $m^2 s^{-1}$, including stratospheric contributions. Using the NCAR general circulation model, Chen and Wiin-Nielsen (1976) obtain DE $\approx$ 2.0 $m^2 s^{-2}$ for a simulated January, suggesting $\bar{R} \approx 0.005$ (see Section 1.3). It is interesting that the results of Experiment 2 reproduce these values quite well.

TABLE 5.1 Description of Experiments 1 - 5

Input non-dimensional. E through QE in J kg^{-1}. VE in f^2.
All results time-mean quantities.

Exp. No.	1	2	3	4	5
INPUT					
$\tilde{T}_o$	.13	.093	0	.52	.035
ν_o	.025	.025	0	.00012	.01
ν_H , k_H	5×10^{-5}	5×10^{-5}	0	7.5×10^{-7}	1×10^{-5}
τ_{rad}	33.	33.	0	8000	100
μ^2	50.	50.	50.	50.	50.
RESULTS					
E	1450.	936.	152.	136.	120.
KE	357.	182.	113.	81.5	24.6
DE	10.8	2.0	42.5	16.0	.024
APE	1090.	754.	38.7	38.2	95.1
θE	1150.	784.	41.0	57.0	99.2
BE	275.	148.	25.8	44.2	20.5
AE	23.	3.7	85.	35.	.039
QE	8.8	.74	86.	35.	.00017
VE	.0115	.0043	.0097	.0063	.0005
R	.01	.0026	.56	.19	.00022
R_Q	.0025	.00013	.56	.19	5×10^{-7}
$\hat{\omega}/f$	.62	.45	1.0	1.0	.066

The time-mean spectra of $G\mathcal{E}_m$, and $A\mathcal{E}_m$ for Experiment 2 appear in Figure 5.1. The $G\mathcal{E}_m$ spectrum peaks at the forced scale where APE is generated by forcing. It drops off at both smaller and larger scales. The ageostrophic spectrum peaks at m=4. This result is directly due to a peak in excitation of the ageostrophic modes at that scale due to geostrophic interactions, as determined by quasi-geostrophic scale analysis to be discussed in Chapter 8. The change in $G\mathcal{E}_m$ between bands 3 and 7 (planetary wave numbers 5 through 26) satisfys a $K^{-3.0}$ decay rate. No conclusions regarding universal spectra for an inertial subrange should be made from this latter result however, even in the context of the model's behavior.

It is estimated that the finite-time-mean values in Table 5.1 differ from the infinite-averaging-period ("true") values by less than 10%. This estimate is obtained by examining how the statistics change with the length of the averaging period. Numerically integrating for a longer time period in order to obtain better statistics was non-trivial on the computer available. Experiments with different integration time steps or numbers of retained bands were also conducted, and the value of 10% includes "errors" from these sources as well. The spectral values presented are accurate to within 20%, except for those of the two largest bands which are subject to intermittancy. For other experiments, the length of the averaging period, the number of retained bands, and the integration time steps are adjusted so that these accuracy limits are maintained.

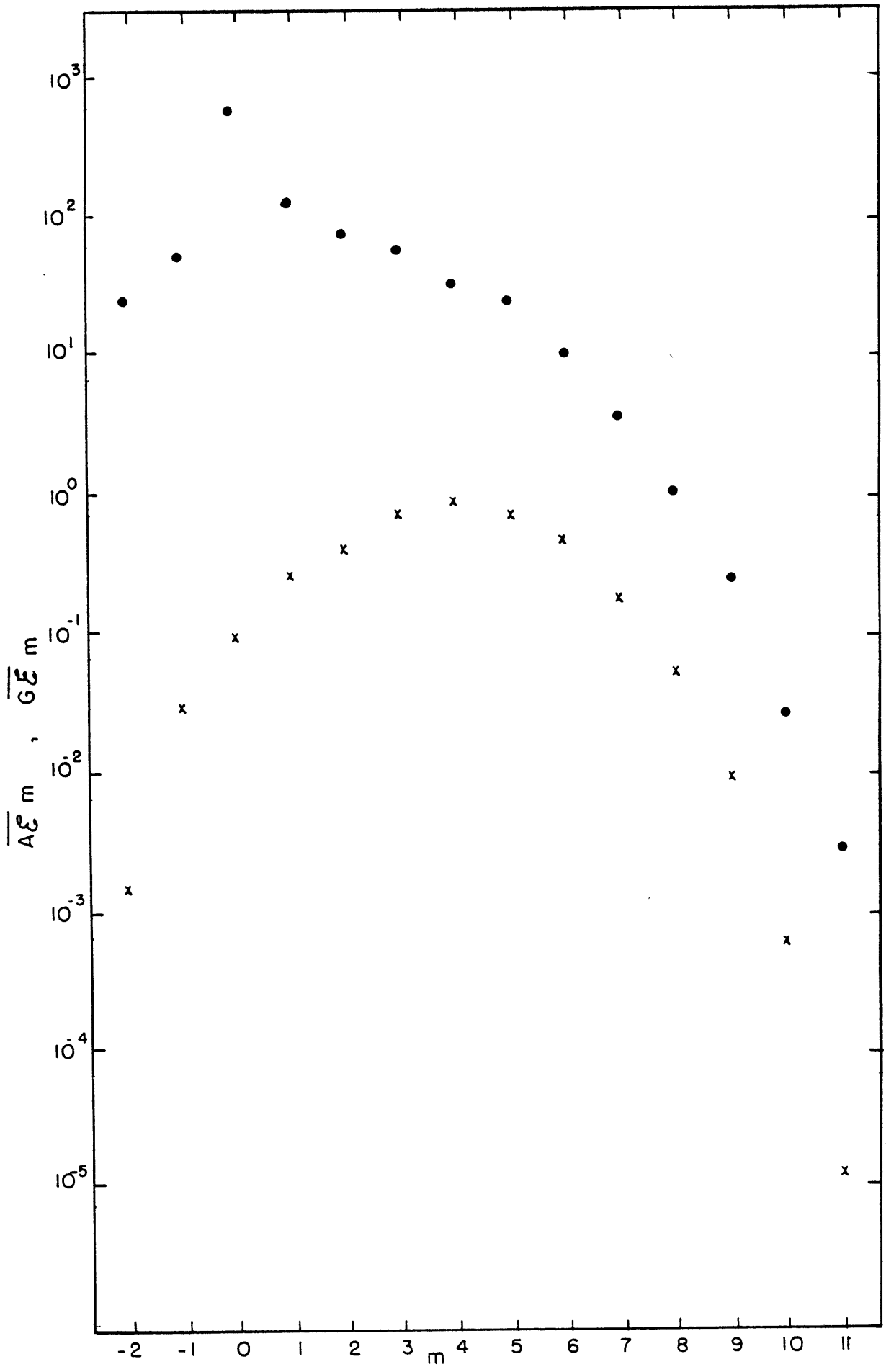
10^3
10^2
10^1
10^0
10^{-1}
10^{-2}
10^{-3}
10^{-4}
10^{-5}
$\overline{\Delta\mathcal{E}}_m$, $\overline{G\mathcal{E}}_m$
-2 -1 0 1 2 3 4 5 6 7 8 9 10 11
m

Figure 5.1

5.2 Inviscid and Non-forced Solution

The importance of the scales of forcing and dissipation in determining the energy partitioning can perhaps best be illustrated by examining the time evolution of a field with the forcing and dissipation removed. An arbitrary initial condition having both non-zero KE and APE is chosen. The time evolution and long-time-mean statistics of the model solution are then numerically determined. The result is that energy tends to be equipartitioned among all the independent modes of the system, as described below.

As an example of this tendency we present Experiment 3. The values of all dissipation and forcing parameters are zero. The initial conditions, for this experiment only, are given by the solution at day 195 for Experiment 5 which has both forcing and dissipation. For Experiment 3 we call this time day 0. Experiments similar to 3 but with different initial conditions were also conducted. These yielded qualitatively similar results and are therefore not described further.

The spectra of $\theta\mathcal{E}_m$ and $A\mathcal{E}_m$ at day 0 appear in Figure 5.2. These spectra have an atmospheric-like shape, although actual values are much smaller than atmospheric. The reduced values have been used to facilitate the numerical calculations. As equipartitioning is approached, the enstrophy of small scales increases by many orders of magnitude. If $V\mathcal{E}_m$ increases beyond 1, then computational stability requires extremely small time steps, greatly increasing the computation time.

The ageostrophic energy as a function of time for Experiment 3

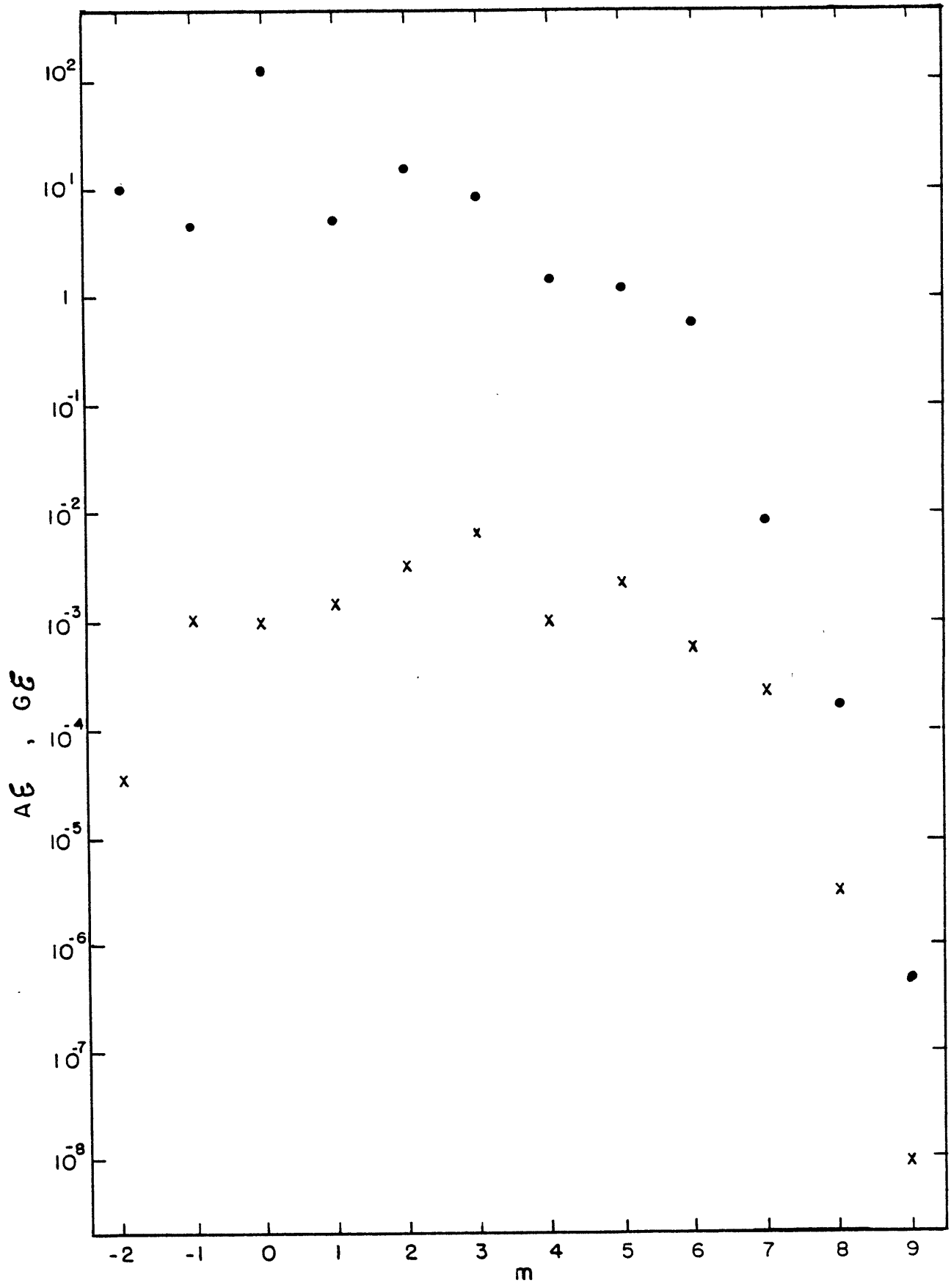
10^2
10^1
1
10^{-1}
10^{-2}
10^{-3}
10^{-4}
10^{-5}
10^{-6}
10^{-7}
10^{-8}
$A\varepsilon$, $G\varepsilon$
-2
-1
0
1
2
3
4
5
6
7
8
9
m

Figure 5.2

appears in Figure 53. It approaches $\frac{1}{2}E$, which is time independent since the invisid-nonforced equations conserve this form of energy. Once AE reaches this value, its time variation becomes relatively small. The elapsed time before the value $\frac{1}{2}E$ is reached depends strongly on the initial conditions. Also appearing in Figure 5.3 is AE as a function of time for Experiment 5, starting from day 195.

The time-mean spectra of $G\mathcal{E}_m$ and $A\mathcal{E}_m$ for Experiment 3, days 200 to 400, appear in Figure 5.4. The energy is approximately partitioned equally to each band m, and to each of $G\mathcal{E}_m$ and $A\mathcal{E}_m$ within each band. Further analysis shows that each linearly independent mode has approximately equal energy. This is to be expected from statistical mechanical arguments; c.f. Salmon, et al. (1976). We note that if both θE and AE are initially zero but BE is nonzero, the flow is barotropic and will remain so, resulting in an equipartitioning analagous to that described by Fox and Orszag (1973).

The equipartitioning we obtain with the very-low-order model is different from that which we would expect with a complete (but truncated, with K^2 less than some large number) spectral model. In the latter, energy is distributed equally among independent modes of each distinct pair $\underset{\sim}{K}$, $-\underset{\sim}{K}$. Each half-octave band then has an energy proportional to the number r_m in Table 4.1. Although for this experiment the very-low-order model results are different from those expected with the complete model, they are indicative of the kind of behavior that does occur; i.e. tendency to equipartition.

We suspect that the slight departures from equipartitioning observed in Figure 5.4 are due to the size of the statistical sample. Since

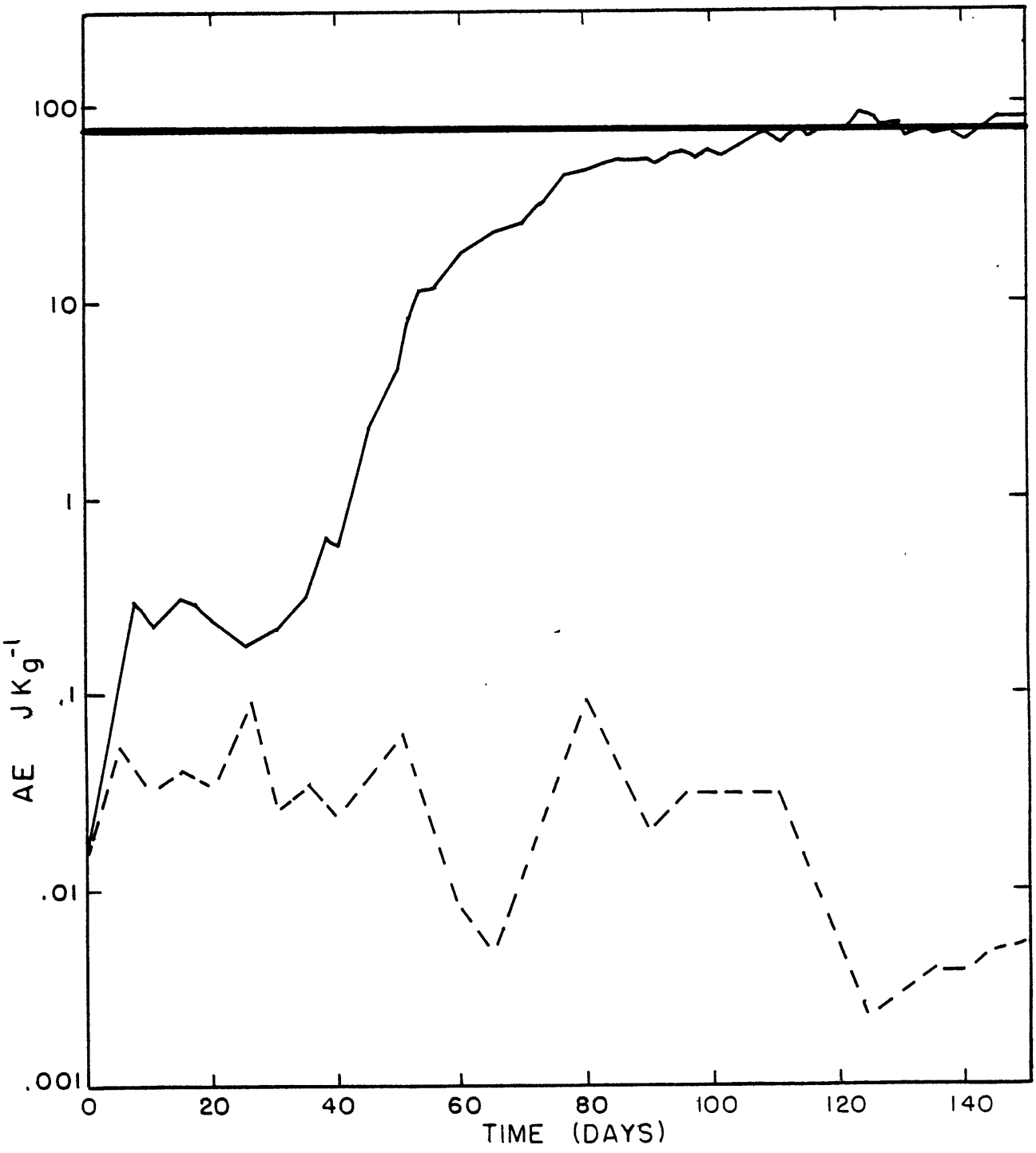

Figure 5.3

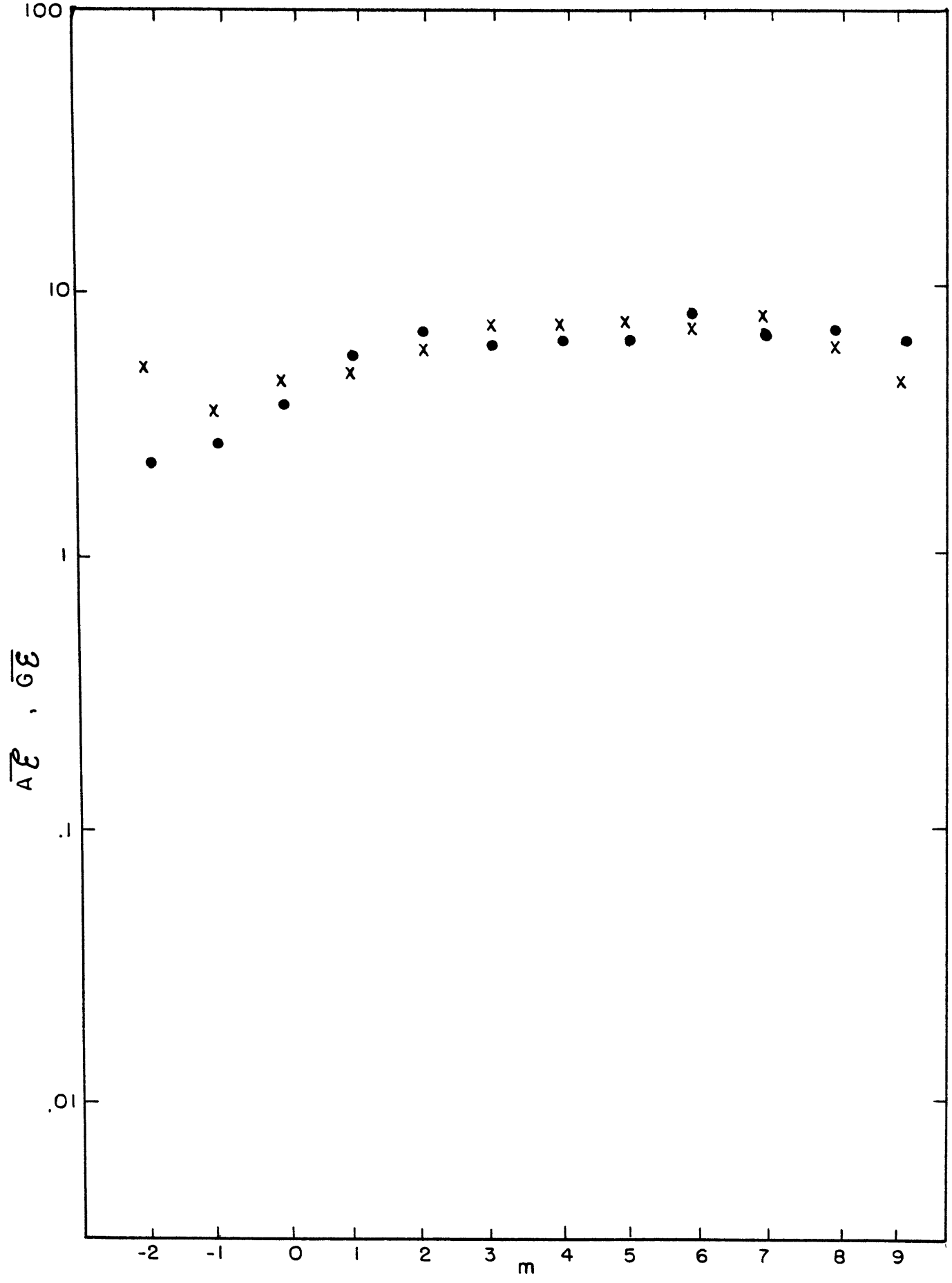
100
10
1
.1
.01
$\overline{A\mathcal{E}}$, $\overline{\mathcal{E}_G}$
-2
-1
0
1
2
3
4
5
6
7
8
9
m

Figure 5.4

energy is equipartitioned, $V\mathcal{E}_m$ is proportional to 2^m. The characteristic time scale of the energy variations of the m^{th} band are on the order of the square root of $V\mathcal{E}_{m\pm1}$, which is a sort of Rossby number for the adjacent scales. (This is expecially true in the very-low-order model for which nonlinear interactions are effectively local in band space). The time scale of the energy variations of $m = -2$ therefore are on the order of 64 times longer than that of $m = 11$. To obtain a better statistical estimate of energy for all the scales, a substantially longer computation time is needed.

The advective processes represented by the nonlinear terms thus tend to distribute the energy equally among all possible modes. Atmospheric-like forcing and dissipation act to oppose this distribution process. The effects of the forcing and dissipation acting independently from the non-linear processes are examined in the next chapter. The nonlinear processes themselves are examined further in Chapter 7. Finally in Chapter 8 the effect of these processes acting together is examined using a detailed scale analysis.

5.3 Small Rossby Number: Ageostrophic Solution

For Experiment 4, the dissipation parameters τ_{rad}^{-1}, ν_H, and ν are greatly reduced from atmospheric-like values so that dissipative processes may be small but present. The forcing $\tilde{T}_{m_F}$ itself is increased, so that the solution's mean enstrophy is approximately that of Experiment 2. Thus the Rossby numbers of Experiments

2 and 4 are similar. μ^2 and m_F are as in Experiment 2. These values and results appear in Table 5.1. The large values of $\bar{R}$ and $\hat{\omega}$ indicate the presence of relatively large amplitude inertial-gravitational waves.

Although $\tilde{T}_o$ is larger than that of Experiment 2, $\tau_{rad}^{-1} \tilde{T}_o$ is smaller. More important than this forcing term itself is the response over all the bands, for example as characterized by the Rossby number. Simce m_F, σ_2 and ε are the same as in Experiment 2, the only parameters which we expect to control the energy partitioning that are different are the dissipative parameters. The dissipative process in reality depends on the influence of internal small scale eddys. A parameterization of these processes more realistic than ours should thus depend on some internal parameter like ε. The very small values of ν, ν_H, and τ_{rad} which we have used may therefore be unrealizable. Yet, this experiment demonstrates the importance of dissipative affects in determining the energy partitioning, and demonstrates that ε by itself is not a measure of geostrophy.

Chapter 6: The Prognostic Equations in terms of Normal Modes

6.1 Non-linear Modal Interactions

Eqs. 2-45 through 2-52 can be transformed into a system of prognostic equations for the modal amplitudes using (2-70). The nonlinearity is then expressed by sums of guadratic functions of the various modes. The interactions of various modes and the resulting energy exchanges become explicit.

The algebra necessary to transform the equations is not difficult for the two-layer model. The inviscid, non-forced modal equations are:

$$\frac{d}{dt} b_{\underset{\sim}{K}} = \sum_{\underset{\sim}{L},\underset{\sim}{M}} \left[C_1 b^*_{\underset{\sim}{L}} b^*_{\underset{\sim}{M}} + C_2 g^*_{\underset{\sim}{L}} g^*_{\underset{\sim}{M}} + C_3 g^*_{\underset{\sim}{L}} a^*_{1\underset{\sim}{M}} + C_3^* g^*_{\underset{\sim}{L}} a^*_{2\underset{\sim}{M}} + C_4 a^*_{1\underset{\sim}{L}} a^*_{1\underset{\sim}{M}} + C_4^* a^*_{2\underset{\sim}{L}} a^*_{2\underset{\sim}{M}} + C_5 a^*_{1\underset{\sim}{L}} a^*_{2,\underset{\sim}{M}} \right] \tag{6-1}$$

$$\frac{d}{dt} g_{\underset{\sim}{K}} = \sum_{\underset{\sim}{L},\underset{\sim}{M}} \left[C_6 b^*_{\underset{\sim}{L}} g^*_{\underset{\sim}{M}} + C_7 b^*_{\underset{\sim}{L}} a^*_{1\underset{\sim}{M}} + C_7^* b^*_{\underset{\sim}{L}} a^*_{2\underset{\sim}{M}} \right] \tag{6-2}$$

$$\frac{d}{dt} a_{1\underset{\sim}{K}} = i\omega_K a_{1\underset{\sim}{K}} + \sum_{\underset{\sim}{L}\underset{\sim}{M}} \left[C_8 b^*_{\underset{\sim}{L}} g^*_{\underset{\sim}{M}} + C_9 b^*_{\underset{\sim}{L}} a^*_{1\underset{\sim}{M}} + C_{10} b^*_{\underset{\sim}{L}} a^*_{2\underset{\sim}{M}} \right] \tag{6-3}$$

$$a_{2\underset{\sim}{K}} = a^*_{1,-\underset{\sim}{K}} \tag{6-4}$$

The later, along with

$$b_{-\underset{\sim}{K}} = b^*_{\underset{\sim}{K}} \tag{6-5}$$

$$g_{-\underset{\sim}{K}} = g^*_{\underset{\sim}{K}} \tag{6-6}$$

insure that the ζ_n, δ_n, and θ_n fields remain real; cf. (2-44).

The interaction coefficients C_i are functions of the ordered set $\underset{\sim}{K}$, $\underset{\sim}{L}$, $\underset{\sim}{M}$, as well as index i. These coefficients are:

$$C_1 = -\tfrac{1}{2}\,\underset{\sim}{L}\times\underset{\sim}{M}\left(L^{-2}-M^{-2}\right) \tag{6-7}$$

$$C_2 = -\tfrac{1}{4}\,\alpha_2\sigma_2\,\underset{\sim}{L}\times\underset{\sim}{M}\left(\omega_L^{-2}-\omega_M^{-2}\right) \tag{6-8}$$

$$C_3 = -\sigma_2\alpha_2\left(2M^2\omega_M^2\omega_L^2\right)^{-1}\left[\underset{\sim}{L}\times\underset{\sim}{M}\left(M^2-L^2\right)+i\omega_m\left(L^2\,\underset{\sim}{M}\cdot\underset{\sim}{K}+M^2\,\underset{\sim}{L}\cdot\underset{\sim}{K}\right)\right] \tag{6-9}$$

$$C_4 = \tfrac{1}{2}\omega_M^{-2}\omega_L^{-2}\left[\underset{\sim}{L}\times\underset{\sim}{M}\left(M^{-2}-L^{-2}\right)\left(1+\omega_M\omega_L\right)-i\left(\omega_L+\omega_M\right)\left(M^{-2}\,\underset{\sim}{M}\cdot\underset{\sim}{K}+L^{-2}\,\underset{\sim}{L}\cdot\underset{\sim}{K}\right)\right] \tag{6-10}$$

$$C_5 = \omega_M^{-2}\omega_L^{-2}\left[\underset{\sim}{L}\times\underset{\sim}{M}\left(M^{-2}-L^{-2}\right)\left(1-\omega_M\omega_L\right)-i\left(\omega_L-\omega_M\right)\left(M^{-2}\,\underset{\sim}{M}\cdot\underset{\sim}{K}+L^{-2}\,\underset{\sim}{L}\cdot\underset{\sim}{K}\right)\right] \tag{6-11}$$

$$C_6 = -\,\underset{\sim}{L}\times\underset{\sim}{M}\;L^{-2}\omega_M^{-2}\left(\omega_M^2-\omega_L^2+1\right) \tag{6-12}$$

$$C_7 = \omega_M^{-2}M^{-2}\left(\underset{\sim}{L}\times\underset{\sim}{M}-i\omega_m\,\underset{\sim}{K}\cdot\underset{\sim}{M}\right) \tag{6-13}$$

$$C_8 = -\tfrac{1}{2}\alpha_2\sigma_2\,\omega_M^{-2}L^{-2}\,\underset{\sim}{L}\times\underset{\sim}{M}\left(\underset{\sim}{K}\cdot\underset{\sim}{L}+i\omega_K\,\underset{\sim}{L}\times\underset{\sim}{M}\right) \tag{6-14}$$

$$C_9 = \left(2\omega_M^2L^2M^2\right)^{-1}\left\{\underset{\sim}{L}\times\underset{\sim}{M}\left[L^2\left(1-\omega_K\omega_M\right)-\omega_K\left(\omega_K M^2-\omega_M K^2\right)\right]-i\left[2\omega_K\left(\underset{\sim}{L}\times\underset{\sim}{M}\right)^2+\omega_M L^2\,\underset{\sim}{K}\cdot\underset{\sim}{M}\right]\right\} \tag{6-15}$$

$$C_{10} = \left(2\omega_M^2L^2M^2\right)^{-1}\left\{\underset{\sim}{L}\times\underset{\sim}{M}\left[L^2\left(1+\omega_K\omega_M\right)-\omega_K\left(\omega_K M^2+\omega_M K^2\right)\right]-i\left[2\omega_K\left(\underset{\sim}{L}\times\underset{\sim}{M}\right)^2-\omega_M L^2\,\underset{\sim}{K}\cdot\underset{\sim}{M}\right]\right\} \tag{6-16}$$

The expressions for C_1, C_2, and C_4 are written symmetrically; e.g. for C_1, since there is redundancy in the summations in (6-1) etc. (i.e. $b_{\underset{\sim}{L}}^* b_{\underset{\sim}{M}}^* = b_{\underset{\sim}{M}}^* b_{\underset{\sim}{L}}^*$), we write C_1 in a form that is independent of the order of L and M. Examination of (6-7) through (6-18) reveals several properties of the energy exchanges among the normal modes which will be discussed in the following chapters.

The tranformed equations maintain forms of the same integral constraints that equations (2-45) through (2-52) maintain. The C_i ($\underset{\sim}{K}$, $\underset{\sim}{L}$, $\underset{\sim}{M}$) must therefore obey certain relationships. Energy conservation requires that

$$K^{-2} C_1(\underset{\sim}{K},\underset{\sim}{L},\underset{\sim}{M}) + L^{-2} C_1(\underset{\sim}{L},\underset{\sim}{M},\underset{\sim}{K}) + M^{-2} C_1(\underset{\sim}{M},\underset{\sim}{K},\underset{\sim}{L}) = 0 \quad (6\text{-}17)$$

$$K^{-2} C_2(\underset{\sim}{K},\underset{\sim}{L},\underset{\sim}{M}) + \tfrac{1}{2} a_2 \sigma_2 \left[\omega_L^{-2} C_6(\underset{\sim}{L},\underset{\sim}{K},\underset{\sim}{M}) + \omega_M^{-2} C_6(\underset{\sim}{M},\underset{\sim}{K},\underset{\sim}{L}) \right] = 0 \quad (6\text{-}18)$$

$$K^{-2} C_3(\underset{\sim}{K},\underset{\sim}{L},\underset{\sim}{M}) + \tfrac{1}{2} a_2 \sigma_2 \omega_L^{-2} C_7(\underset{\sim}{L},\underset{\sim}{K},\underset{\sim}{M}) + 2\omega_M^{-2} M^{-2} C_8(\underset{\sim}{M},\underset{\sim}{K},\underset{\sim}{L}) = 0 \quad (6\text{-}19)$$

$$K^{-2} C_4(\underset{\sim}{K},\underset{\sim}{L},\underset{\sim}{M}) + 2\omega_L^{-2} L^{-2} C_9(\underset{\sim}{L},\underset{\sim}{K},\underset{\sim}{M}) + 2\omega_M^{-2} M^{-2} C_9(\underset{\sim}{M},\underset{\sim}{K},\underset{\sim}{L}) = 0 \quad (6\text{-}20)$$

$$K^{-2} C_5(\underset{\sim}{K},\underset{\sim}{L},\underset{\sim}{M}) + 2\omega_L^{-2} L^{-2} C_{10}(\underset{\sim}{L},\underset{\sim}{K},\underset{\sim}{M}) + 2\omega_M^{-2} M^{-2} C_{10}^*(\underset{\sim}{M},\underset{\sim}{K},\underset{\sim}{L}) = 0 \quad (6\text{-}21)$$

In the absence of ageostrophic effects (i.e. C_3, C_4, C_5, and C_7 set equal to zero), the pseudo-potential vorticity is conserved by a fluid element (Charney and Stern, 1962). In particular then, a form of potential enstrophy P defined as

$$P = \tfrac{1}{2} \sum_{\underset{\sim}{K}} \left(b_{\underset{\sim}{K}}^* b_{\underset{\sim}{K}} + g_{\underset{\sim}{K}}^* g_{\underset{\sim}{K}} \right) \quad (6\text{-}22)$$

is conserved, requiring

$$C_1(\underset{\sim}{K},\underset{\sim}{L},\underset{\sim}{M}) + C_1(\underset{\sim}{L},\underset{\sim}{M},\underset{\sim}{K}) + C_1(\underset{\sim}{M},\underset{\sim}{K},\underset{\sim}{L}) = 0 \qquad (6\text{-}23)$$

$$C_2(\underset{\sim}{K},\underset{\sim}{L},\underset{\sim}{M}) + C_6(\underset{\sim}{L},\underset{\sim}{K},\underset{\sim}{M}) + C_6(\underset{\sim}{M},\underset{\sim}{K},\underset{\sim}{L}) = 0 \qquad (6\text{-}24)$$

Eq's (6-17) through (6-21), (6-23), and (6-24) provide a check that C_1 through C_{10} have been determined correctly. Alternatively, the above relations can provide a method of generating remaining coefficients from a smaller set independently determined.

It is possible to omit certain terms in (6-1) through (6-3), yet still conserve some form of energy, if it is done in accordance with (6-17) through (6-24). For example, if all the terms involving C_3 are omitted, then omitting those of C_7 and C_8 as well conserves energy as defined by (2-71). Some of the other possibilities are more familiar. Retaining only the $\frac{d}{dt} b_{\underset{\sim}{K}}$ and C_1 terms results in the barotropic vorticity equation on an f plane. The quasi-geostrophic system of equations is obtained by omitting all terms involving a_1 and a_2 as well as C_8. It conserves geostrophic energy. Omitting C_4, C_5, C_9, and C_{10} terms and the $da_{1\underset{\sim}{K}}/dt$ term results in a kind of balanced system. It too conserves geostrophic energy.

This last system deserved special notice since its solution approximates that of (6-1) through (6-4) very well under nearly geostrophic conditions, i.e. $a_{1\underset{\sim}{K}} << g_{\underset{\sim}{K}}$ and $a_{1\underset{\sim}{K}} << b_{\underset{\sim}{K}}$. For this modified system, the ageostrophic equation is diagnostic:

$$i\omega_K\, a_{1\underset{\sim}{K}} = -\sum_{\underset{\sim}{L},\underset{\sim}{M}} C_8\, b^*_{\underset{\sim}{L}}\, g^*_{\underset{\sim}{M}} \qquad (6\text{-}25)$$

Eq. (6-25) can be combined with (6-4) to yield diagnostic equations for $\omega_{2\underset{\sim}{K}}$ and the quantity $\zeta_{1\underset{\sim}{K}} - \zeta_{3\underset{\sim}{K}} + \alpha_2 K^2 \theta_{2\underset{\sim}{K}}$. The resulting equations are spectral forms of the quasi-geostrophic omega equation and a balance equation where the nonlinear terms depend only on geostrophic approximations to the temperature and momentum fields.

6.2 Effects of Dissipative Processes

The forcing and dissipative terms given by (2-84), (2-85), and (2-86), along with the terms for the divergence equations, can be written in the notation of Section 2.2 as

$$\frac{d}{dt} \underset{\sim}{X}_{\underset{\sim}{K}} = \ldots + F_K' \underset{\sim}{X}_{\underset{\sim}{K}} + \underset{\sim}{G}_{\underset{\sim}{K}} \qquad (6\text{-}26)$$

where the first four elements of $\underset{\sim}{G}_{\underset{\sim}{K}}$ are zero, and the last is $\tau_{rad}^{-1} \theta_{rad,\underset{\sim}{K}}$, and where F_K' is the appropriate matrix for expressing the remaining terms. For an understanding of how these terms affect the modal amplitudes, (6-26) can be transformed into

$$\frac{d}{dt} \underset{\sim}{Y}_{\underset{\sim}{K}} = \ldots + F_K \underset{\sim}{Y}_{\underset{\sim}{K}} + C_K^{-1} \underset{\sim}{G}_{\underset{\sim}{K}} \qquad (6\text{-}27)$$

where

$$F_K = C_K^{-1} F_K' C_K \qquad (6\text{-}28)$$

Excluding the forcing term $C_K^{-1} \underset{\sim}{G}_{\underset{\sim}{K}}$, (6-27) states

$$\frac{d}{dt} b_{\underset{\sim}{K}} = -e_1 b_{\underset{\sim}{K}} + 2K' e_2 g_{\underset{\sim}{K}} + e_2 (a_{1\underset{\sim}{K}} + a_{2\underset{\sim}{K}}) \qquad (6\text{-}29)$$

$$\frac{d}{dt} g_{\underset{\sim}{K}} = e_2 \omega_K^2 b_{\underset{\sim}{K}} + (e_3 - e_4) g_{\underset{\sim}{K}} - e_3 (a_{1\underset{\sim}{K}} + a_{2\underset{\sim}{K}}) \quad (6\text{-}30)$$

$$\frac{d}{dt} a_{1\underset{\sim}{K}} = \tfrac{1}{2} e_2 \omega_K^2 b_{\underset{\sim}{K}} - K' e_3 g_{\underset{\sim}{K}} + (K' e_3 - e_4) a_{1\underset{\sim}{K}} + K' e_3 a_{2\underset{\sim}{K}} \quad (6\text{-}31)$$

The e_i are functions of scale:

$$e_1 = \tfrac{1}{2} \nu + K^2 \nu_H \quad (6\text{-}32)$$

$$e_2 = \tfrac{1}{2} \nu \omega_K^{-2} \quad (6\text{-}33)$$

$$e_3 = \omega_K^{-2} \left[\tfrac{5}{2} \nu + (\nu_H - k_H) K^2 - \tau_{rad}^{-1} \right] \quad (6\text{-}34)$$

$$e_4 = e_1 + 2\nu \quad (6\text{-}35)$$

$$K' = \tfrac{1}{2} (\omega_K^2 - 1) \quad (6\text{-}36)$$

These terms act to exchange energy between modes (indicated by the non-zero off-diagonal elements of F_K) as well as to dissipate energy. For example, the difference in stress acting upon the top and bottom of the model "atmosphere" acts on the vertical-mean (i.e. barotropic) velocity to create vertical shear, thereby affecting modes which are functions of this shear. Likewise, this difference in stress can destroy vertical shear and generate barotropic modes.

Further insight into the influence of the dissipative affects can be obtained by examining F_K for both the large ($K^2 \to 0$) and small ($K^2 \to \infty$) scale limits. We set $\nu_H = k_H$ for simplicity. We have avoided scaling the modal amplitudes also, although they too are K dependent and vary in magnitude.

For $K^2 \to 0$,

$$\frac{d}{dt} b_{\underset{\sim}{K}} = \ldots - \nu b_{\underset{\sim}{K}} + \tfrac{1}{2}\nu \left(a_{1\underset{\sim}{K}} + a_{2\underset{\sim}{K}}\right) \tag{6-37}$$

$$\frac{d}{dt} g_{\underset{\sim}{K}} = \ldots + \tfrac{1}{2}\nu b_{\underset{\sim}{K}} - \tau_{rad}^{-1} g_{\underset{\sim}{K}} + \left(\tau_{rad}^{-1} - \tfrac{5}{2}\nu\right)\left(a_{1\underset{\sim}{K}} + a_{2\underset{\sim}{K}}\right) \tag{6-38}$$

$$\frac{d}{dt} a_{1\underset{\sim}{K}} = \ldots + \tfrac{1}{4}\nu b_{\underset{\sim}{K}} - \tfrac{5}{2}\nu a_{1\underset{\sim}{K}} \tag{6-39}$$

The baroclinic geostrophic mode does not appear in (6-37) and (6-39) because at large scale the ageostrophic modes become inertial in character (i.e. approximately Θ independent), as is the barotropic mode. Horizontal eddy diffusion is also negligible at large scales.

The barotropic mode has only a boundary stress acting on it. Besides this stress acting on it, the ageostrophic mode has an implicit internal structure (i.e. vertical shear) upon which an internal stress acts as well. Consequently, the magnitude of the coefficient of $b_{\underset{\sim}{K}}$ in (6-37) is smaller than that of $a_{1\underset{\sim}{K}}$ in (6-39).

If the non-linear terms are ignored and $\Theta_{rad}\, \underset{\sim}{K} = 0$, the solutions to the linear equations are given by the eigenvalues and eigenvectors of $A_K + F_K$. The real parts of the eigenvectors describe a damping rate. For $K^2 \to 0$, these rates are $-2.5\ \nu$, $-2.5\ \nu$, $-\tau_{rad}^{-1}$, and $-1.0\ \nu$ (that for the $d_{\underset{\sim}{K}}$ mode is ignored). The eigenvectors corresponding to the first two eigenvalues have only ageostrophic components, and that for the third only geostrophic. The remaining eignevector has both geostrophic and ageostrophic components, with the latter smaller by a factor $\sim \nu/4$. Thus, at large scales, if $\tau_{rad}\, \nu \geq 0.2$,

dominant ageostrophic modes dissipate faster than dominant geostrophic modes, if other effects are excluded.

For $K^2 \to \infty$, the largest terms of F_K become the diagonal ones, all asymptotic to $-\nu_H K^2$. That is, horizontal diffusion becomes most important. As long as $\nu_H = k_H$, the rate of energy dissipation is identical for all modes.

6.3 Effect of Heating

The heating process represented by $C_K^{-1} G_{\underset{\sim}{K}}$ acts upon the baroclinic modes. For the remainder of this chapter we will investigate the effects of this particular heating function upon the generation of $\theta\mathcal{E}_{\underset{\sim}{K}}$ and $A\mathcal{E}_{\underset{\sim}{K}}$ using the two-layer model. These comments can be readily generalized to an N-layer model with linearized radiative heating functions. In chapter 8 these results will be combined with results previously discussed and others to be presented in order to demonstrate how forcing, dissipation, and hydrodynamic instability act together to partition the energy.

In the two-layer model

$$C_K^{-1} G_{\underset{\sim}{K}} = -\sigma_2^{-1}\tau_{rad}^{-1}\theta_{rad\,\underset{\sim}{K}}\left(0,\ 0,\ 1,\ \omega_K^2-1,\ \omega_K^2-1\right)^T \qquad (6\text{-}40)$$

At larger horizontal scales, where $\omega_K \sim 1$, this heating function mainly drives the baroclinic geostrophic mode, while for small scales the ageostrophic modes are more strongly driven. This is simply a result of the ageostrophic modes depending on a higher (horizontal) derivative of the temperature field compared with that of the geostrophic modes;

i.e. $a_{1\underset{\sim}{K}}$ depends on the horizontal gradient of temperature while $g_{\underset{\sim}{K}}$ depends on a vertical shear proportional to temperature.

The rates of change of $\theta\mathcal{E}_{\underset{\sim}{K}}$ and $A\mathcal{E}_{\underset{\sim}{K}}$ due to the heating term (6-40) are

$$\frac{d}{dt}\theta\mathcal{E}_{\underset{\sim}{K}} = \ldots - \alpha_2 \left(2\tau_{rad}\,\omega_K^2\right)^{-1} Re\left[g^*_{\underset{\sim}{K}}\,\theta_{rad\,\underset{\sim}{K}}\right] \quad (6\text{-}41)$$

$$\frac{d}{dt}A\mathcal{E}_{\underset{\sim}{K}} = \ldots - \alpha_2 \left(2\tau_{rad}\,\omega_K^2\right)^{-1} Re\left[\frac{a^*_{1\underset{\sim}{K}} + a^*_{2\underset{\sim}{K}}}{2}\,\theta_{rad\,\underset{\sim}{K}}\right] \quad (6\text{-}42)$$

(The ... indicates that there are rates of change produced by other processes). Each type of energy generation depends on the correlation between a modal amplitude and $\theta_{rad\,\underset{\sim}{K}}$. In particular, if $\theta_{rad\,\underset{\sim}{K}}$ is time independent, then the time-mean generation of $\theta\mathcal{E}_{\underset{\sim}{K}}$ and $A\mathcal{E}_{\underset{\sim}{K}}$ is dependent on only the time-mean values of $g_{\underset{\sim}{K}}$ and $a_{1\underset{\sim}{K}} + a_{2\underset{\sim}{K}}$ respectively. In this case, any high frequency components of $a_{1\underset{\sim}{K}}$ and $a_{2\underset{\sim}{K}}$ (e.g. inertial-gravitational waves) will not generate any time-mean $A\mathcal{E}_{\underset{\sim}{K}}$ by this heating process.

The equality of the coefficients appearing in (6-41) and (6-42) is perhaps misleading because of the rather arbitrary way the normal modes have been defined. Any normal mode is only determined up to an arbitrary, scale dependent, coefficient. The modes have been defined so as to be familiar, e.g. $b_{\underset{\sim}{K}}$ as the vertical-mean potential vorticity of scale $\underset{\sim}{K}$.

The modes can be redefined so that equal (modulus of) amplitudes implies equal energy. Define $b'_{\underset{\sim}{K}}$, $g'_{\underset{\sim}{K}}$, $a'_{1\underset{\sim}{K}}$, and $a'_{2\underset{\sim}{K}}$ as

$$b'_{\underset{\sim}{K}} = \left(2K^2\right)^{-1/2} b_{\underset{\sim}{K}} \quad (6\text{-}43)$$

$$g'_{\underset{\sim}{K}} = \frac{(\alpha_2 \sigma_2)^{1/2}}{2\omega_K} g_{\underset{\sim}{K}} \tag{6-44}$$

$$a'_{1\underset{\sim}{K}} = \frac{1}{\omega_K |\underset{\sim}{K}|} a_{1\underset{\sim}{K}} \tag{6-45}$$

$$a'_{2\underset{\sim}{K}} = \frac{1}{\omega_K |\underset{\sim}{K}|} a_{2\underset{\sim}{K}} \tag{6-46}$$

The various energies are then simply expressed as

$$B\mathcal{E}_{\underset{\sim}{K}} = b'_{\underset{\sim}{K}} b'^{*}_{\underset{\sim}{K}} \tag{6-47}$$

$$\Theta\mathcal{E}_{\underset{\sim}{K}} = g'_{\underset{\sim}{K}} g'^{*}_{\underset{\sim}{K}} \tag{6-48}$$

$$A\mathcal{E}_{\underset{\sim}{K}} = a'_{1\underset{\sim}{K}} a'^{*}_{1\underset{\sim}{K}} + a'_{2\underset{\sim}{K}} a'^{*}_{2\underset{\sim}{K}} \tag{6-49}$$

The energy generation due to heating is now

$$\frac{d}{dt} \Theta\mathcal{E}_{\underset{\sim}{K}} = \ldots - \tau_{rad}^{-1} \omega_K^{-1} \left(\frac{\alpha_2}{\sigma_2}\right)^{1/2} Re\left[g'^{*}_{\underset{\sim}{K}} \Theta_{rad\,\underset{\sim}{K}} \right] \tag{6-50}$$

$$\frac{d}{dt} A\mathcal{E}_{\underset{\sim}{K}} = \ldots - \tau_{rad}^{-1} \omega_K^{-1} \left(\frac{\alpha_2}{4}\right) |\underset{\sim}{K}| Re\left[\frac{a'_{1\underset{\sim}{K}} + a'^{*}_{2\underset{\sim}{K}}}{2} \Theta_{rad\,\underset{\sim}{K}} \right] \tag{6-51}$$

Even if the baroclinic geostrophic and ageostrophic modes have equal energies and identical time spectra at those scales forced, so that their correlations with $\theta_{rad\,\underset{\sim}{K}}$ are identical, their respective energy generations will not be equal. For equal correlations, the ratio of generation due to the heating function $G_{\underset{\sim}{K}}$ is

$$\frac{d\ \Theta\mathcal{E}_{\underset{\sim}{K}} / dt}{d\ A\mathcal{E}_{\underset{\sim}{K}} / dt} = 2\sqrt{2}\ \mu\ |\underset{\sim}{K}|^{-1} \tag{6-52}$$

For atmospheric-like values (Section 5.1)

$$\frac{d\theta E_K / dt}{dA E_S / dt} : L'_K / 920 \text{ kilometers} \qquad (6\text{-}53)$$

where L'_K is the (dimensional) wave length

$$L'_k = |\underset{\sim}{K}|^{-1} 2\pi L \qquad (6\text{-}54)$$

Eq. (6-53) states that heating (as parameterized) acts on horizontal scales larger than 920 kilometers to produce geostrophic energy at a faster rate than ageostrophic energy, even if other processes have acted to distribute the energy so as to make the correlations $\overline{g^{*'}_K \theta_{rad\,\underset{\sim}{K}}}$ and $\overline{\tfrac{1}{2}(a^{*'}_{1k} + a^{*'}_{2k})\theta_{rad\,\underset{\sim}{K}}}$ equal. In actuality, the other processes are not that efficient at redistributing the energy (as will be discussed), so that $\overline{g^{*'}_k \theta_{rad\,\underset{\sim}{K}}} \gg \overline{\tfrac{1}{2}(a^{*'}_{1k} + a^{*'}_{2k})\theta_{rad\,\underset{\sim}{K}}}$, and the heating process generates negligible amounts of $A\underset{\sim}{\mathcal{E}}_k$ at large scales.

Chapter 7: Stability of Geostrophic Modes

7.1 General Problem

The numerical results presented in Chapter 5 suggest that ageostrophic modes of an atmospheric-like initial condition will amplify if dissipative processes are weak, even if the Rossby number describing the solution is less than or equal to its atmospheric value. On the other hand, with atmospheric values of the Rossby number and dissipation parameters, energy is readily exchanged among geostrophic modes, but only weakly between geostrophic and ageostrophic modes. An atmospheric-like spectrum is thereby maintained. This suggests that geostrophic modes may be more unstable with respect to interaction with geostrophic modes than with ageostrophic modes. An alternative possibility, that the dissipation by small scale eddies (e.g., by eddy viscosity) acts more strongly on ageostrophic than geostrophic modes, has been discussed in Chapter 6 and will again be discussed in Chapter 9. The former possibility will be addressed here.

To study the stability of an atmospheric-like initial condition with respect to geostrophic and ageostrophic pertubations in the absence of dissipation processes would be a highly nonlinear problem not easily investigated or described. Examining the stability of simple geostrophic solutions is more amenable to study. If the parameterized forcing and dissipation terms are ignored, each pair of geostrophic modes $b_{\underset{\sim}{K}}$, $b_{-\underset{\sim}{K}}$ or $g_{\underset{\sim}{K}}$, $g_{-\underset{\sim}{K}}$ is an independent, time independant solution to (6-1) through (6-6). Since either member of a pair is

determined by the other, each pair will be denoted by its first member only. We call any of these independent solutions a basic state, denoted by an overbar, e.g., $\bar{b}_{\underset{\sim}{K}}$, so as to distinguish it from pertubation modes.

The modulus of the basic state amplitude defines a scaling parameter ε. Examining the stability of a basic state with respect to pertubations of order $\varepsilon_1 << \varepsilon$ yields systems of equations in which terms quadratic in pertubation modes can be ignored. The system then becomes linear. As long as $\varepsilon_1 << \varepsilon$ the basic state remains uninfluenced by the pertubations.

Each basic state $\bar{b}_{\underset{\sim}{K}}$ or $\bar{g}_{\underset{\sim}{K}}$ yields different sets of linearized systems. For $\bar{b}_{\underset{\sim}{K}}$ the linear problem is separable into two distinct sets: one involving only barotropic pertubations, the other only baroclinic. There are therefore three sets of problems to discuss. The systems of equations in each set are completely determined by the values of $\bar{b}_{\underset{\sim}{K}}$ or $\bar{g}_{\underset{\sim}{K}}$, $\underset{\sim}{K}$, u^2, and the pertubation scales $\underset{\sim}{L}'_n$.

Any scale $\underset{\sim}{L}'_n$ can interact with the basic state scale $\underset{\sim}{K}'_n = (-1)^n \underset{\sim}{K}$ to affect scale $\underset{\sim}{L}'_{n+1} = -\underset{\sim}{L}'_n - \underset{\sim}{K}'_n$, and with the scale $-\underset{\sim}{K}'_n$ to affect scale $\underset{\sim}{L}'_{n-1} = -\underset{\sim}{L}'_n + \underset{\sim}{K}'_n$. Therefore the $\underset{\sim}{L}'_n$ can be defined in general by the sequence

$$\underset{\sim}{L}'_n = (-1)^n \underset{\sim}{L}_n \tag{7-1}$$

$$\underset{\sim}{L}_n = \underset{\sim}{L}_o + n\underset{\sim}{K} \tag{7-2}$$

for integral n. $\underset{\sim}{L}_o$ is arbitrary. A convenient choice is to make $\underset{\sim}{L}_o$ that scale in the sequence $\underset{\sim}{L}_n$ which has a minimum value of $\underset{\sim}{L}_n^2$ (Gill, 1974). The systems of equations for sets $\underset{\sim}{L}_n'$ generated by different $\underset{\sim}{L}_o$'s are then independent of each other.

In principle, the set L_n is infinite. In practice, however, it is not necessary to consider an infinite number of pertubation modes. Therefore we will consider only finite sets of $\underset{\sim}{L}_n$ with $|n| \leq \mathcal{N}$. For small enough ε, the growth rates associated with characteristically ageostrophic solutions converge rapidly to a limiting value as $\mathcal{N}$ is increased. The same is true for the most unstable characteristically geostrophic solutions. Not all the solutions converge rapidly however.

Each linear system can be written in the general form

$$\frac{d}{dt}\underset{\sim}{X} = A\underset{\sim}{X} \qquad (7\text{-}3)$$

The components of $\underset{\sim}{X}$ are the amplitudes of the various pertubation modes of the scales $\underset{\sim}{L}_n$ for a given $\underset{\sim}{L}_o$. The modes of scales $\underset{\sim}{L}_n$ are related to those of $\underset{\sim}{L}_n'$ through (7-1), (6-4), (6-5), and (6-6). A is the appropriate matrix describing the modal interactions. If the components of $\underset{\sim}{X}$ are arranged in order of descending or ascending n, then the matrix A is made up of overlapping blocks, each centered along the diagonal. Each block by itself describes the interaction between the basic state and two pertubation modes of different (vector) scales.

The general solution to (7-3) is of the form

$$\underset{\sim}{X} = \sum_m \underset{\sim}{X}_m e^{\lambda_m t} \qquad (7\text{-}4)$$

each term of which is a particular solution. λ_m and $\underset{\sim}{X}_m$ are the eigenvalues and corresponding eigenvectors of A, λ_m satisfying $\mathrm{Det}(\lambda I - A) = 0$. The real part of λ_m defines the growth rate for the m^{th} solution. The corresponding $\underset{\sim}{X}_m$ defines the relationships between the various pertubation modal amplitudes for that particular solution.

The elements of the upper and lower triangular portions of A, not including the diagonal, are interaction coefficients multiplied by basic state amplitudes of scales $\underset{\sim}{K}$ and $-\underset{\sim}{K}$ respectively. Any terms $\bar{b}_{\underset{\sim}{K}}$ appearing in the evaluation of the determinant $\lambda I - A$ only appear in pairs $\bar{b}_{\underset{\sim}{K}} \bar{b}_{-\underset{\sim}{K}} = \varepsilon^2$. Thus, the eigenvalues of A depend only on ε and not on the phase of the basic state amplitude. This result is consistent with the arbitrary location of the origin x = 0, y = 0 on a periodic f-plane. The phase of the complex amplitude $\bar{b}_{\underset{\sim}{K}}$ is altered by a translation of the origin, but the dynamics (and time scale λ_m) do not depend on the coordinate system for this simple geometry.

For a particular solution, it may be that the pertubation mode of greatest modulus is an ageostrophic mode, with all the geostrophic moduli smaller by an order of magnitude. Or geostrophic modes may dominate. In these cases a solution may be characterized as either ageostrophic or geostrophic respectively depending on the structure of the eigenvector. Our intention is to compare the growth rates of characteristically ageostrophic solutions to those characteristically

geostrophic. The significance of our results will then be discussed in Chapter 10.

We obtain numerical results using a FORTRAN version of ALGOL routines developed by Wilkinson et. al. (1971). The numerical results are used to obtain solutions with large N. These are then compared with solutions which are obtained analytically by considering fewer equations. Each stability problem depends on values of K^2, $\underset{\sim}{K} \cdot \underset{\sim}{L}_o$, $\underset{\sim}{K} \times \underset{\sim}{L}_o$, μ^2, and ε in a manner possibly difficult to determine numerically. Fortunately, the geostrophic and ageostrophic solutions we wish to compare are in fact adequately described by the analytic approximations. We therefore avoid presenting tables of numerical solutions since the results we do present satisfy our intended purpose.

The stability of geostrophic modes in quasi-geostrophic models has already been investigated by others. Lorenz (1972) studied the stability of Rossby waves on a β-plane using a barotropic model. His results were generalized by Gill (1974). Kim (1975) investigated the stability of baroclinic Rossby waves on a β-plane. These studies are reviewed and extended by Lin (1979). Our results will be compared with these in the appropriate limits where both should agree.

The stability of barotropic geostrophic modes in a shallow water model has been investigated by Duffy (1974) and 1975). In the first, only resonant interactions were investigated. However, his results are invalidated by an error to be discussed below. In the second study, he concluded that barotropic geostrophic modes are neutral with respect to ageostrophic pertubations. This result will be compared with ours for baroclinic ageostrophic pertubations.

7.2 Stability of a Baroclinic Geostrophic Mode

The stability of a single finite-amplitude baroclinic geostrophic mode $\bar{g}_{\underset{\sim}{K}}$ with respect to infinitessimal pertubations in other modes is discussed first. The appropriate linearized equations are

$$\frac{d}{dt} g_{\underset{\sim}{L}'_{2n}} = C_6(\underset{\sim}{L}'_{2n}, \underset{\sim}{K}, \underset{\sim}{L}'_{2n-1}) \bar{g}^*_{\underset{\sim}{K}} b^*_{\underset{\sim}{L}'_{2n+1}} + C_6(\underset{\sim}{L}'_{2n}, -\underset{\sim}{K}, \underset{\sim}{L}'_{2n-1}) \bar{g}^*_{-\underset{\sim}{K}} b^*_{\underset{\sim}{L}'_{2n-1}} \tag{7-5}$$

$$\frac{d}{dt} a_{1\underset{\sim}{L}'_{2n}} = i\omega_{\underset{\sim}{L}'_{2n}} a_{1\underset{\sim}{L}'_{2n}} + C_8(\underset{\sim}{L}'_{2n}, \underset{\sim}{K}, \underset{\sim}{L}'_{2n+1}) \bar{g}^*_{\underset{\sim}{K}} b^*_{\underset{\sim}{L}'_{2n+1}} + C_8(\underset{\sim}{L}'_{2n}, -\underset{\sim}{K}, \underset{\sim}{L}'_{2n-1}) \bar{g}^*_{-\underset{\sim}{K}} b^*_{\underset{\sim}{L}'_{2n-1}} \tag{7-6}$$

$$\frac{d}{dt} a_{2\underset{\sim}{L}'_{2n}} = -i\omega_{\underset{\sim}{L}'_{2n}} a_{2\underset{\sim}{L}'_{2n}} + C^*_8(\underset{\sim}{L}'_{2n}, \underset{\sim}{K}, \underset{\sim}{L}'_{2n+1}) \bar{g}^*_{\underset{\sim}{K}} b^*_{\underset{\sim}{L}'_{2n+1}} + C^*_8(\underset{\sim}{L}'_{2n}, -\underset{\sim}{K}, \underset{\sim}{L}'_{2n-1}) \bar{g}^*_{-\underset{\sim}{K}} b^*_{\underset{\sim}{L}'_{2n-1}} \tag{7-7}$$

$$\begin{aligned} \frac{d}{dt} b_{\underset{\sim}{L}_{2n-1}} = {} & \bar{g}^*_{-\underset{\sim}{K}} \left[C_2(\underset{\sim}{L}'_{2n-1}, -\underset{\sim}{K}, \underset{\sim}{L}'_{2n}) g^*_{\underset{\sim}{L}'_{2n}} + C_3(\underset{\sim}{L}'_{2n-1}, -\underset{\sim}{K}, \underset{\sim}{L}'_{2n}) a^*_{1\underset{\sim}{L}'_{2n}} \right] \\ & + \bar{g}^*_{-\underset{\sim}{K}} C^*_3(\underset{\sim}{L}'_{2n-1}, -\underset{\sim}{K}, \underset{\sim}{L}'_{2n}) a^*_{2\underset{\sim}{L}'_{2n}} + \bar{g}^*_{\underset{\sim}{K}} C_2(\underset{\sim}{L}'_{2n-1}, \underset{\sim}{K}, \underset{\sim}{L}'_{2n-2}) g^*_{\underset{\sim}{L}'_{2n-2}} \\ & + \bar{g}^*_{\underset{\sim}{K}} \left[C_3(\underset{\sim}{L}'_{2n-1}, \underset{\sim}{K}, \underset{\sim}{L}'_{2n-2}) a^*_{1\underset{\sim}{L}'_{2n-2}} + C^*_3(\underset{\sim}{L}'_{2n-1}, \underset{\sim}{K}, \underset{\sim}{L}'_{2n-2}) a^*_{2\underset{\sim}{L}'_{2n-2}} \right] \end{aligned} \tag{7-8}$$

The barotropic and baroclinic modes can instead be defined for even and odd subscripted scales respectively yielding a system of equations similar in structure but with different values for the scale dependent coefficients. Such an exchange of subscripts causes the scale L_o to be associated with a barotropic mode rather than baroclinic mode as above. The systems of equations are independend from each other. [If the ageostrophic effects are ignored and $\underset{\sim}{L}_o \cdot \underset{\sim}{K} = 0$, these two systems are what Kim (1975) calls Branch II and Branch I problems respectively.]

Equations (7-5) through (7-8) have been written in a form closely resembling (6-1) through (6-3). Alternatively, using the relations (7-4) and (6-4) through (6-6), they can be written in the form (7-3). The right-hand side of the prognostic equations are then in terms of the pertubation amplitudes themselves, rather than their complex conjugates. The transformed equations may be written as

$$\frac{d}{dt} g_{2n} = \bar{g}^*_{\underset{\sim}{K}} C_{6,2n} b_{2n+1} + \bar{g}_{\underset{\sim}{K}} C'_{6,2n} b_{2n-1} \tag{7-9}$$

$$\frac{d}{dt} a_{1,2n} = i\omega_{2n} a_{1,2n} + \bar{g}^*_{\underset{\sim}{K}} C_{8,2n} b_{2n+1} + \bar{g}_{\underset{\sim}{K}} C'_{8,2n} b_{2n-1} \tag{7-10}$$

$$\frac{d}{dt} a_{2,2n} = -i\omega_{2n} a_{2,2n} + \bar{g}^*_{\underset{\sim}{K}} C^*_{8,2n} b_{2n+1} + \bar{g}_{\underset{\sim}{K}} C'^*_{8,2n} b_{2n-1} \tag{7-11}$$

$$\frac{d}{dt}b_{2n+1} = \bar{g}^{*}_{\underset{\sim}{K}}\left[\bar{C}_{2,2n+1}g_{2n+2} + C_{3,2n+1}a_{1,2n+2}\bar{C^{*}_{3,2n+1}}a_{2,2n+2}\right]$$

$$+ \bar{g}_{\underset{\sim}{K}}\left[\bar{C'_{2,2n+1}}g_{2n} + C'_{3,2n+1}a_{1,2n} + \bar{C'^{*}_{3,2n+1}}a_{2,2n}\right] \tag{7-12}$$

where, for the modal amplitudes and ω_n, the subscript n is to imply a subscript $\underset{\sim}{L}_n$, and where $C_{i,n}$ and $C'_{i,n}$ are functions of the ordered sets $\underset{\sim}{L}_n$, $\underset{\sim}{K}$, $-\underset{\sim}{L}_{n+1}$ and $-\underset{\sim}{L}_n$, $\underset{\sim}{K}$, $\underset{\sim}{L}_{n-1}$ respectively. The vector $\underset{\sim}{X}$, for odd $\mathcal{N}$ for example, is then

$$X = (b_{\mathcal{N}}, g_{\mathcal{N}-1}a_{1,\mathcal{N}-1}a_{2,\mathcal{N}-1}b_{\mathcal{N}-2} \cdots b_{-\mathcal{N}+2}, g_{-\mathcal{N}+1}, a_{1,-\mathcal{N}+1}, a_{2,-\mathcal{N}+1}, b_{-\mathcal{N}})^{T} \tag{7-13}$$

The matrix A is of the form

$$A = \begin{pmatrix}
0 & C_2 & C_3 & C_3^* & 0 & & & & & & & & & \\
C_6 & 0 & 0 & 0 & C_6 & & & & & & & & & \\
C_8 & 0 & i\omega & 0 & C_8 & & & & 0 & & & & & \\
C_8^* & 0 & 0 & -i\omega & C_8^* & & & & & & & & & \\
0 & C_2 & C_3 & C_3^* & 0 & C_2 & C_3 & C_3^* & & & & & & \\
0 & 0 & 0 & 0 & C_6 & 0 & 0 & 0 & & & & & & \\
 & & & & C_8 & 0 & i\omega & 0 & & & & 0 & & \\
 & 0 & & & C_8^* & 0 & 0 & -i\omega & & & & & & \\
 & & & & & & & & 0 & C_2 & C_3 & C_3^* & 0 & \\
 & & & & & & & & C_6 & 0 & 0 & 0 & C_6 & \\
 & & & & & & & & C_8 & 0 & i\omega & 0 & C_8 & \\
 & & & & & & & & C_8^* & 0 & 0 & -i\omega & C_8^* & \\
 & & & & & & & & 0 & C_2 & C_3 & C_3^* & 0 &
\end{pmatrix} \tag{7-14}$$

The scale dependences of the C's are not shown for ease of notation. That portion of A appearing in the blocked square describes the interactions between modes of scales $\underset{\sim}{L}_{N-2}$ and $\underset{\sim}{L}_{N-1}$.

This system will be examined analytically for $\varepsilon \to 0$. The ordering parameter ε_1 does not appear since the equations are linear. With $\underset{\sim}{K}$, $\underset{\sim}{L}_o$, and μ^2 fixed, the only remaining ordering parameter is ε. For $\varepsilon << 1$, we can seek particular solutions of the form

$$\underset{\sim}{X}(t) = \varepsilon_1 \left(\sum_{P=0}^{\infty} \varepsilon^P \underset{\sim}{X}_m^{(P)} \right) \exp \left(t \sum_{P=0}^{\infty} \varepsilon^P \lambda_m^{(P)} \right) \tag{7-15}$$

for each independent solution m (c.f. Bender and Orszag; 1978; pp 330 ff.). The coefficients $\lambda_m^{(P)}$ and $\underset{\sim}{X}_m^{(P)}$ are independent of ε.

We substitute (7-15) into the system described by (7-9) through (7-12). The resulting equations for each component of $\underset{\sim}{X}$ must be satisfied for each power of ε independently. The coefficients $\lambda_m^{(P)}$ are evaluated through some order p thus yielding a p^{th} order approximation to the solution. The difference between the true value and this approximation is asymptotic to the product of an ε-independent constant and ε^{p+1} as $\varepsilon \to 0$. For ε near 1 and p small, this approximation is not expected to be a good one, yet even in that case, with numerical guidance, conclusions can be made.

The order zero equations are

$$\lambda^{(o)} g_{2n}^{(o)} = 0 \tag{7-16}$$

$$\lambda^{(o)} a_{1,2n}^{(o)} = i\omega_{2n} a_{1,2n}^{(o)} \tag{7-17}$$

$$\lambda^{(o)} a_{2,2n}^{(o)} = -i\omega_{2n} a_{2,2n}^{(o)} \tag{7-18}$$

$$\lambda^{(o)} b_{2n-1}^{(o)} = 0 \tag{7-19}$$

There are characteristically geostrophic solutions: $\lambda^{(o)} = 0$, $a_{1,2n}^{(o)} = 0$, $a_{2,2n}^{(o)} = 0$ with $b_{2n-1}^{(o)}$ and $g_{2n}^{(o)}$ arbitrary, for all n. There are also characteristically ageostrophic solutions for each n: $\lambda^{o} = i\omega_{2n}$, $a_{1,2n}^{(o)}$ arbitrary, and all other modes zero to lowest order, or $\lambda^{(o)} = -i\omega_{2n}$, $a_{2,2n}^{(o)}$ arbitrary, and all other modes zero to lowest order. These ageostrophic solutions describe inertial-gravitational waves to lowest order.

7.2.1 Characteristically Geostrophic Solutions

The first order equations for the characteristically geostrophic solutions are

$$\lambda^{(1)} g_{2n}^{(o)} = g'^{*} C_{6,2n} b_{2n+1}^{(o)} + g' C'_{6,2n} b_{2n-1}^{(o)} \tag{7-20}$$

$$0 = i\omega_{2n} a_{k,2n} + g'^{*} C_{8,2n} b_{2n+1}^{(o)} + g' C'_{8,2n} b_{2n-1}^{(o)} \tag{7-21}$$

$$0 = -i\omega_{2n} a_{2,2n} + g'^{*} C^{*}_{8,2n} b_{2n+1}^{(o)} + g' C'^{*}_{8,2n} b_{2n-1}^{(o)} \tag{7-22}$$

$$\lambda^{(1)} b_{2n-1}^{(o)} = g'^{*} C_{2,2n-1} g_{2n}^{(o)} + g' C'_{2,2n-1} g_{2n-2}^{(o)} \tag{7-23}$$

where

$$g' = \bar{g}_{\underset{\sim}{K}} / |\bar{g}_{\underset{\sim}{K}}| \tag{7-24}$$

The $\lambda^{(1)}$ are eigenvalues of the quasi-seostrophic system (7-20) and (7-23). This first order problem with $\underset{\sim}{L}_o \cdot \underset{\sim}{K} = 0$ is the same as that presented by Kim (1975) and Lin (1979) in the limit where both their zonal wind speed $U \to 0$ and $\beta \to 0$. The solutions describe stable, neutral, and unstable ($Re\lambda^{(1)} < 0$, $= 0$, and > 0 respectively) modes. These may be either stationary ($I_m \lambda^{(1)} = 0$) or propagating ($I_m \lambda^{(3)} \neq 0$). Through this order the ageostrophic modes satisfy the balance condition (3-10) and the quasi-geostrophic omega equation (3-7), linearized about the basic state.

Analytic approximations to the unstable first-order characteristically geostrophic solutions can be obtained. As long as $L_o^2 > 2|\underset{\sim}{L}'_o \cdot \underset{\sim}{K}|$, the only pertubation scale $\underset{\sim}{L}_n$ satisfying $L_n^2 \leq K^2$ is the scale $\underset{\sim}{L}_o$. The $\mathcal{N} = 1$ approximation in this case includes all interactions

among wave number triples which have as their central scale the basic state; i.e., $L_{\pm 1}{}^2 > K^2 > L_o{}^2$. The importance of this scale relationship in yielding instability in this linearized quasi-geostrophic solution is discussed by Lin (1979) in relation to Fjortoft's theorem (1953). The $\mathcal{N} = 1$ solution for $\lambda^{(1)}$ is easily determined. For the scale $\underset{\sim}{L}_o$ associated with a barotropic mode

$$\lambda^{(1)} = \mu^{-4}(\underset{\sim}{K}\times\underset{\sim}{L}_o)^2\,\omega_K^{-4}L_o^2(\omega_K^2 - \omega_{L_o}{}^2 + 1)\left[L_o^2(\omega_{L1}^{-1} + \omega_{L-1}^{-2}) + 2L_o{}^{\bullet}K(\omega_{L1}^{-2} - \omega_{L-1}^{-2})\right] \tag{7-25}$$

For $\underset{\sim}{L}_o$ associated with baroclinic modes

$$\lambda^{(1)} = u^{-6}(\underset{\sim}{K}\times\underset{\sim}{L}_o)^2\omega_K^{-2}\omega_{L_o}^{-2}(K^2 - L_o{}^2)\;\frac{L_o{}^2 + 2\underset{\sim}{L}_o{}^{\bullet}\underset{\sim}{K} + u^2}{L_o{}^2 + K^2 + 2\underset{\sim}{L}_o{}^{\bullet}\underset{\sim}{K}} + \frac{L_o{}^2 - 2\underset{\sim}{L}_o{}^{\bullet}\underset{\sim}{K} + u^2}{L_o{}^2 + K^2 - 2\underset{\sim}{L}_o{}^{\bullet}\underset{\sim}{K}} \tag{7-26}$$

Eq. (7-25) is indentical with the result presented by Lin (1979) for $\underset{\sim}{L}_o \cdot \underset{\sim}{K} = 0$, and in the limits $U \to 0$, and $\beta \to 0$.

For $L_o{}^2 \leq 2|\underset{\sim}{L}_o \cdot \underset{\sim}{K}|$ the $\mathcal{N} = 2$ approximation is necessary to describe all interactions with wave number triples having $|\underset{\sim}{K}|$ as the central scale. The $\mathcal{N} = 2$ solution can be determined analytically, and numerical results show it is a good approximation to larger $\mathcal{N}$ solutions. Our interest however is not in describing the characteristically geostrophic solutions in any great detail. For the simpler solutions, the interested reader can consult Lin (1979).

Before investigating the characteristically ageostrophic solutions we would like to see what effect the ageostrophic modes can have on

the characteristically geostrophic solutions. This requires looking at the next order characteristically geostrophic problem. The second order equations are:

$$\lambda^{(1)} g_{2n}^{(1)} + \lambda^{(2)} g_{2n}^{(o)} = g'^{*} C_{6,2n} b_{2n+1}^{(1)} + g' C'_{6,2n} b_{2n-1}^{(1)} \tag{7-27}$$

$$\lambda^{(1)} a_{1,2n}^{(1)} = i\omega_{2n} a_{1,2n}^{(2)} + g'^{*} C_{8,2n} b_{2n+1}^{(1)} + g' C'_{8,2n} b_{2n-1}^{(1)} \tag{7-28}$$

$$\lambda^{(1)} a_{2,2n}^{(1)} = -i\omega_{2n} a_{2,2n}^{(2)} + g'^{*} C^{*}_{8,2n} b_{2n+1}^{(1)} + g' C'^{*}_{8,2n} b_{2n-1}^{(1)} \tag{7-29}$$

$$\begin{aligned} \lambda^{(1)} b_{2n-1}^{(1)} + \lambda^{(2)} b_{2n-1}^{(o)} = {} & g'^{*} \left[C_{2,2n-1} g_{2n}^{(1)} + 2\,\mathrm{Im}\left[\frac{C_{3,2n-1} C_{8,2n}}{\omega_{2n}} \right] g^{*} b_{2n+1}^{(o)} \right] \\ & + g' g'^{*} 2\,\mathrm{Im}\left[\frac{C_{3,2n-1} C'_{8,2n}}{\omega_{2n}} + \frac{C'_{3,2n-1} C_{8,2n-2}}{\omega_{2n-2}} \right] b_{2n-1}^{(o)} \\ & + g' \left[C'_{2,2n-1} g_{2n-2}^{(1)} + 2\,\mathrm{Im}\left[\frac{C'_{3,2n-1} C'_{8,2n-2}}{\omega_{2n-2}} \right] g' b_{2n-3}^{(o)} \right] \end{aligned} \tag{7-30}$$

We prefer to combine second and first order problems to yield a system like (7-3). To do this we add ε^2 times (7-27) to ε times (7-20), ε^2 times (7-28) to ε times (7-21), etc. Third-order terms like $\varepsilon^3 \lambda^{(2)} g_{2n}^{(1)}$ can be added to the resulting equations since they are negligible. Define $\lambda' = \varepsilon\lambda^{(1)} + \varepsilon^2\lambda^{(2)}$, $a'_{1,n}$ and $a'_{2,n}$ analogously, $g'_n = g_n^{(o)} + \varepsilon g_n^{(1)}$ and b'_n analogously. We obtain an eigenvalue problem for λ'

$$\lambda' g'_{2n} = g'^{*} C_{6,2n} b'_{2n+1} + g' C'_{6,2n} b'_{2n-1} \tag{7-31}$$

$$\begin{aligned}\lambda' b'_{2n-1} = {} & g'^{*} C_{2,2n-1} g'_{2n} + g\, C_{2,2n-1} g'_{2n-2} \\ & + 2\varepsilon \mathrm{Im} \left(\frac{C_{3,2n-1} C'_{8,2n}}{\omega_{2n}} + \frac{C'_{3,2n-1} C_{8,2n-2}}{\omega_{2n-2}} \right) b'_{2n-1} \\ & + 2\varepsilon (g'^{*})^2 \, \mathrm{Im} \, \frac{C_{3,2n-1} \, C_{8,2n}}{\omega_{2n}} \, b'_{2n+1} \\ & + 2\varepsilon (g')^2 \, \mathrm{Im} \, \frac{C'_{3,2n-1} \, C'_{8,2n-2}}{\omega_{2n-2}} b'_{2n-3}\end{aligned} \tag{7-32}$$

The ageostrophic terms are given by

$$-i(\omega_{2n} + i\lambda') a'_{1,2n} = g'^{*} C_{8,2n} b'_{2n+1} + g' C'_{8,2n} b'_{2n-1} \tag{7-33}$$

$$i(\omega_{2n} - i\lambda') a'_{2,2n} = g'^{*} C^{*}_{8,2n} b'_{2n+1} + g' C'^{*}_{8,2n} b'_{2n-1} \tag{7-34}$$

Aside from the quasi-geostrophic unstable solutions obtained from the $\mathcal{N} = 1$ or $\mathcal{N} = 2$ approximations as discussed, the remaining characteristically geostrophic numerical solutions converge very slowly (if at all) as $\mathcal{N}$ increases. An example of only weak-convergence by $\mathcal{N} = 17$ for $K^2 = 36$, $\underset{\sim}{K} \cdot \underset{\sim}{L}_o = 6$, and $\underset{\sim}{K} \times \underset{\sim}{L}_o = 12$, $u^{-2} = .02$ appears in Fig. 7.1.

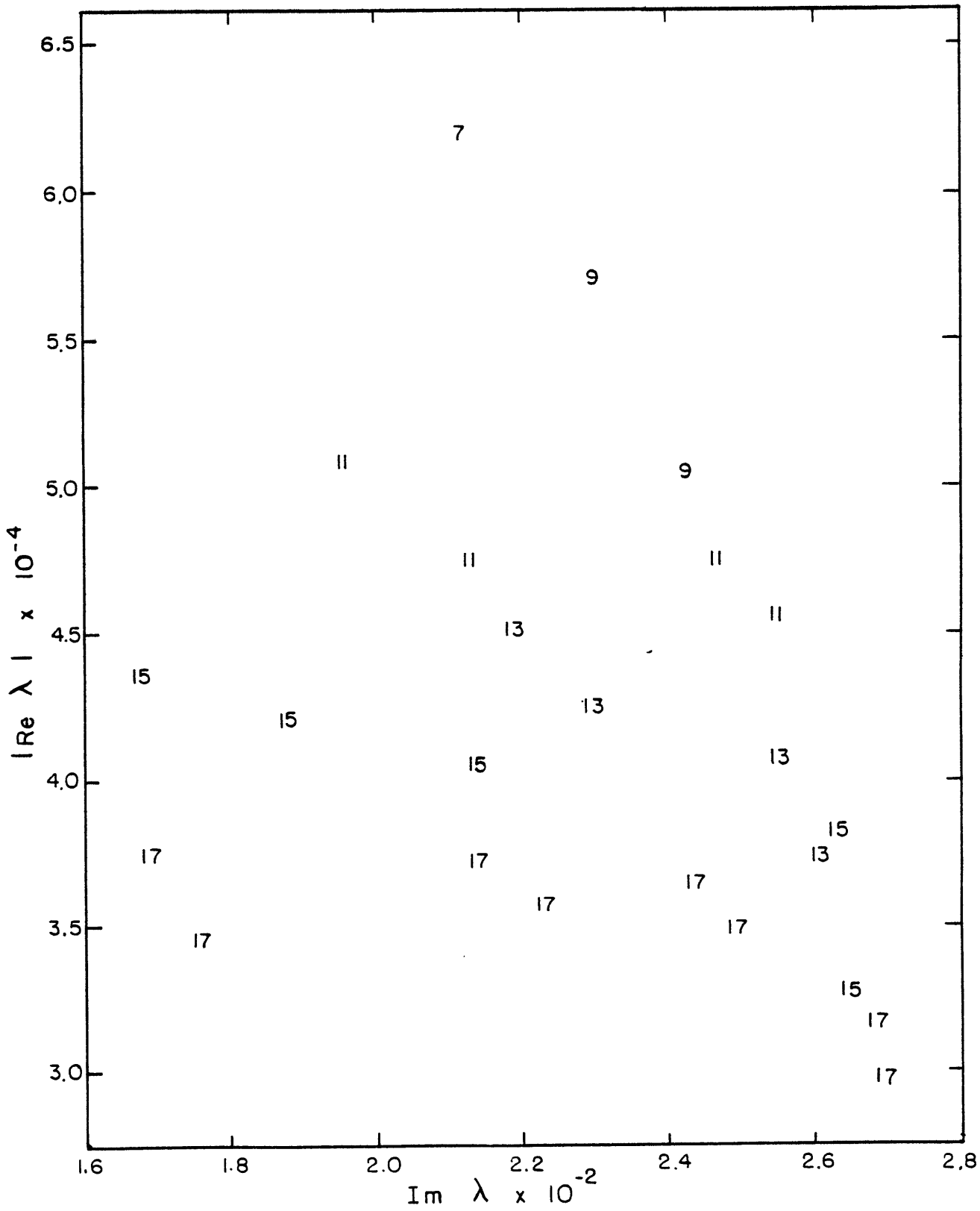
6.5
6.0
5.5
5.0
4.5
4.0
3.5
3.0
1.6
1.8
2.0
2.2
2.4
2.6
2.8
Re λ | x 10^-4
Im λ x 10^-2
7
9
11
9
11
11
13
15
13
15
13
15
17
13
17
17
17
17
15
17
17

Figure 7.1

The form of the equations suggest that the presence of the ageostrophic effects may in fact create an instability different from that discussed earlier, with growth rates proportional to ε^2 in the small ε limit. This is also suggested by the convergence of numerical solutions, although weak.

For the purpose of this study, the result we particularly wish to note is that characteristically geostrophic solutions do exist with growth rates proportional to ε for small ε. These solutions have a small non-zero ageostrophic components which satisfy (7-21) and (7-22) to first order in small ε. Second order analysis yields ageostrophic relations (7-33) and (7-34) which describe a similar balance but with an "adjusted inertial-gravitational frequency" $\omega_{2n} \pm i\lambda'$.

7.2.2 Characteristically ageostrophic solutions

We next examine the characteristically ageostrophic solutions. In particular we choose one with

$$a_{1\underset{\sim}{L}_m} = a \exp(i\omega_{\underset{\sim}{L}_m} + O(\varepsilon))t \qquad (7\text{-}35)$$

and other modes zero to lowest order. Since $a_{1\underset{\sim}{L}_m}^{(o)}$ is arbitrary, we can set it equal to $a = a_{1\underset{\sim}{L}_m}$ at the initial time $t = 0$. The higher order $a_{1\underset{\sim}{L}_m}$ terms are then zero.

The first order equations for this zero order solution are easy to solve, and yield

$$\lambda^{(1)} = 0 \tag{7-36}$$

$$b_{m+1}^{(1)} = -i\omega_m^{-1} C'_{3,m+1} a\, g' \tag{7-37}$$

$$b_{m-1}^{(1)} = -i\omega_m^{-1} C_{3,m-1} a\, g'^{*} \tag{7-38}$$

The first order expansion coefficients of all other modes are zero.

The second order equations yield a solution for $\lambda^{(2)}$

$$\lambda^{(2)} = i\omega_m^{-1} \left[C_{8,m} C'^{*}_{3,m+1} + C'_{8,m} C^{*}_{3,m-1} \right] \tag{7-39}$$

The growth rate is proportional to $\mathrm{Re}\lambda^{(2)}$

$$\mathrm{Re}\,\lambda^{(2)} = 2\mu^{-4} \omega_{L_m}^{-2} \omega_K^{-4} (\underset{\sim}{K} \times \underset{\sim}{L}_m)(\underset{\sim}{K} \cdot \underset{\sim}{L}_m) \tag{7-40}$$

Denoting θ_m as the angle between the vectors $\underset{\sim}{K}$ and $\underset{\sim}{L}_m$, our principal result is

$$\mathrm{Re}\lambda \to \omega_K^{-2} \frac{K^2 L_m^2}{(\mu^2 + K^2)(\mu^2 + L_m^2)} (\sin 2\theta_m) \varepsilon^2 \qquad \varepsilon \to 0 \tag{7-41}$$

as the growth rate. Increasing the static stability (i.e., μ^{-2}) may increase or decrease $\mathrm{Re}\lambda$ depending on the particular values of $\underset{\sim}{K}$, $\underset{\sim}{L}_m$ and μ^2. For a given K^2 and u^2, the largest growth rate is one for which $\theta_m = \pi/4$ and $L_m^2 \to \infty$. For a given θ_m and L_m^2 the growth rate is a maximum for the basic state length scale $|\underset{\sim}{K}|^{-1}$ equal to the baroclinic radius of deformation μ^{-1}. $\mathrm{Re}\lambda$ therefore has an upper bound

$$\mathrm{Re}\ \lambda \ < 1/4\ \varepsilon^2 \qquad (7\text{-}42)$$

for the characteristically ageostrophic solutions for small enough values of ε. Numerical results suggest that (7-41) is a good approximation to the infinite-N value (with maximum error $\leq 20\%$) for $\varepsilon \leq 1$.

Ageostrophic effects are responsible for two kinds of instability. One is that described by any solution to (7-31) and (7-32) which has $\mathrm{Re}\lambda' \to +0$ as $\varepsilon \to 0$ explicitly in (7-32). The other is described by a characteristically ageostrophic solution. Both kinds of instability are similar, differing only in the time scales and relative magnitudes of the pertubations. A characteristically ageostrophic solution necessarily has an inertial time scale. A characteristically geostrophic solution introduces an advective (i.e. progapating wave) time scale of order ε.

There are two physical processes involved in either of these two kinds of instability as revealed by the modal equations. One is the forcing of ageostrophic modes by the advection of the geostrophic wind and temperature field by the geostrophic wind, a sort of non-linear

geostrophic adjustment, described by the C_8 terms. The other is the mutual advection of the ageostrophic and geostrophic wind and temperature fields. This interplay, described by the C_3 terms, affects the geostrophic modes which in turn affects the ageostrophic modes, ad infinitum. The processes may be unstable, neutral, or stable, depending on the scales involved.

7.3 Stability of a Barotropic Mode: Barotropic Pertubations

The linearized equations describing the interactions between barotropic pertubations b_n and a barotropic basic state $\bar{b}_{\underset{\sim}{K}}$ are for our model

$$\frac{d}{dt}b_n = C_{1,n}\bar{b}^*_{\underset{\sim}{K}}b_{n+1} + C'_{1,n}\bar{b}_{\underset{\sim}{K}}b_{n-1} \tag{7-43}$$

This is identical to Lorenz's (1972) system with his $\beta = 0$ and $U = 0$, and has been discussed in detail by Gill (1974). We therefore do not repeat those studies. Gill has demonstrated that for small ε (the parameter b in his study) an instability with growth rate of order ε is present if $L_o^2 < K^2$.

7.4 Stability of a Barotropic Mode: Baroclinic Pertubations

We now investigate the stability of a finite-amplitude barotropic geostrophic mode $\bar{b}_{\underset{\sim}{K}}$ with respect to infinitessimal baroclinic

pertubations. The linearized equations in the form (7-3) are

$$\frac{d}{dt}g_n = \bar{b}^*_{\underset{\sim}{K}}\left[C_{6,n}g_{n+1} + C^*_{7,n}a_{1,n+1} + C_{7,n}a_{2,n+1}\right]$$

$$+ \bar{b}_{\underset{\sim}{K}}\left[C'_{6,n}g_{n-1} + C'^*_{7,n}a_{1,n-1} + C'_{7,n}a_{2,n-1}\right] \tag{7-44}$$

$$\frac{d}{dt}a_{1,n} = i\omega_n a_{1,n} + \bar{b}^*_{\underset{\sim}{K}}\left[C_{8,n}g_{n+1} + C_{10,n}a_{1,n+1} + C_{9,n}a_{2,n+1}\right]$$

$$+ \bar{b}_{\underset{\sim}{K}}\left[C'_{8,n}g_{n-1} + C'_{10,n}a_{1,n-1} \quad C'_{9,n}a_{2,n-1}\right] \tag{7-45}$$

$$\frac{d}{dt}a_{2,n} = -i\omega_n a_{2,n} + \bar{b}^*_{\underset{\sim}{K}}\left[C^*_{8,n}g_{n+1} + C^*_{9,n}a_{1,n+1} + C^*_{10,n}a_{2,n+1}\right]$$

$$+ \bar{b}_{\underset{\sim}{K}}\left[C'^*_{8,n}g_{n-1} + C'^*_{9,n}a_{1,n-1} + C'^*_{10,n}a_{2,n-1}\right] \tag{7-46}$$

We proceed to study solutions of the form (7-15) as done in Section 7.2.

The order zero equations are

$$\lambda^{(o)}g_n^{(o)} = 0 \tag{7-47}$$

$$\lambda^{(o)}a_{1,n}^{(o)} = i\omega_n a_{1,n}^{(o)} \tag{7-48}$$

$$\lambda^{(o)}a_{2,n}^{(o)} = -i\omega_n a_{2,n}^{(o)} \tag{7-49}$$

The characteristically geostrophic solutions have $\lambda^{o} = 0$, $a_{1,n}^{(o)} = 0$, $a_{2,n}^{(o)} = 0$, $g_n^{(o)}$ arbitrary for all n. The characteristically ageostrophic solutions have, for each n, $\lambda^{(o)} = i\omega_n$, $a_{1,n}^{(o)}$ arbitrary, and all other modes zero to lowest order, or $\lambda^{(o)} = -i\omega_n$, $a_{2,n}^{(o)}$ arbitrary, and all other modes zero to lowest order. The characteristically ageostrophic solutions are inertial-gravitational waves to lowest order.

7.4.1 Characteristically geostrophic solutions

The first and second order characteristically geostrophic problem can be combined to yield an eigenvalue problem for λ' as done earlier in (7-31) and (7-32). The system of equations is given by

$$\lambda' g_n' = b'^{*}\left[C_{6,n}' g_{n+1}' - \varepsilon 2\omega_{n+1}^{-1}\ \mathrm{Im}(C_{8,n+1}' C_{7,n}^{*}) b'^{*} g_{n+2}'\right]$$

$$- \varepsilon\left[\omega_{n+1}^{-1}\mathrm{Im}(C_{8,n+1}' C_{7,n}^{*}) + \omega_{n-1}^{-1}\mathrm{Im}(C_{8,n-1}' C_{7,n}'^{*})\right] g_n'$$

$$+ b'\left[C_{6,n}' g_{n-1}' - \varepsilon 2\omega_{n-1}^{-1}\ \mathrm{Im}(C_{8,n-1}' C_{7,n}'^{*}) b' g_{n-2}'\right] \qquad (7\text{-}50)$$

where the prime notation is as in (7-31) and (7-32) and

$$b' = \bar{b}_{\underset{\sim}{K}} / |\bar{b}_{\underset{\sim}{K}}| \qquad (7\text{-}51)$$

Ageostrophic effects are included through this order and produce an effect that depends on ε. The ageostrophic terms are given through first order by (7-21) and (7-22) and second order by (7-33) and (7-34), but with b's and g's exchanged, and C_7^* replacing C_3.

With ε set explicitly equal to zero in (7-50), yielding a linearized form of the quasi-geostrophic equations, numerical results indicate only neutral propagating solutions exist. This result agrees with that of Lin (1979) who showed that on a β-plane, with $|\bar{g}_{\underset{\sim}{K}}|/|\bar{b}_{\underset{\sim}{K}}| \ll 1$, the instability is characteristically barotropic. With ageostrophic effects included however, unstable propagating solutions are obtained, as determined from numerical solutions. The wave frequencies (i.e. $I_m\lambda$) are asymptotic to those obtained with the quasi-geostrophic system as $\varepsilon \to 0$. The growth rates are proportional to ε^2 for $\varepsilon \ll 1$ (the numerical solutions indicated that $\varepsilon < 1/2$ is sufficient for this ε behavior to be a good description). Convergence of these solutions as $\mathcal{N}$ increases is slow. An example of solutions for $K^2 = 36$, $K \cdot L = 6$, $K \times L = -12$, and $\varepsilon = 10^{-3/2}$, as a function of $\mathcal{N}$, appear in Fig. 7.2. Most of the solutions appear to converge at a uniform rate as $\mathcal{N}$ increases. Physically, this instability is similar to that described at the end of section 7.2.2.

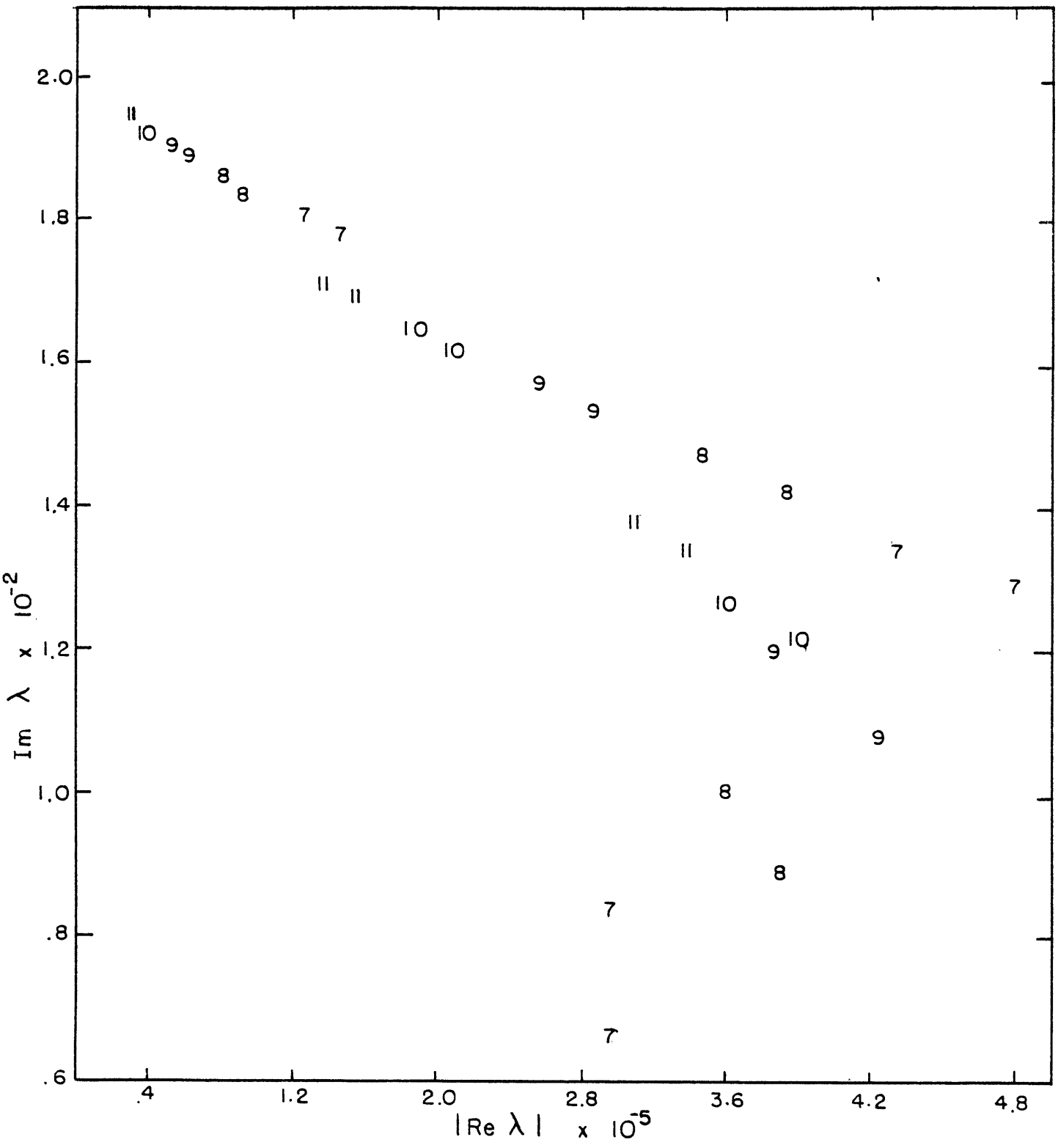
2.0
1.8
1.6
1.4
1.2
1.0
.8
.6
Im λ x 10^-2
.4
1.2
2.0
2.8
3.6
4.2
4.8
|Re λ| x 10^-5
11
10
9
9
8
8
7
7
11
11
10
10
9
9
8
8
11
11
7
7
10
9
10
9
8
8
7
7

Figure 7.2

7.4.2 Characteristically ageostrophic solutions

Characteristically ageostrophic solutions of the form (7-35) are examined for $\varepsilon << 1$. We set $\lambda^{(o)} = i\omega_n$, $a_{1,n}^{(o)} = a$, and all other modes zero to lowest order. The first order solution is

$$\lambda^{(1)} = 0 \tag{7-54}$$

$$a_{1,n+1}^{(1)} = i(\omega_{n+1} - \omega_n)^{-1} C'_{10,n+1}\, a \tag{7-55}$$

$$a_{1,n-1}^{(1)} = i(\omega_{n-1} - \omega_n)^{-1} C_{10,n-1}\, a \tag{7-56}$$

$$a_{2,n+1}^{(1)} = -i(\omega_{n+1} + \omega_n)^{-1} C'^{*}_{9,n+1}\, a \tag{7-57}$$

$$a_{2,n-1}^{(1)} = -i(\omega_{n-1} + \omega_n)^{-1} C^{*}_{9,n-1}\, a \tag{7-58}$$

$$g_{n+1}^{(1)} = -i\omega_n^{-1} C'^{*}_{7,n+1}\, a \tag{7-59}$$

$$g_{n-1}^{(1)} = i\omega_n^{-1} C^{*}_{7,n-1}\, a \tag{7-60}$$

with all other order-one variables zero.

We omit writing out the higher order solutions except for the values of $\lambda^{(p)}$.

$$\lambda^{(2)} = i\Big[\omega_n^{-1}(C'^{*}_{7,n+1}C_{8,n} + C^{*}_{7,n-1}C'_{8,n}) + (\omega_n - \omega_{n+1})^{-1}C'^{*}_{9,n+1}C_{9,n}$$

$$+ (\omega_n - \omega_{n-1})^{-1}C^{*}_{9,n-1}C'_{9,n} + (\omega_n + \omega_{n+1})^{-1}C'_{10,n+1}C_{10,n}$$

$$+ (\omega_n + \omega_{n-1})^{-1}C_{10,n-1}C'_{10,n}\Big] \tag{7-61}$$

It is not hard to show that the second order growth rate is identically zero.

$$\text{Re } \lambda^{(2)} = 0 \tag{7-62}$$

It is easy to discern that all even order pertubations of all scales $\underset{\sim}{L}_{n\pm1}$, with i even, are zero. From that it readily follows that

$$\lambda^{(2m-1)} = 0 \qquad m = 1,2,3,... \tag{7-63}$$

It is possible to obtain an expression for $\lambda^{(4)}$, yet it is given by a sum of 132 terms, each containing a product of four interaction coefficients. Numerical results indicate that Re $\lambda^{(4)} \neq 0$ is usually the case. Also they indicate that replacing $\underset{\sim}{L}_o$ by $-\underset{\sim}{L}_o$ changes the sign of Re $\lambda^{(4)}$.

If the system (7-44), (7-45), (7-46) in truncated (i.e. $\mathcal{N}$ finite) then the characteristically ageostrophic solutions having lowest order modes of scales $\underset{\sim}{L}_{\mathcal{N}}$ and $\underset{\sim}{L}_{-\mathcal{N}}$ will not have $\lambda^{(2)}$ given by (7-61) since the

$\underset{\sim}{L}_{N+1}$ or $\underset{\sim}{L}_{-N-1}$ modes will be missing. In this case there are instead solutions

$$\text{Re } \lambda^{(2)} = -(\underset{\sim}{K} \times \underset{\sim}{L}) K^{-2} \omega_L^{-2} \tag{7-64}$$

for either $\underset{\sim}{L}_N$ or $\underset{\sim}{L}_{-N}$. Limited spatial resolution in a model will therefore result in increased instability of barotropic modes with respect to ageostrophic distrubances. In particular, this is the case for the very-low-order model at all scales.

Fortunately, this enhancement of instability is not critical in our numerical model. The most unstable characteristically geostrophic solutions have growth rates an order ε larger than those characteristically ageostrophic solutions whose growth rates are in error. Baroclinic geostrophic modes in any case may be unstable with respect to inertial gravitational waves, with a second-order growth rate. This enhancement should have little if any effect on the energy partitioning if atmospheric-like values of ε are considered.

7.5 Resonant Inertial-Gravitational Wave Interactions

There is one particular barotropic stability problem we would like to examine in more detail. If $K^2 = -2\underset{\sim}{K} \cdot \underset{\sim o}{L}$, then $L_o^2 = L_1^2$, and $\omega_o = \omega_1$. There is therefore a solution for small ε which has $\lambda^{(o)} = i\omega_o$,

both $a_{1\underset{\sim}{L}_o}^{(o)}$ and $a_{1\underset{\sim}{L}_1}^{(o)}$ arbitrary, and other modes zero to lowest order. This is also the lowest order solution when L_o^2 and L_1^2 differ by a small amount so that $\omega_o = \omega_1 + 0(\varepsilon)$. We shall therefore continue to distinguish between ω_o and ω_1.

The first order eigenvalue problem in this case is

$$\lambda^{(1)} a_{1\underset{\sim}{L}_o}^{(o)} = b'^{*} C_{10}(\underset{\sim}{L}_o, \underset{\sim}{K}, -\underset{\sim}{L}_1) a_{1\underset{\sim}{L}_1}^{(o)} \tag{7-65}$$

$$\lambda^{(1)} a_{1\underset{\sim}{L}_1}^{(o)} = b' C_{10}(-\underset{\sim}{L}_1, \underset{\sim}{K}, \underset{\sim}{L}_o) a_{1\underset{\sim}{L}_o}^{(o)} \tag{7-66}$$

This interaction among $a_{1\underset{\sim}{L}_o}$, $a_{1\underset{\sim}{L}_1}$, and $\bar{b}_{\underset{\sim}{K}}$ is called a (near) resonant triad interaction. The natural frequency of $\bar{b}_{\underset{\sim}{K}}$ (i.e. the associated eigenvalue in the linear analysis of Section 2.2) is zero while those of the other two modes are similar. The relationship between resonance and the energy partitioning is explored further in Chapter 8. If the interactions described by (7-65) and (7-66) are written in the form of (6-3) by applying (6-4) (in order to obtain $a_{1\underset{\sim}{L}_1} = a^{*}_{2-\underset{\sim}{L}_1}$), then the resonant triad conditions appear in the more usual form

$$\underset{\sim}{K} + \underset{\sim}{L} + \underset{\sim}{M} = 0 \tag{7-67}$$

$$\omega(b_{\underset{\sim}{K}}) + \omega(a_{1\underset{\sim}{L}_o}) + \omega(a_{2\underset{\sim}{L}_o}) = 0 \tag{7-68}$$

where $\omega(b_{\underset{\sim}{K}})$ refers to the natural frequency of the mode $b_{\underset{\sim}{K}}$, etc.

The solution for $\lambda^{(1)}$ is

$$\lambda^{(1)} = \pm \left[C_{10}(\underset{\sim}{L}_o, \underset{\sim}{K}, -\underset{\sim}{L}_1) C_{10}(-\underset{\sim}{L}_1, \underset{\sim}{K}, \underset{\sim}{L}_o) \right]^{1/2} \tag{7-69}$$

Substitution for C_{10} using (6-16) yields a complicated expression of the form

$$\lambda^{(1)} = \pm \left[-S^2 + O(\varepsilon) \right] \tag{7-70}$$

where S is real and the $O(\varepsilon)$ terms may be complex. Thus, for $\varepsilon << 1$, $\lambda^{(1)}$ is imaginary indicating that resonant interactions are stable through first order in ε.

Duffy (1974) investigated the stability of a Rossby wave on an f-plane with respect to resonantly interacting pairs of ageostrophic pertubations using a shallow-water model. He used the method of multiple time scales (c.f. Bender and Orszag, 1978) rather than the modal analysis employed here. He obtains unstable solutions to his order-ε problem, and suggests that such a response should therefore be observable.

Further analysis of our problem (7-65), (7-66), indicates that his problem should have as its solution an expression like (7-70). Applying a multiple time scale argument to our problem does not alter our result. Examination of his analysis indicates that his interaction coefficient C_{pq} is determined incorrectly. This can be readily

discovered by substituting his (5.1) and (5.2) into the right-hand side of his (5.3) and observing that C_{pq} must in general be complex although his expression is real. A correct determination of C_{pq} yields a result similar to ours.

Chapter 8: Ordering Analysis 2

In Chapter 3, the terms of the inviscid equations for ζ , δ , θ, etc were ordered in terms of ε . For a given $\varepsilon << 1$, two time scales were shown to be possible, each with characteristically different solutions. This complicated the ordering analysis, since for each equation multiple time scales needed consideration. In Chapter 5 the importance of dissipation in partitioning the energy was demonstrated using a numerical model. It has thus been made clear that both dissipation and multiple time scales need to be explicitly considered in any answer to the questions posed in Chapter 1.

In this chapter two ordering parameters, ε and ν are considered. The modal equations derived in Chapter 6 are analyzed rather than the equations discussed in Chapter 3 because multiple time scales are more easily considered using the former. The time scale of the largest variations of the geostrophic modes is clearly the advective time scale (as long as the ageostrophic modes do not dominate the geostrophic modes). The inertial time scale only enters the lowest order problem in the prognostic equations for the ageostrophic modes.

8.1 Re-scaling with the Dissipative Time Scale

Equations 6-1, 6-2, and 6-3 with forcing and dissipation can be written as

$$\frac{db}{dt} = \sum \left(C_1 bb + C_2 gg + C_3 ga + C_{4,5} aa \right) + \nu \left(e_{11} b + e_{12} g + e_{13} a \right) \quad (8\text{-}1)$$

$$\frac{dg}{dt} = \sum \left(C_6 bg + C_7 ba \right) + \nu \left(e_{21} b + e_{22} g + e_{23} a \right) + \nu G \quad (8\text{-}2)$$

$$\frac{da}{dt} = i\omega a + \sum \left(C_8 bg + C_{9,10} ba \right) + \nu \left(e_{31} b + e_{32} g + e_{33} a \right) + \nu G_a \quad (8\text{-}3)$$

where subscripted notation of the scale dependence has been omitted. The $\nu\ e_{ij}$ are the elements of the matrix F in Section 6.2. ν G and $\nu\ G_a$ are the external forcing functions acting on the geostrophic and ageostrophic modes respectively. G_a shall subsequently be ignored since its effect is small at large scales as long as the time scale of the forcing is long compared with the inertial time scale (Section 6.3 and Blumen, 1972). By considering only one scale forced, almost all the $a_{\underset{\sim}{K}}$ and $g_{\underset{\sim}{K}}$ equations have zero external forcing. Yet there is a result we wish to obtain by considering G.

The viscosity coefficient can be removed from the geostrophic equations by re-scaling. We denote $g'=g/\nu$, $b'=b/\nu$, $a'=a/\nu$, $G'=G/\nu$, and $t'=t\nu$. In effect, the time scale f^{-1} used to non-dimensionalize the equations is now replaced by the (dimensional) dissipative time scale $\nu_v^{-1} (\Delta p)^2$. The re-scaled equations are like (8-1) through (8-3) with primed quantities replacing the corresponding unprimed quantities, and ν removed except for a replacement of ω by ω/ν in (8-3).

The rescaled quasi-geostrophic system

$$\frac{db'}{dt} = \sum (C_1 b'b' + C_2 g'g') + e_{11} b' + e_{12} g' \qquad (8\text{-}4)$$

$$\frac{dg'}{dt} = \sum C_6 b'g' + e_{21} b' + e_{22} g' + G' \qquad (8\text{-}5)$$

is completely determined by G', the matrix F, and the initial conditions for b', g'. The effect of varying ν with fixed G', F, and initial conditions b', g' is simply determined by inserting factors of ν into the solution to (8-4), (8-5). However, a second time scale 0(1) enters if non-quasi-geostrophic effects are included, and the factor ν is then not removed by simple scaling. With G', F, and initial conditions b', g', a' fixed, any ν - dependence of b'(t') and g'(t') is a result of non-quasi-geostrophic effects described by terms with coefficients C_4, C_5, and C_7.

The above discussion applies to the very-low-order model as well. Therefore, in Experiments 6a through 6g we investigate solutions with $T_0 = 52.4\ \nu/\nu_o$, $\nu_H = k_H = \nu_{Ho}\ \nu/\nu_o$ $\tau_{rad} =$ and ν varying. The initial conditions b', g', a' are fixed. These experiments are described in Table 8.1.

Time-mean statistics of AE, QE, BE, ΘE, and VE appear as a function of ν in Figure 8.1. If only (8-4) and (8-5) were considered, with the parameters set as described, $\overline{\Theta E}$ and $\overline{BE}$ would both be proportional to ν^2. Because of ageostrophic effects, however, only $\overline{\Theta E}$

TABLE 8.1 Description of Experiments 6a - 6g

Input non-dimensional. E through QE in J kg^{-1}. VE in f^2.
All results time-mean quantities.

No.	6a	6b	6c	6d	6e	6f	6g
r							
	1.04	.52	.26	.155	.13	.065	.0325
ν	.5	1.	2.	3.38	4.	8.	16.
ν_{Ho}/k_H	.5	1.	2.	3.38	4.	8.	16.
$d)^{-1}$	.5	1.	2.	3.38	4.	8.	16.
	50.	50.	50.	50.	50.	50.	50.
TS							
	44700.	9740.	2450.	861.	580.	175.	57.8
	9350.	2900.	823.	347.	206.	65.9	27.8
	2480.	510.	97.2	19.7	7.28	.28	.018
	35300.	6840.	1630.	514.	374.	109.	30.
	36000.	7109.	1730.	548.	397.	118.	32.2
	3820.	1620.	524.	273.	169.	56.7	25.6
	4810.	1020.	204.	40.	14.7	.61	.041
	10100.	1120.	184.	32.8	11.6	.215	.0006
	1.42	.408	.070	.015	.0066	.0022	.0009
	.13	.10	.069	.039	.014	.0025	.0005
	.17	.084	.048	.028	.00803	.00049	$4x10^{-6}$
	1.45	1.00	.95	.91	.89	.59	.13

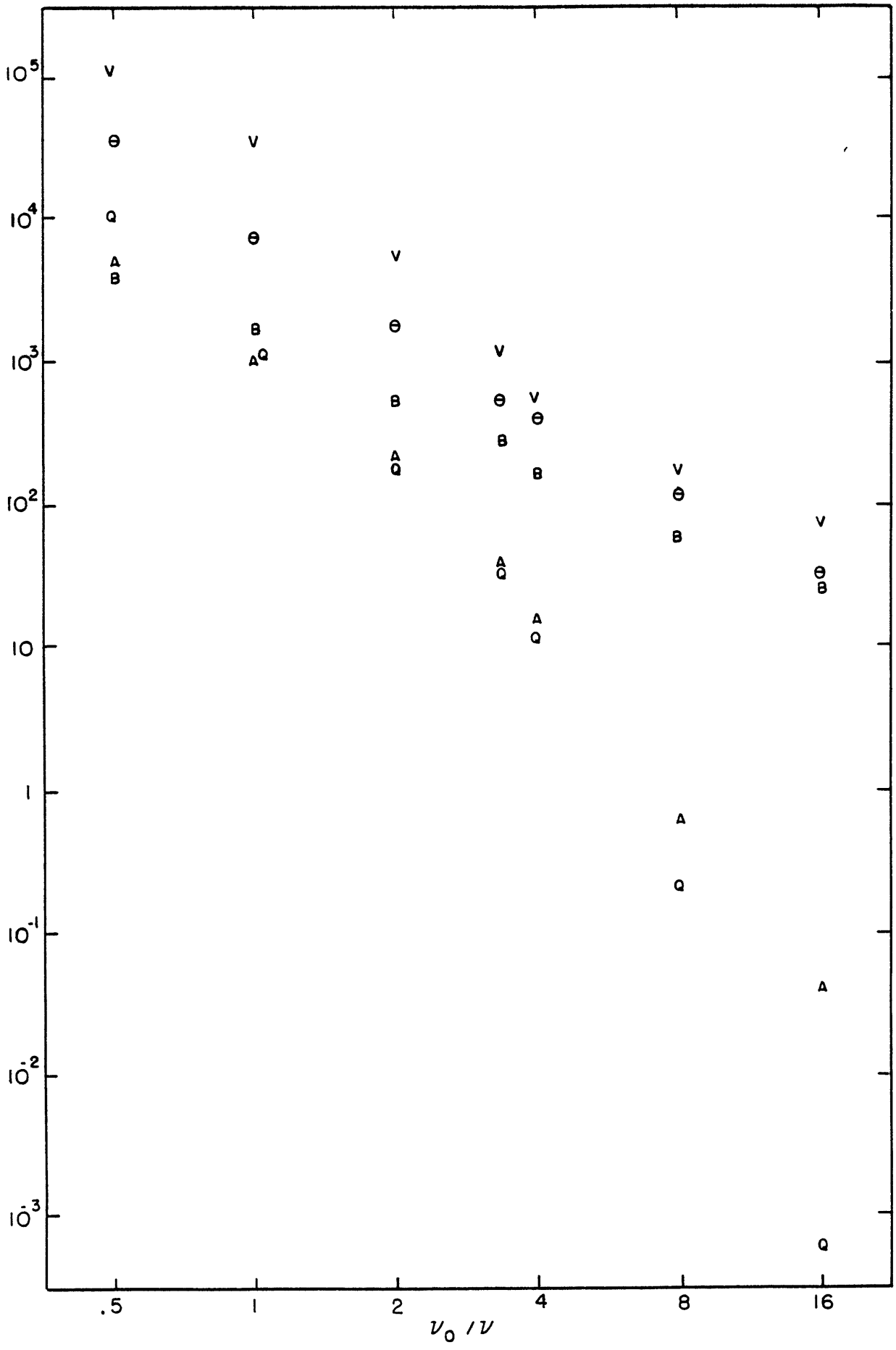

Figure 8.1

appears to behave in this manner. $\overline{BE}$ increases with ν more slowly than $\overline{\theta E}$.

If the fields are quasi-geostrophic, or very nearly so, then (6-25) applies and a is a quadratic function of b and g , so that $\overline{AE}$ is proportional to ν^4. This behavior is observed for $\nu \ll 1$. $\hat{\omega}$ is then very small, implying that the time scale for these ageostrophic modes is the advective rather than inertial time scale. Yet, as $\nu \to 1$, $\hat{\omega}$ rapidly approaches 1, and finally exceeds that value. The ageostrophic modes then describe high frequency waves.

The spectra $(\nu_o/\nu)^2\, \overline{\theta\mathcal{E}}_m$, $(\nu_o/\nu)^2\, \overline{B\mathcal{E}}_m$, and $(\nu_o/\nu)^2 \overline{A\mathcal{E}}_m$ are examined as functions of ν in Figures 8.2, 8.3, and 8.4 respectively. The factor $(\nu_o/\nu)^2$ is used as a normalizing factor because, in the absence of ageostrophic effects, such normalized spectra for the geostrophic modes would be independent of ν . The observed differences in spectra are thus a result of ageostrophic effects. There appear to be two kinds of small scale behaviors, one for large ν dynamics, and one for quasi-geostrophic dynamics. At larger scales $\overline{B\mathcal{E}}_m$ is more sensitive to ageostrophic effects than $\overline{\theta\mathcal{E}}_m$ is. This may be simply because $\overline{B\mathcal{E}}_m$ is smaller than $\overline{\theta\mathcal{E}}_m$ at those scales. Under nearly quasi-geostrophic conditions, the lowest order effect of the ageostrophic modes on the geostrophic modes is simply to exchange energy between $b_{\underset{\sim}{K}}$ and $g_{\underset{\sim}{K}}$. This effect on $B\mathcal{E}_{\underset{\sim}{K}}$ is given by

$$\frac{d}{dt} B\mathcal{E}_{\underset{\sim}{K}} = -\frac{1}{2} K^{-2} \sum_{\underset{\sim}{L},\underset{\sim}{M}} g^*_{\underset{\sim}{L}}\, b^*_{\underset{\sim}{K}}\, b_{\underset{\sim}{M}}\, g_{\underset{\sim}{L}+\underset{\sim}{K}-\underset{\sim}{M}}$$

$$\mathrm{Im}\left(\omega^{-1}_{-K-L}\, C_3\left(\underset{\sim}{K},\underset{\sim}{L},-\underset{\sim}{K}-\underset{\sim}{L}\right) C_8\left(-\underset{\sim}{K}-\underset{\sim}{L},\underset{\sim}{M},\underset{\sim}{L}+\underset{\sim}{K}-\underset{\sim}{M}\right)\right) \quad (8\text{-}6)$$

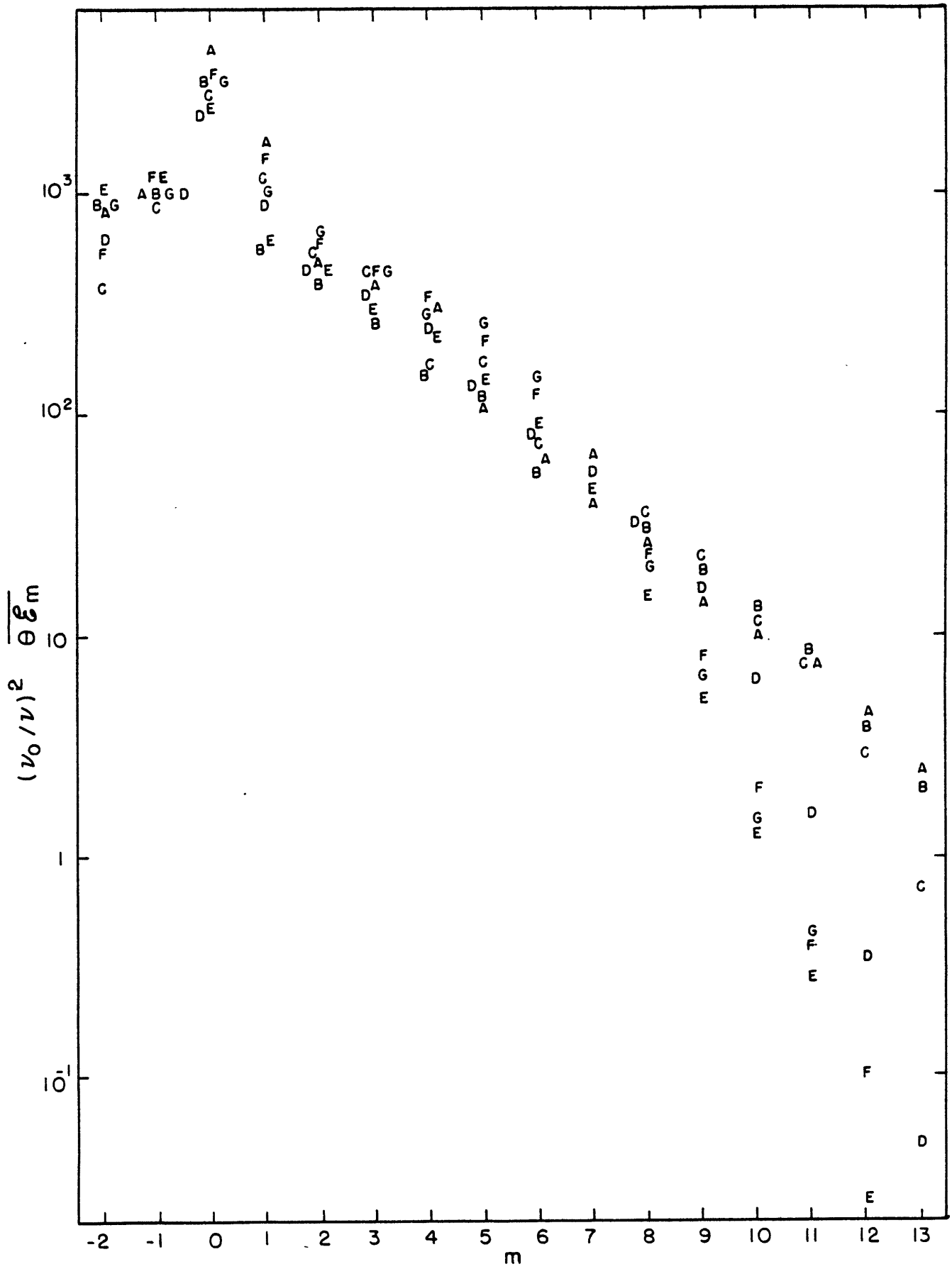
$(\nu_0/\nu)^2 \frac{\partial \mathcal{E}_m}{\partial \theta}$
10^3
10^2
10
1
10^{-1}
-2 -1 0 1 2 3 4 5 6 7 8 9 10 11 12 13
m

Figure 8.2

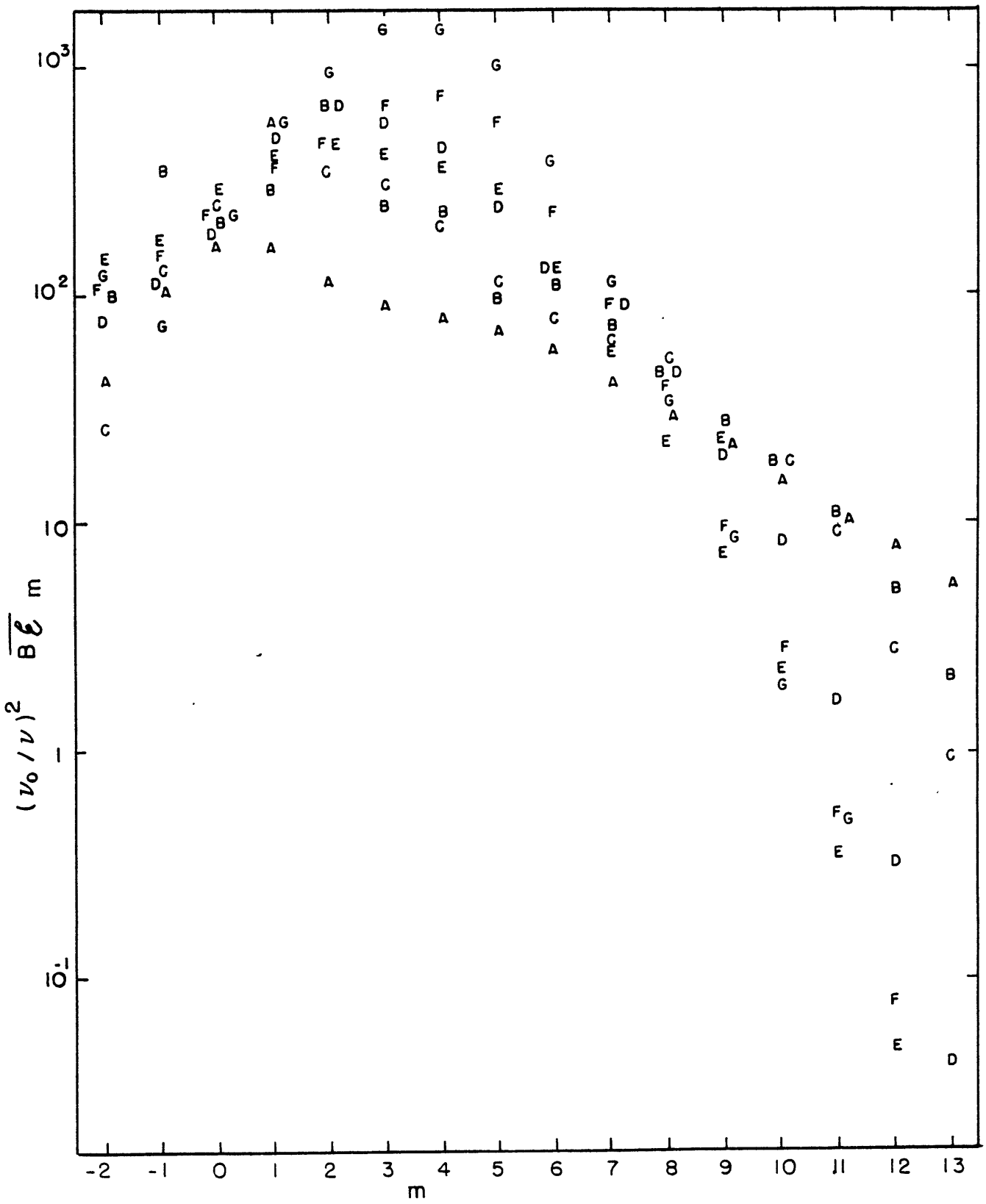
10^3
10^2
10
1
10^{-1}
$(\nu_0/\nu)^2$ $\overline{B\mathcal{E}}$ m
-2 -1 0 1 2 3 4 5 6 7 8 9 10 11 12 13
m

Figure 8.3

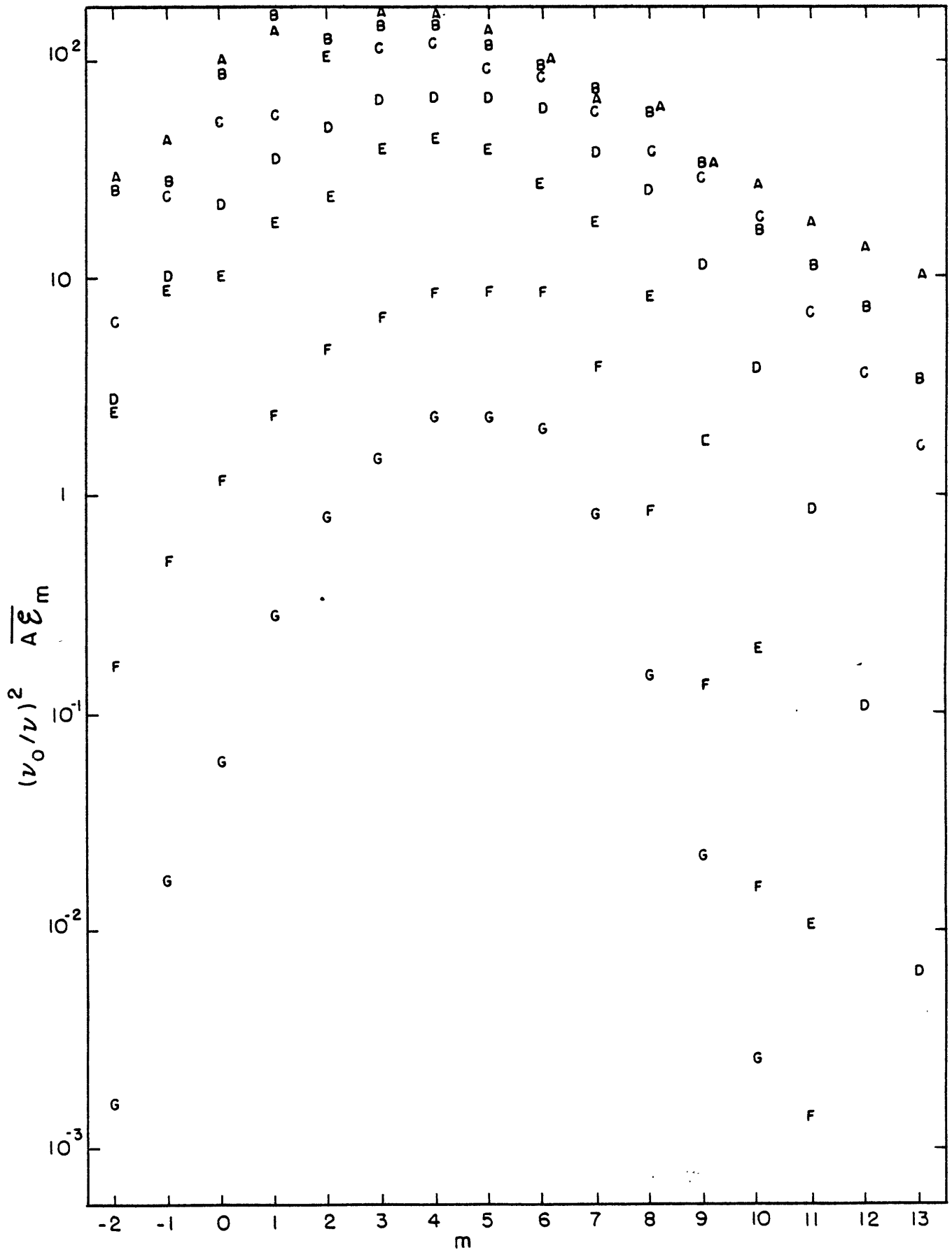
10^2
10
1
10^{-1}
10^{-2}
10^{-3}
$(\nu_0/\nu)^2 \overline{A\mathcal{E}}_m$
-2 -1 0 1 2 3 4 5 6 7 8 9 10 11 12 13
m

Figure 8.4

with the negative effect on $\theta\mathcal{E}_{\underset{\sim}{K}}$. This exchange is fourth order in the modal amplitudes, whereas the precisely quasi-geostrophic energy exchanges are third order. In the very-low-order model at least, this ageostrophic effect seems to have a significant effect on the geostrophic spectra, even when the order of the geostrophic modal amplitudes is very small as in Experiments 11 and 12.

For nearly quasi-geostrophic conditions, using (6-25) for $a_{1\underset{\sim}{K}}$,

$$A\mathcal{E}_{\underset{\sim}{K}} \approx 2K^{-2}\omega_{\underset{\sim}{K}}^{-4} \sum_{\underset{\sim}{L},\underset{\sim}{M}} b^*_{\underset{\sim}{L}} b_{\underset{\sim}{M}} g^*_{-\underset{\sim}{K}-\underset{\sim}{L}} g_{-\underset{\sim}{K}-\underset{\sim}{M}} C_s(\underset{\sim}{K},\underset{\sim}{L},-\underset{\sim}{K}-\underset{\sim}{L}) C_s^*(\underset{\sim}{K},\underset{\sim}{M},-\underset{\sim}{K}-\underset{\sim}{M}) \qquad (8\text{-}7)$$

If also the time-mean correlation $\overline{b^*_{\underset{\sim}{L}} b_{\underset{\sim}{M}} g^*_{-\underset{\sim}{K}-\underset{\sim}{L}} g_{-K-\underset{\sim}{M}}}$ can be approximated by $|b_{\underset{\sim}{L}}|^2 |g_{-\underset{\sim}{K}-\underset{\sim}{L}}|^2$ for $\underset{\sim}{L} = \underset{\sim}{M}$ and zero otherwise, then $\overline{A\mathcal{E}}_{\underset{\sim}{K}}$ can be approximated by

$$\overline{A\mathcal{E}}_{\underset{\sim}{K}} \approx \frac{16}{\sigma_1\alpha_2\omega_{\underset{\sim}{K}}^4 K^2} \sum_{\underset{\sim}{L}} L^2 \omega_{-\underset{\sim}{K}-\underset{\sim}{L}} / C_s(\underset{\sim}{K},\underset{\sim}{L},-\underset{\sim}{K}-\underset{\sim}{L})/^2 \overline{B\mathcal{E}}_{\underset{\sim}{L}} \overline{\theta\mathcal{E}}_{-\underset{\sim}{K}-\underset{\sim}{L}} \qquad (8\text{-}8)$$

The time-mean ageostrophic energy spectrum can thus be related directly to the time-mean geostrophic spectra under the described conditions. In the numerical model, the scale dependent factor appearing on the right-hand side of (8-8) increases rapidly with $|\underset{\sim}{K}|_m$ before approaching a constant value. Thus, in combination with the shape of the geostrophic energy spectra, $\overline{A\mathcal{E}}_m$ peaks at a scale slightly smaller than that at which $\overline{B\mathcal{E}}_m$ peaks in Experiments 10, 11, and 12.

8.2 Sample Power Spectra of Modes

As demonstrated in Chapter 3, the geostrophic modes have a time scale $0(\varepsilon)$ unless ageostrophic modes dominate (in which case the restricted scale analysis in Chapter 3 does not apply). Both inertial and advective time scales are possible for the ageostrophic modes to lowest order. As an illustration, some examples of power spectra for various modes and numerical solutions are presented. These are given by

$$B\hat{\mathcal{E}}_m(\hat{\omega}_j) = 2^{-m-3} \Big/ \sum_n \left(X_{1,m} + X_{2,m}\right)_{t_n} \exp(-i\hat{\omega}_j t_n) \Big/^2 \tag{8-9}$$

$$\Theta\hat{\mathcal{E}}_m(\hat{\omega}_j) = \frac{\alpha_2\sigma_2}{16}\omega_m^{-2} \Big/ \sum_n \left(X_{1,m} - X_{2,m} - 2T_m\sigma_2^{-1}\right)_{t_n} \exp(-i\hat{\omega}_j t_n) \Big/^2 \tag{8-10}$$

$$A\hat{\mathcal{E}}_m(\hat{\omega}_j) = 2^{-m-3}\omega_m^{-2} \Big/ \sum_n \left(X_{1,m} - X_{2,m} + \alpha_2 2^m T_m\right)_{t_n} \exp(-i\hat{\omega}_j t_n) \Big/^2 + 2^{m-1} \Big/ \sum_n \left(Y_m\right)_{t_n} \exp(-i\omega_j t_n) \Big/^2 \tag{8-11}$$

where a subscript t_n signifies a quantity evaluated at time

$$t_n = t_0 + n\,\Delta t \qquad n = 0, 1, \ldots, n_{max} \tag{8-12}$$

and

$$\hat{\omega}_j = \frac{2\pi}{\Delta t\, n_{max}}\, j \qquad j = 0, \ldots, n_{max} \tag{8-13}$$

Data is obtained from both Experiments 2 and 3 with $n_{max} = 512$, $\Delta t = 0.80\ f^{-1}$ and $0.66\ f^{-1}$ respectively, and t_o = day 200.

In Experiment 3, low frequency dominates $B\hat{\mathcal{E}}_m$ and $\theta\hat{\mathcal{E}}_m$. As m increases, the enstrophy of scale m increases, and the advective time scale becomes shorter as discussed in Chapter 5. This is observed qualitatively in Figure 8.5 which compares $B\hat{\mathcal{E}}_o$, $B\hat{\mathcal{E}}_4$, $\theta\hat{\mathcal{E}}_4$, and $B\hat{\mathcal{E}}_{11}$. For the smaller m, a greater portion of $B\overline{\mathcal{E}}_m$ is contributed by lower frequencies. There is small but measurable power in the inertial frequencies, too. This is presumably due to ageostrophic effects. $A\hat{\mathcal{E}}_4$ appears in Figure 8.6. It has a maximum at $\hat{\omega}_i \approx \omega_m$.

Approximate quasi-geostrophic power spectra are obtained from Experiment 2 data. $B\hat{\mathcal{E}}_4$ and $G\hat{\mathcal{E}}_4$ appear in Figure 8.7. Low frequencies again dominate. Significant power at the inertial frequency is absent. $A\hat{\mathcal{E}}_4$, and $D\hat{\mathcal{E}}_4$ defined by

$$D\hat{\mathcal{E}}_m(\hat{\omega}_j) = 2^{m-1} \Big/ \sum_n (Y_m)t_n \exp(-i\hat{\omega}_j t_n) \Big/^2 \qquad (8\text{-}14)$$

appear in Figure 8.8. The ageostrophic mode is dominated by low frequencies also. There is a small response at the inertial frequency $\hat{\omega}_i \approx \omega_m$. Note too that $D\hat{\mathcal{E}}_4$ is approximately one-half $A\hat{\mathcal{E}}_4$. This is to be expected if the phase of the ageostrophic mode has a uniform distribution in time.

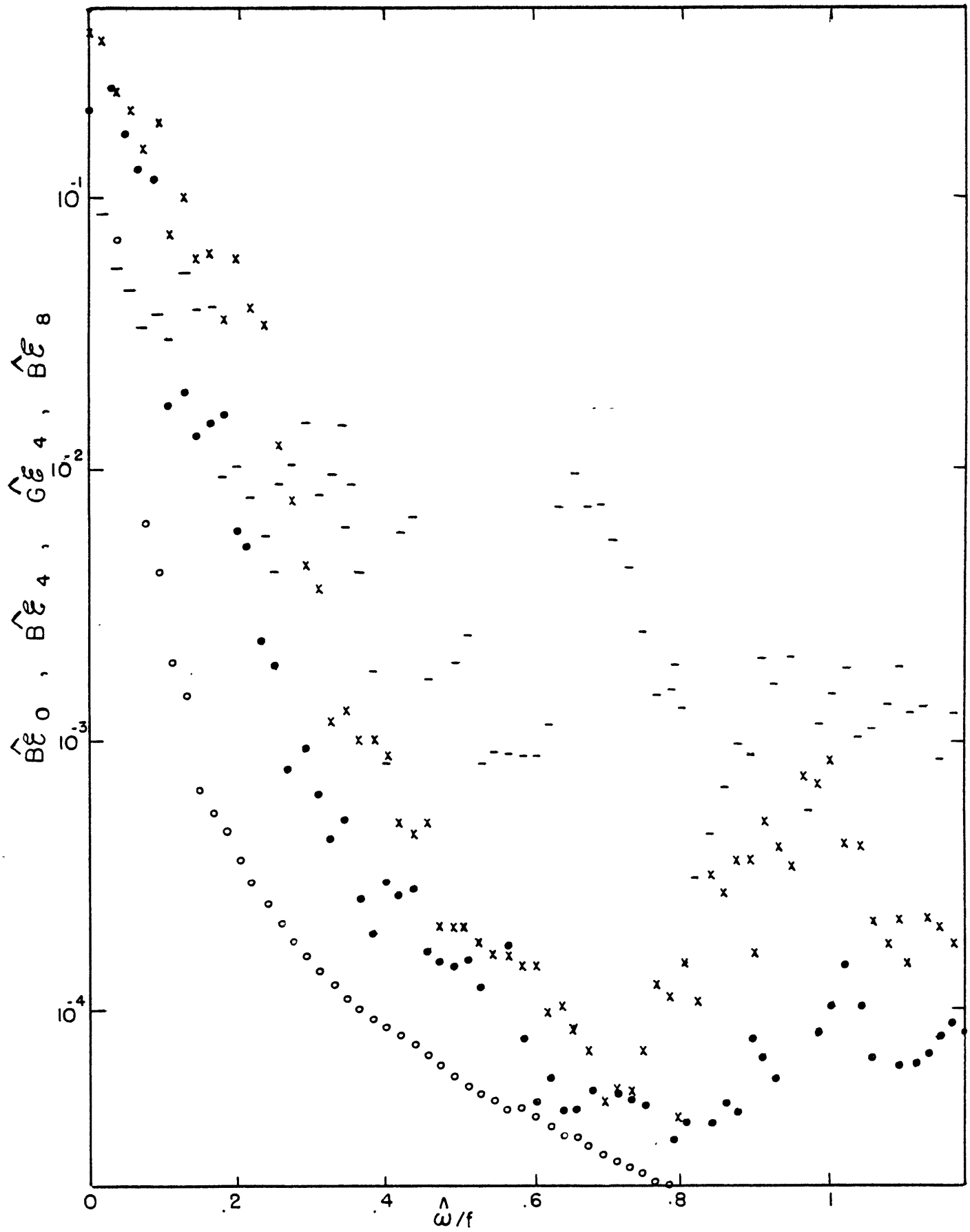
$\hat{B\varepsilon}_0$, $\hat{B\varepsilon}_4$, $\hat{G\varepsilon}_4$, $\hat{B\varepsilon}_8$
10^{-1}
10^{-2}
10^{-3}
10^{-4}
0
.2
.4
.6
.8
1
$\hat{\omega}/f$

Figure 8.5

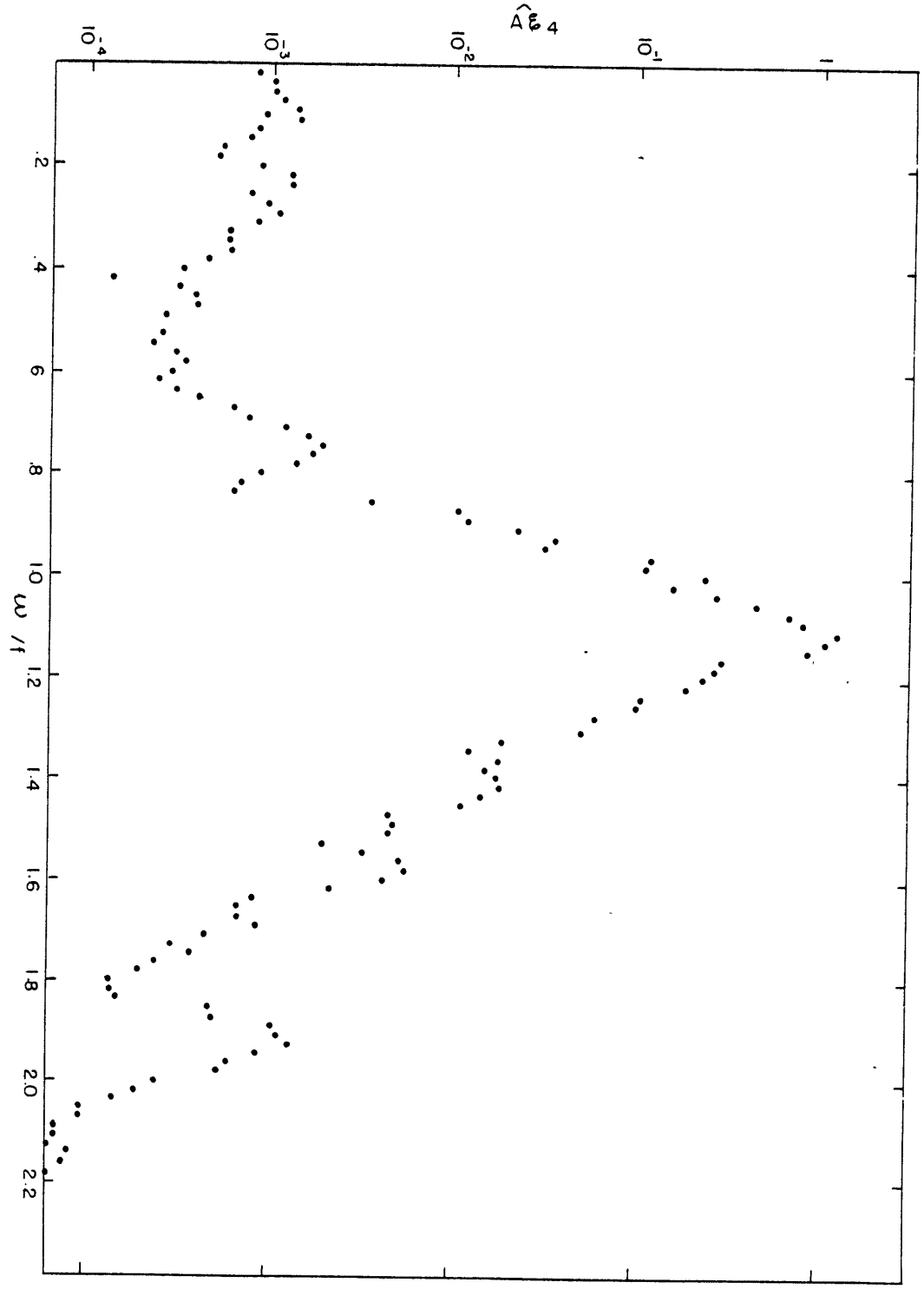

Figure 8.6

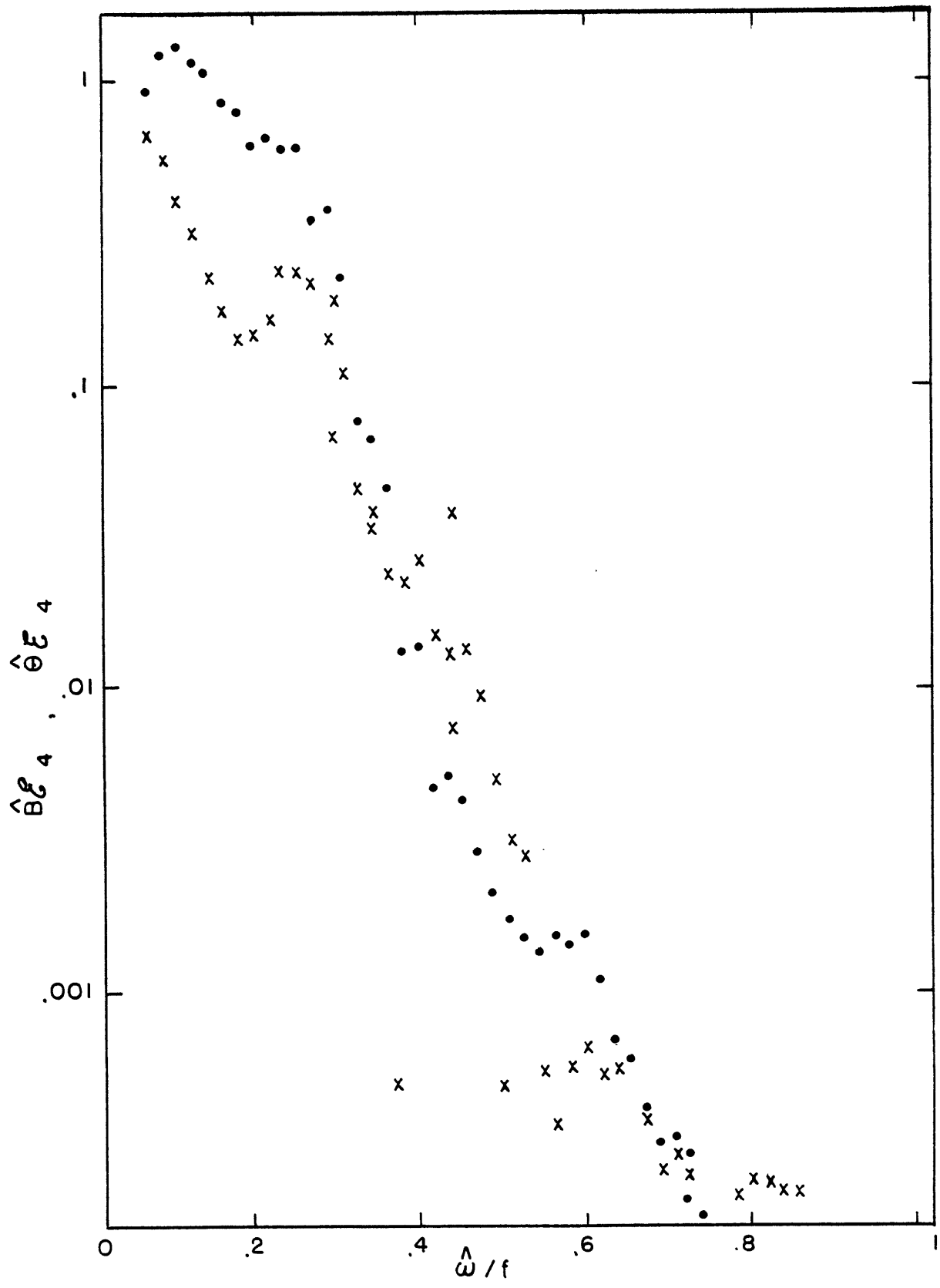
1
.1
.01
.001
0
.2
.4
.6
.8
1
$\hat{\omega}$ / f
$\hat{B}\hat{\ell}_4 \cdot \hat{\Theta}\hat{\ell}_4$

Figure 8.7

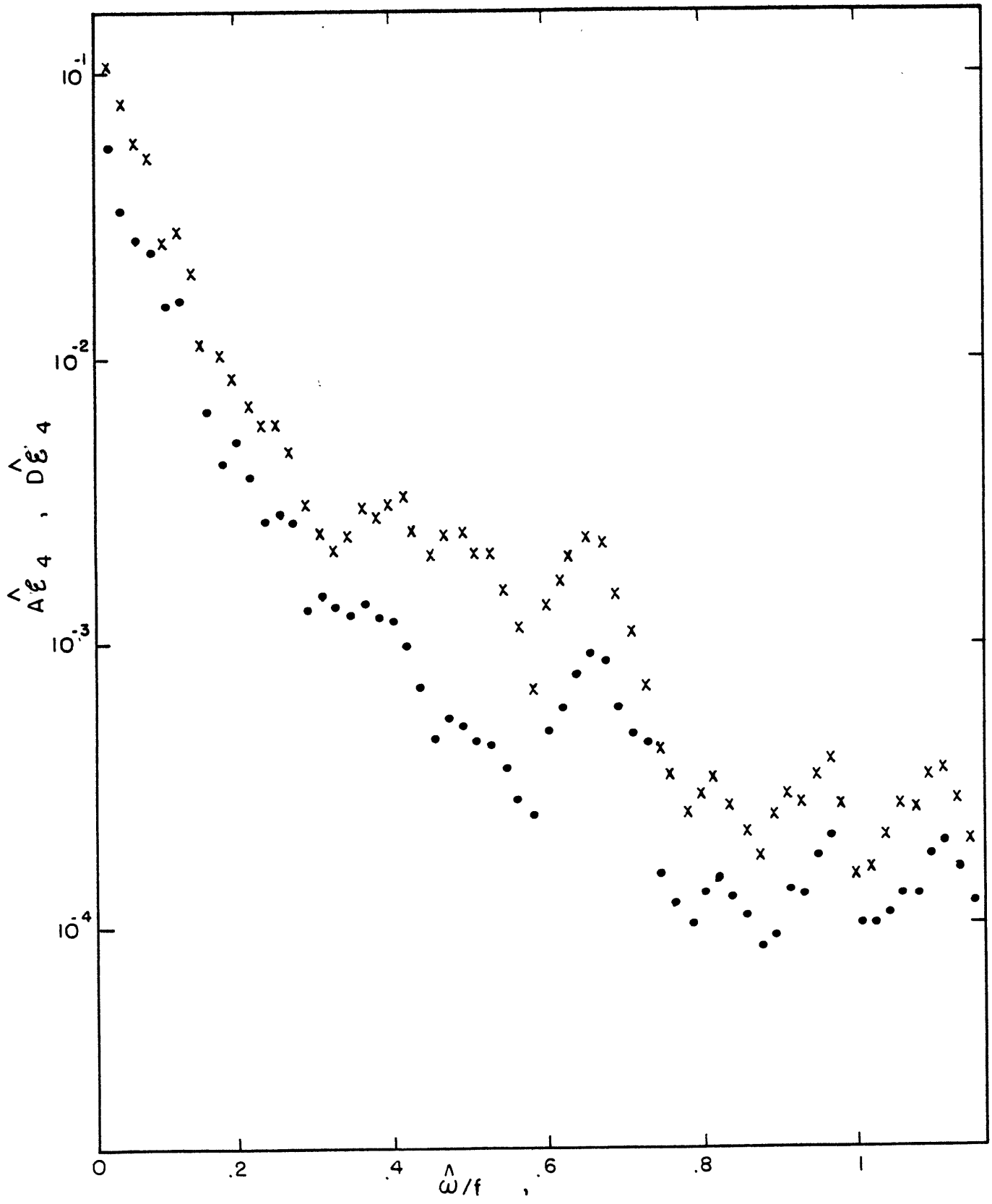
10^{-1}
10^{-2}
10^{-3}
10^{-4}
$\hat{A}\hat{\varepsilon}_4$, $\hat{D}\hat{\varepsilon}_4$
0
.2
.4
.6
.8
1
$\hat{\omega}/f$,

Figure 8.8

8.3 Multiple Time Scale Analysis

Some aspects of the power spectra of the modes and their energy exchanges become apparent if (8-1), (8-2), and (8-3) are considered in the general form

$$\frac{d}{dt}\gamma_i = (i\omega_i - \nu_i)\gamma_i + f_i(t) \tag{8-15}$$

γ_i is any particular mode. $f_i(t)$ represents all terms not linear in γ_i, and $f_i(t)$, ω_i, and ν_i depend on which mode and scale γ_i represents. In particular, $\omega_i = 0$ for a geostrophic mode, and $\omega_i = \omega_K$ for an ageostrophic mode $a_{1\underset{\sim}{K}}$. $f_i(t)$ is in general unknown. Yet knowing something of its power spectrum yields information regarding the power spectrum of $\gamma_i(t)$.

Equation (8-15) is the same as that for a forced damped linear harmonic oscillator with velocity γ_i. Denote the Fourier transform of any function $s(t)$ as $\hat{s}(\hat{\omega})$; i.e.

$$\hat{s}(\hat{\omega}) = \int_0^\infty s(t)\, e^{-i\hat{\omega}t}\, dt \tag{8-16}$$

A particular solution to (8-15) can then be described simply by

$$\hat{\gamma}_i(\hat{\omega}) = \left[\nu_i + i(\hat{\omega} - \omega_i)\right]^{-1} \hat{f}_i(\hat{\omega}) \tag{8-17}$$

The power spectra of $f_i(t)$ and $\gamma_i(t)$ are thus simply related. The general solution to (8-15) also contains initial-condition dependent transient terms whose moduli decrease exponentially in time. These latter terms can be ignored after a sufficient time. The statistics of the solution represented by (8-17) are thus those that determine the time-mean statistics of γ_i.

The inverse transform for $\hat{s}(\hat{\omega})$ can be written in a form which isolates a time scale ω_i, e.g.

$$s(t) = \int_{|\hat{\omega}-\omega_i| \leq \varepsilon_1} \hat{s}(\hat{\omega})\, e^{i\hat{\omega}t} d\hat{\omega} + \int_{|\hat{\omega}-\omega_i| \geq \varepsilon_1} \hat{s}(\hat{\omega})\, e^{i\hat{\omega}t} d\hat{\omega} \tag{8-18}$$

ε_1 is some ordering parameter such that $\varepsilon << \varepsilon_1 << 1$. Denote the first integral in (8-18) as $s^{(1)}$ and the second as $s^{(2)}$. Then the relation between order and time scale can be described explicitly. For example, $0(\gamma_i^{(1)}) >> 0(\gamma_i^{(2)})$ implies that, to lowest order, mode γ_i has a time scale on the order of its natural frequency as illustrated in Figures 8.5 and 8.6. For the behavior illustrated in Figure 8.8, on the other hand, $0(\gamma_i^{(1)}) << 0(\gamma_i^{(2)})$ since the power is relatively very small at the frequency ω_m.

Substitution of (8-17) into (8-16) yields

$$\gamma_i(t) = \int_{|\hat{\omega}-\omega| \leq \varepsilon_1} \frac{\hat{f}(\hat{\omega})\, e^{i\hat{\omega}t}}{\nu_i + i(\hat{\omega}-\omega_i)} d\hat{\omega} + \int_{|\hat{\omega}-\omega| \geq \varepsilon_1} \frac{\hat{f}(\hat{\omega})\, e^{i\hat{\omega}t}}{\nu_i + i(\hat{\omega}-\omega_i)} d\hat{\omega} \tag{8-19}$$

If $O(\nu) \lesssim \varepsilon$, then the ordering for $f(t)$ is like that described for the nonlinear terms in Chapter 3. Therefore the lowest order of $f^{(1)}$ and $f^{(2)}$ is ε^2. The following inequalities can be established:

$$O(\nu^{-1})\, o(f^{(1)}) \gtrsim o(\gamma^{(1)}) \gg o(f^{(1)}) \tag{8-20}$$

$$o(\gamma^{(2)}) \ll \varepsilon \tag{8-21}$$

Thus only $\gamma^{(1)}$ may be order ε. This describes the phenomenon of resonance, by which the response amplitude may be much greater than that of the forcing only if the forcing frequency occurs near a natural frequency.

If $O(\nu) \sim \varepsilon$, then demonstrating that $O(f_i^{(1)}) \ll \varepsilon^2$ ($f^{(1)}$ defined as for $\zeta^{(1)}$) for some $\gamma_i \equiv a_{1\underset{\sim}{K}}$ is sufficient to claim that $O(a_{1\underset{\sim}{K}}) \ll \varepsilon$. We will investigate the ordering of $f_i^{(1)}$ by assuming an order for the γ_j ($j \neq i$). Specifically, we first assume that both geostrophic and ageostrophic modes are order $\varepsilon \ll 1$. Thus $\gamma_j \sim \gamma_j^{(1)} + O(\varepsilon^2)$ and all modes are characterized by their natural frequencies. Then we can demonstrate, but only by considering sources and sinks of energy, that order ε ageostrophic modes can not be maintained.

$f_i(t)$ is a sum of linear terms $\nu e_{ij}\gamma_j$ ($j \neq i$) and nonlinear terms of the form

$$f_{ijk}(t) = C_{ijk}\ \gamma_j^*(t)\ \gamma_k^*(t) \tag{8-22}$$

By our ordering assumptions as $\varepsilon \to 0$

$$f_{ijk}(t) = C_{ijk}\ \gamma_j^{(1)}(t)\ \gamma_k^{(1)}(t) + O(\varepsilon^3) \tag{8-23}$$

Thus, through order ε^2, $f_{ijk}(t)$ is dominated by frequencies which are nearly resonant with the natural frequencies ω_j and ω_k. Specifically, as $\varepsilon \to 0$

$$o\left\{\int \sum_{jk}^{} \hat{f}_{ijk}(\hat{\omega})\, e^{i\hat{\omega}t}\, d\hat{\omega}\right\} \lesssim \varepsilon^2 \tag{8-24}$$
$$|\hat{\omega} + \omega_j + \omega_k| \leq \varepsilon_1$$

but

$$o\left\{\int \sum_{jk} \hat{f}_{ijk}(\hat{\omega})\, e^{i\hat{\omega}t}\, d\hat{\omega}\right\} \ll \varepsilon^2 \tag{8-25}$$
$$|\hat{\omega} + \omega_j + \omega_k| \geq \varepsilon_1$$

If the resonant condition

$$/\omega_i + \omega_j + \omega_k / \lesssim \varepsilon_1 \tag{8-26}$$

does not hold, then the integration regions of $f^{(1)}$ and the integral in (8-24) do not overlap and therefore $0(f^{(1)}) << \varepsilon^2$.

It is clear that in the geostrophic equations, (8-26) is satisfied for all the interactions involving only geostrophic modes, for then $\omega_i = \omega_j = \omega_k = 0$. In the ageostrophic equation (6-3), the only possible near-resonant interaction having order ε^2 is that described by the $C_{10}(\underset{\sim}{K}, \underset{\sim}{L}, \underset{\sim}{M})\, b^*_{\underset{\sim}{L}}\, a^*_{2\underset{\sim}{M}}$ terms where $\omega_K - \omega_M \lesssim \varepsilon_1$ and therefore $/K^2 - M^2/ \lesssim \mu^2 \varepsilon_1$. We have thus established which nonlinear effect must be responsible for maintaining large amplitude ageostrophic modes. Since resonant interactions for the ageostrophic modes do exist, the question remains why such forcing does not maintain order ε ageostrophic amplitudes.

Why resonant interactions in the two-layer model are ineffective in maintaining ageostrophic modes is explained by considering energy transfer. Since $0(\nu) \sim \varepsilon$ by assumption, ageostrophic energy is dissipated at a rate of order ε. The nonlinear interaction among the modes $a_{1\underset{\sim}{K}}$, $a_{2\underset{\sim}{M}}$, and $b_{\underset{\sim}{L}}$ conserves energy according to (6-21). Thus this nonlinear interaction exchanges geostrophic and ageostrophic energies at the rate

$$\frac{d}{dt}\left(A\mathcal{E}_{\underset{\sim}{K}} + A\mathcal{E}_{\underset{\sim}{M}}\right) = -L^{-2}\,\mathrm{Re}\left(C_5\, b^*_{\underset{\sim}{L}}\, a^*_{1\underset{\sim}{K}}\, a^*_{2\underset{\sim}{M}}\right) = -\frac{d}{dt} B\mathcal{E}_{\underset{\sim}{L}} \tag{8-27}$$

By the resonance conditions we have established, ordering (6-11) indicates $0(C_5) \sim \varepsilon_1$, and by assumption $0(b_{\underset{\sim}{L}})\ 0(a_{1\underset{\sim}{K}})\ 0(a_{2\underset{\sim}{M}}) \leq \varepsilon^3$. Energy is a quadratic quantity and therefore order ε^2. This implies that the rate of energy exchange has least order $\varepsilon\varepsilon_1 << \varepsilon$, not large enough to counter the dissipation of ageostrophic energy by eddy viscosity. Thus if there is at any time ageostrophic energy of order ε^2, it will dissipate if $0(\nu) >> \varepsilon^2$.

The fact that $0(C_5) \sim \varepsilon_1$ for resonating ageostrophic modes is a result of the spatial symmetry necessary in order to have resonating scales. If $\omega_M \sim \omega_{\underset{\sim}{K}}$, then $|\underset{\sim}{K}| \sim |\underset{\sim}{M}|$ and the vectors $\underset{\sim}{K}$, $\underset{\sim}{M}$, and $\underset{\sim}{L}$ must form nearly an isosceles triangle. Thus the inertial-gravitational waves must by summetrically situated with respect to the quasi-stationary barotropic wave. This symmetry apparently results in an exchange of energy between waves rather than with the mean field.

The ordering arguments used here are valid only for small enough ε. The arguments do not determine at all what a sufficiently small value may be. Whether the atmospheric or model values of ε fall within this category is uncertain.

Chapter 9: Numerical Results 2

We do not expect to be able to understand quantitative details of the relationship between $\bar{R}$ and most other parameters. In particular, $\bar{R}$ is related to the shape of the geostrophic spectra in a complex way as discussed in Section 8.1. In any case, details of the very-low-order model are not to be suggestive of atmospheric behavior or even the behavior of the complete spectral form of our model. As discussed in Section 5.1 there is some statistical uncertainty in the numerical results we present. For these reasons we avoid describing any complicated quantitative behavior of the numerical solutions presented below.

9.1 Effects of Forcing and Dissipation

In the following set of experiments, the behavior of $\bar{R}$ as a function of ν and $\tilde{T}_o$ is explored. The values of ν are $\nu_o/4$, ν_o, and $4\nu_o$ in Experiments 7a-d, 8a-b, and 9a-d, respectively. $\tilde{T}_o$ is varied from .065 to 0.65. Other parameters are given by $\tau_{rad} = 33.$, $\nu_H = \nu_{Ho}\nu/\nu_o$, and $\mu^2 = 50$. Results are presented in Table 9.1.

Values of $\bar{E}(\nu, T_o)$ and $\overline{VE}(\nu, T_o)$ appear in Figures 9.1 and 9.2 respectively. The latter quantity is the time-mean enstrophy defined by (4-15). Data from Experiments 1, 2, and 6b appear also since they differ from 8a-b only in their values of $\tilde{T}_o$. $\bar{E}$ is relatively ν-independent and increases at a rate faster than $\tilde{T}_o$ (approximately $E \propto \tilde{T}_o^{1.5}$). $\overline{VE}$ increases with $\tilde{T}_o$ at an even faster rate (approximately

Table 9.1 Effects of Forcing and Dissipation

All imput is dimensionless. E through QE are in units of J kg^{-1}. VE is in units of f^2. All Results time-mean quantities.

Exp. No.	7a	7b	7c	7d	8a	8b	9a	9b	9c	9d
INPUT										
$\tilde{T}_o$	.065	.13	.26	.52	.065	.26	.13	.26	.52	.65
ν/ν_o	.25	.25	.25	.25	1.0	1.0	4.0	4.0	4.0	4.0
ν_H/ν_{Ho}	.25	.25	.25	.25	1.0	1.0	4.0	4.0	4.0	4.0
k_H/ν_{Ho}	.25	.25	.25	.25	1.0	1.0	4.0	4.0	4.0	4.0
τ_{rad}	33.	33.	33.	33.	33.	33.	33.	33.	33.	33.
μ^2	50.	50.	50.	50.	50.	50.	50.	50.	50.	50.
RESULTS										
E	648.	1440.	4460.	12700.	539.	3900.	1470.	4180.	10100.	14200.
KE	233.	690.	1700.	5150.	90.	874.	132.	459.	1230.	1840.
DE	3.83	51.8	337.	1310.	.458	73.8	3.35	28.7	167.	303.
APE	415.	748.	2760.	7520.	449.	3030.	1340.	3720.	8690.	12400.
θE	436.	803.	2870.	7780.	465.	3160.	1370.	3840.	9140.	12800.
BE	204.	532.	906.	2200.	74.	587.	90.	301.	683.	944.
AE	7.9	110.	680.	2700.	.66	150.	4.2	42.	278.	517.
QE	4.7	92.	760.	3700.	.008	95.	.025	7.0	119.	278.
VE	.0059	.0335	.228	2.50	.0019	.0456	.0021	.0116	.050	.078
R	.0078	.062	.14	.20	.0006	.033	.0025	.0075	.023	.035
R_Q	.0031	.048	.14	.23	2×10^{-6}	.019	7×10^{-6}	.0004	.0056	.013
$\hat{\omega}/f$	.77	.91	1.06	1.17	.11	.79	.077	.41	.65	.73

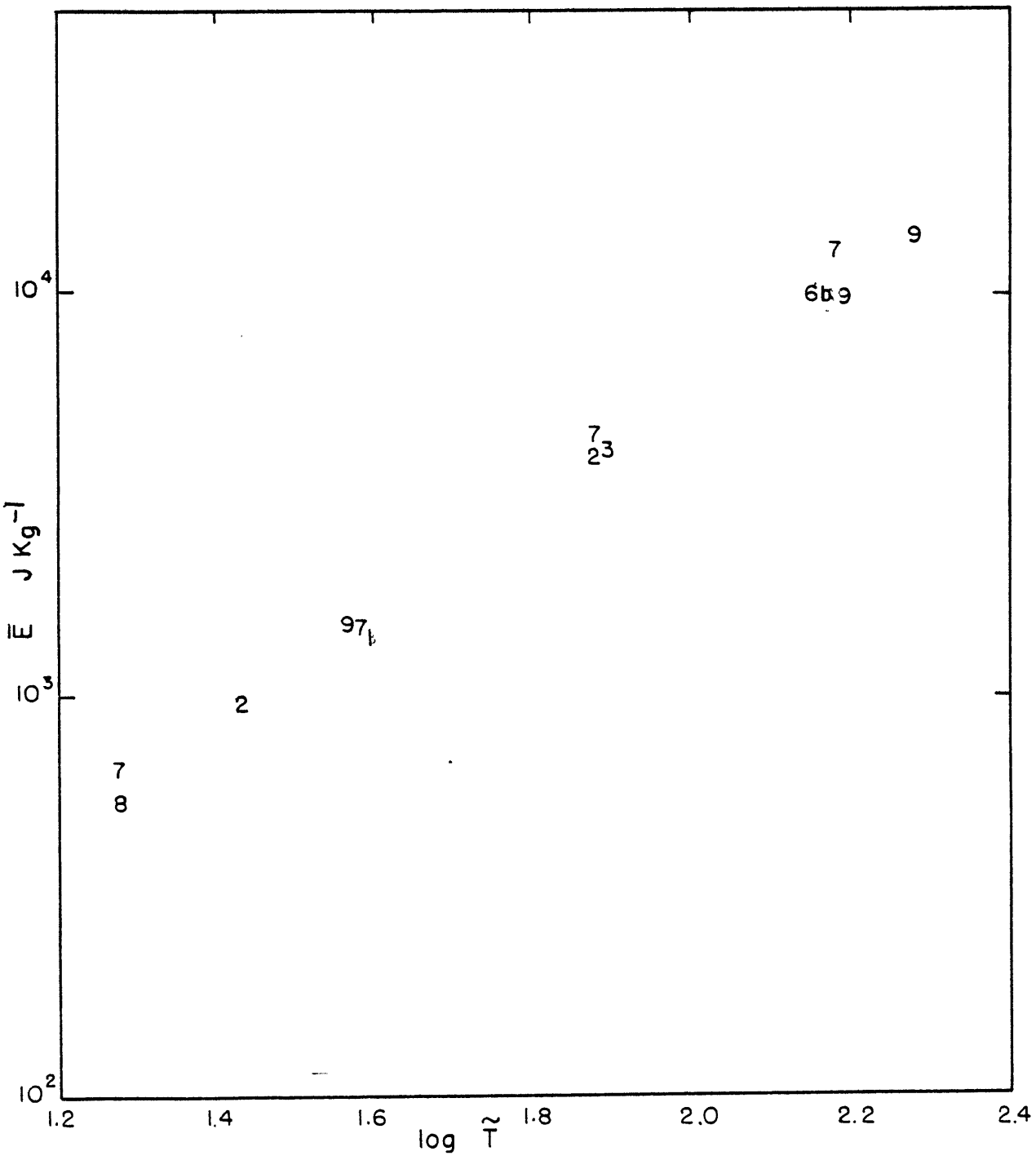

Figure 9.1

$\overline{VE} \propto \nu^{-2.4}$). The ratio between $\bar{E}$ and $\overline{VE}$ defines the square of a length scale. The decrease of this scale with $\tilde{T}_o$ indicates that the portion of energy in smaller scales increases with $\tilde{T}_o$ (other parameters fixed). The square root of $\overline{VE}$ defines a Rossby number as described in Section 3.1.

Values of $\bar{R}(\nu,T_o)$ appear in Figure 9.3. For fixed $\tilde{T}_o$, $\bar{R}$ increases with decreasing ν. For fixed ν, $\bar{R}$ increases rapidly with $\tilde{T}_o$ as long as R is very small. It approaches what may be a ν-dependent, $\tilde{T}_o$-independent value for larger values of $\tilde{T}_o$. This result is also suggested by experiments 6a-6g.

For large $\tilde{T}_o$ and small ν, viscous terms become relatively small. We may expect the equipartitioning results of Experiment 3 to apply, except that our choice of forcing acts to generate GE more so than AE. Therefore, if $\bar{R}$ does approach a constant value as $\tilde{T}_o$ increases, it is likely less than the equipartitioning value of 1/2.

For values of $\tilde{T}_o$ not much smaller than those presented, the nature of the numerical solutions change rather abruptly. For those $\tilde{T}_o$, the value of $\overline{GE}$ is within 1% of that given by the linear problem with forcing. The value of $\overline{AE}$ may be two or three times that given by the linear problem, but negligibly small even so. The energy generated by forcing does not appreciably propagate to other scales in these solutions. Thus, dissipative effects dominate the nonlinear effects for these low values of $\tilde{T}_o$.

At values of $\tilde{T}_o$ larger than presented, the amount of computation necessary to obtain statistically significant results increases

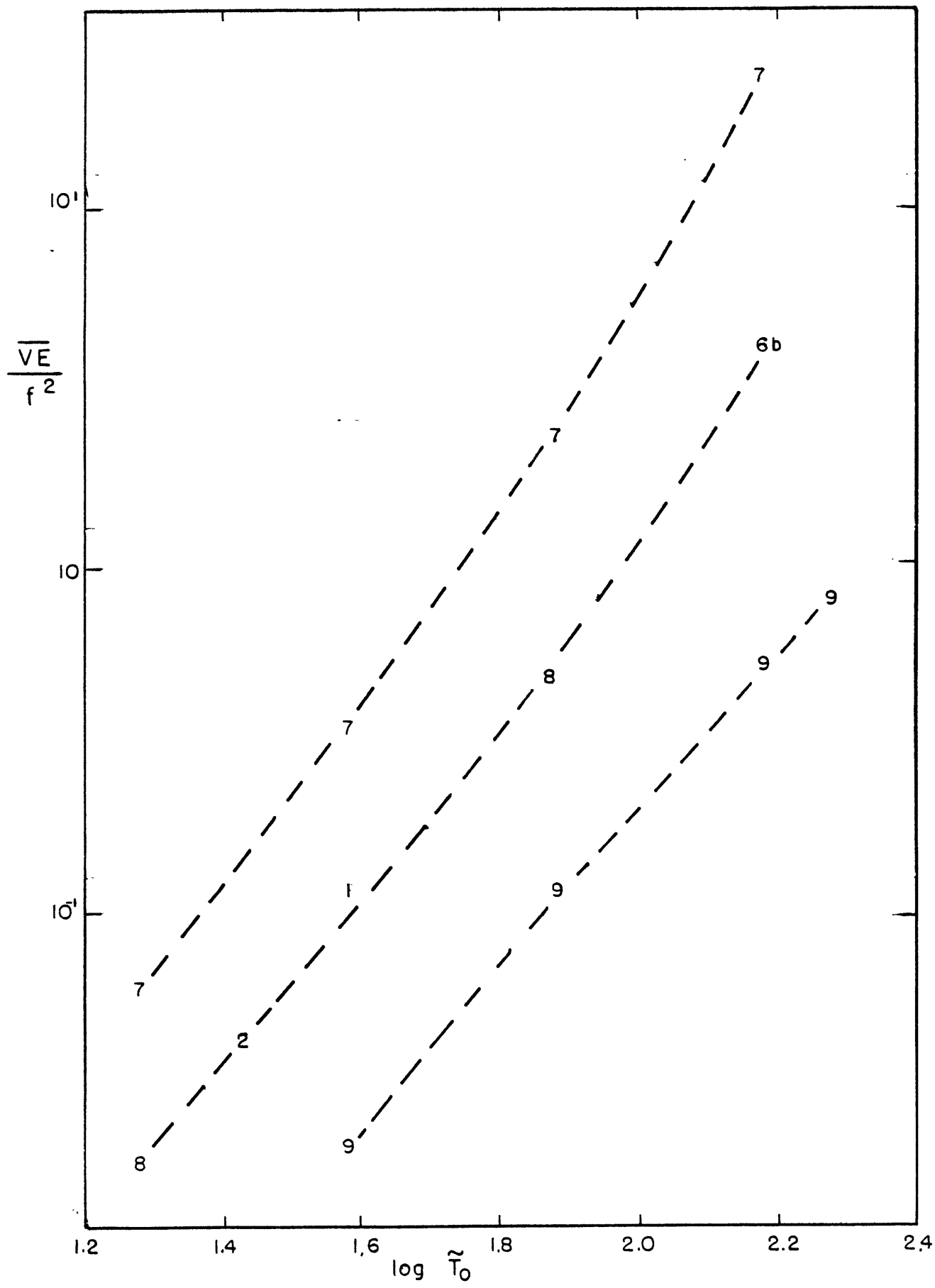
$\frac{\overline{VE}}{f^2}$
10^1
10
10^{-1}
1.2
1.4
1.6
1.8
2.0
2.2
2.4
log $\tilde{T}_0$
7
7
7
6b
8
8
9
9
9
1
2

Figure 9.2

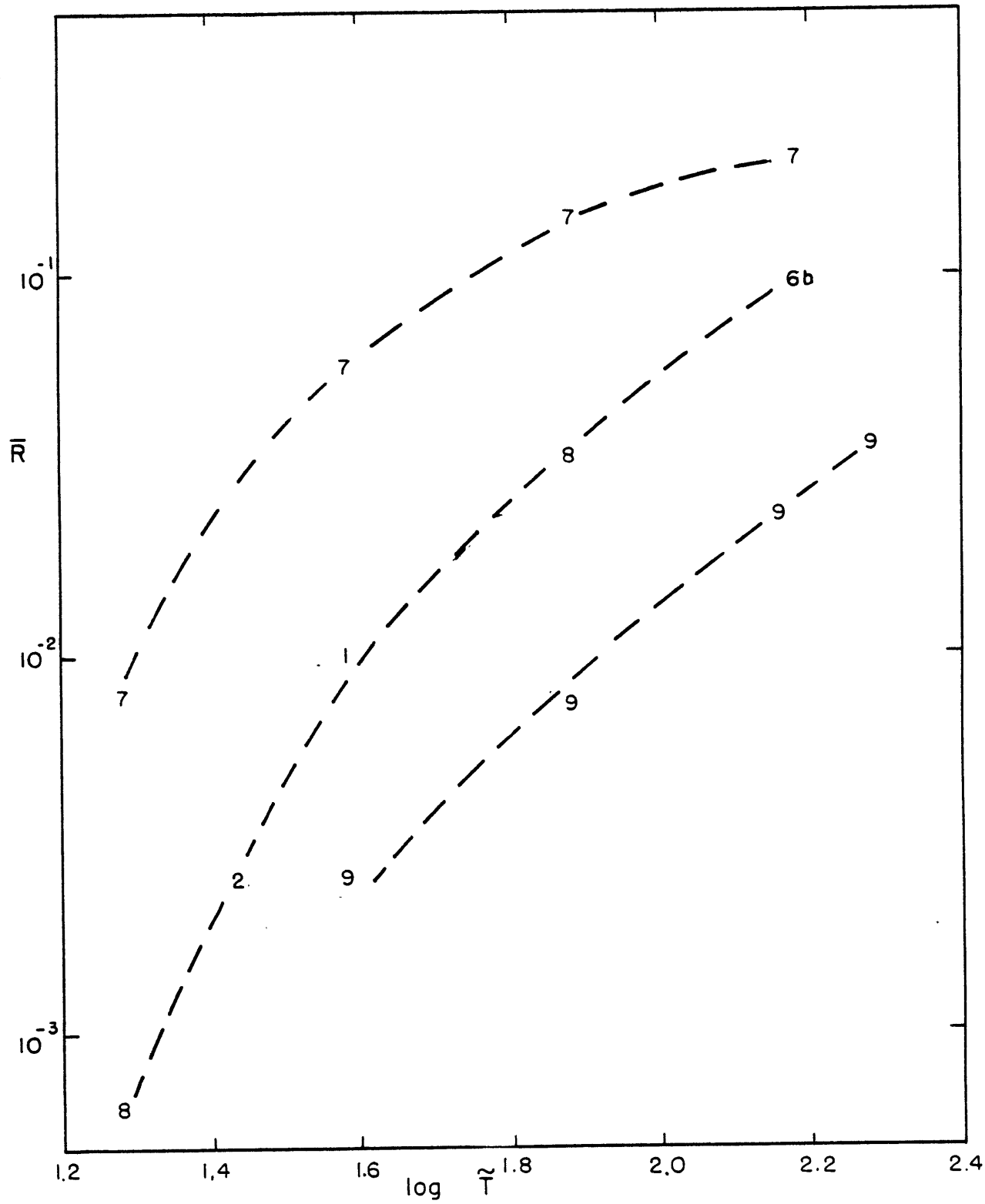

Figure 9.3

substantially. It is necessary to increase the horizontal resolution and the simulated intergration period as well as decrease the integration time-step considerably. The large requirement of computation time seemed to outweigh the expected significance of new data to be obtained.

9.2 Effects of Mean Static Stability

The dimensional value of σ_2 is varied between 5K and 80K in the next set of experiments. $\tilde{T}_o$ is equal to .066, .13, and .26 in Experiments 10a-c, 11a-d, and 12a-b, respectively. Dissipative parameters are as in Experiment 1. Results are presented in Table 9.2.

Variations of σ_2 can significantly affect the solution in many respects, although between Experiments 10b and 10c this was not the case. In most cases both $\overline{VE}$ and $\bar{R}$ are inversely related to σ_2. $\bar{R}$ is much more sensitive to the value of $\tilde{T}_o$ than to the value of σ_2.

The value of $\tilde{T}_o$ does not describe the numerical solution well (e.g. as $\overline{VE}$ does) unless the functional relationships between $\tilde{T}_o$ and the solution's statistics are known. $\tilde{T}_o$ explicitly describes only the forcing in one band, while $\overline{VE}$ describes the mean response of all the bands. For this reason we present $\bar{R}$ as a function of $\overline{VE}$ and σ_2 in Figure 9.4. Data appear from Table 9.2 and Experiments 1, 2, 8a, and 8b. Dissipative parameters are identical in all of these experiments.

Within the range of values appearing in Figure 9.4, $\bar{R}$ is approximately proportional to $\overline{VE}$ for constant σ_2. Thus, within this range, $\bar{R}$

Table 9.2 Effects of Mean Static Stability

For all experiments $\nu = .025$, $\nu_H = k_H = 5\times10^{-5}$, $\tau_{rad} = 33.$
T_o and μ^2 are dimensionless. E through QE are
units of J kg^{-1}. VE is in units of f^2. All Results time-mean quantities.

Exp. No.	10a	10b	10c	11a	11b	11c	11d	12a	12b
INPUT									
$\tilde{T}_o$	.065	.065	.065	.13	.13	.13	.13	.26	.26
σ_2 (K)	5.	10.	40.	5.	10.	40.	80.	40.	80.
μ^2	200.	100.	25.	200.	100.	25.	12.5	25.	12.5
RESULTS									
E	1930.	275.	260.	5610.	2970.	945.	401.	2140.	1100.
KE	144.	55.	51.0	549.	380.	254.	156.	740.	518.
DE	4.87	.140	.131	66.3	23.6	1.97	.610	34.1	7.80
APE	1790.	220.	209.	5060.	2590.	691.	245.	1400.	578.
θE	1810.	177.	221.	5121.	2650.	737.	276.	1514.	670.
BE	111.	42.3	38.5	348.	269.	204.	124.	558.	420.
AE	9.6	.20	.17	140.	49.	3.6	.86	68.	12.
QE	4.1	.0004	.0003	120.	27.	.35	.0041	36.	2.4
VE	.0095	.0005	.0004	.060	.0192	.0030	.0010	.0129	.0043
R	.0025	.0007	.0006	.022	.013	.003	.002	.025	.0085
R_Q	.0005	1×10^{-6}	6×10^{-7}	.016	.0056	.0001	6×10^{-6}	.01	.0006
$\hat{\omega}/f$	.65	.04	.04	.92	.74	.31	.07	.73	.45

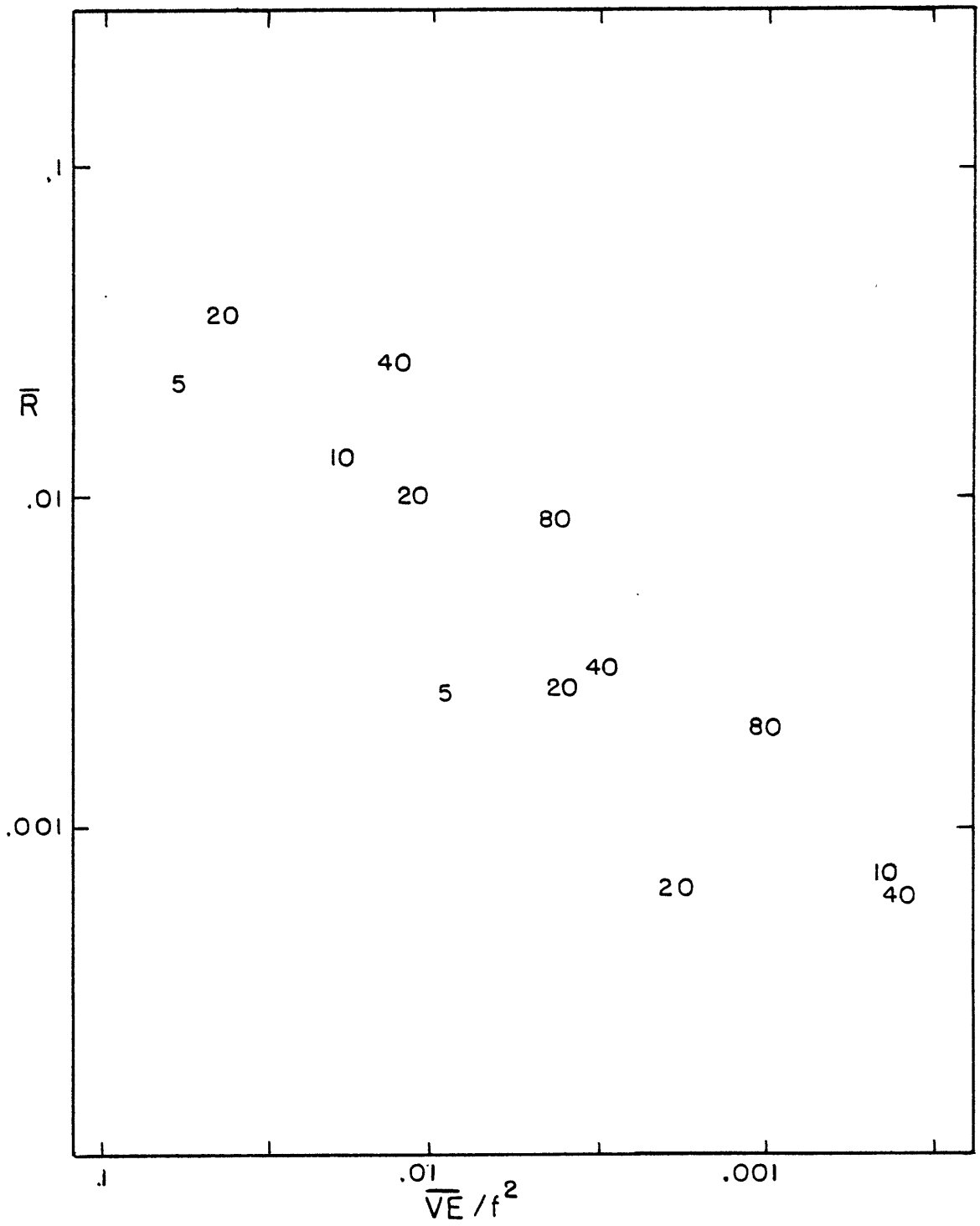
.1
.01
.001
$\overline{R}$
20
40
5
10
20
80
40
5
20
80
20
10
40
.1
.01
.001
$\overline{VE}/f^2$

Figure 9.4

is approximately proportional to the Rossby number squared. Judiciously interpolating between values of constant σ_2 in Figure 9.4, we observe that $\bar{R}$ increases approximately proportionally to σ_2 for fixed $\overline{VE}$. Since increasing σ_2, with other parameters fixed, acts to decrease $\overline{VE}$, which in turn tends to decrease $\bar{R}$, the actual effect of increasing σ_2 is to decrease $\bar{R}$.

9.3 Effect of a Change in the Dissipative Mechanism

We present an experiment here to investigate a possibility presented in Section 6.2. There it was suggested that at large scales a realistic eddy viscosity and radiative heating parameterization may tend to dissipate AE faster than GE.

In Experiment 13, the additional dissipative term $-1.5\nu X_{n,m}$ is added to the right hand side of the prognostic equation for $X_{n,m}$, Equation 4-2. This modification acts to increase the dissipative rate for any value of ν. It also acts to change the relative magnitude of the dissipation coefficients in the modal form of the very-low-order equations. Specifically, the new term only acts directly on the barotropic mode (i.e., other modes will be influenced only through the effect of this term on b). It modifys the linear problem in Section 6.2 so that it can not be claimed that the dissipation significantly favors geostrophic modes. Additionally reducing ν by a factor 2.5 reduces the effective dissipative rate to a value similar to that of Experiments 1

Table 9.3: Effect of a Change in Dissipative Mechanism

All input is dimensionless. E through QE are in units of J kg^{-1}. VE is in units of f^2. All Results time-mean quantities.

Exp. No.	13
INPUT	
$\tilde{T}_o$	.13
ν	.025
ν_H , k_H	$5x10^{-}$
τ_{rad}	33.
μ^2	50.
RESULTS	
E	1710.
KE	207.
DE	7.43
APE	1500.
θE	1560.
BE	131.
AE	14.7
QE	7.62
VE	.0083
R	.0047
R_Q	.0016
$\hat{\omega}/f$	.72

and 2.

Results of this experiment appear in Table 9.3. The change in dissipative terms does act to alter statistics of the solution. However, both $\overline{VE}$ and $\bar{R}$ in Experiment 13 are between the corresponding values in Experiments 1 and 2. This suggests that the differences in dissipative effects as determined by the linear problem in Section 6.2 do not significantly influence the value of $\bar{R}$ in the non-linear problem.

Chapter 10: Summary and Conclusion

Examination of the meteorological literature reveals that an adequate demonstration that the extra-tropical troposphere should be quasi-geostrophic has not been presented. Specifically, we mean quasi-geostrophic in the sense of approximate geostrophic balance, and do not intend to imply that small non-geostrophic effects are unimportant. Former studies are either speculative (suggesting what presumably the explanation must be), or ignore nonlinear effects, or implicitly assume the atmosphere is quasi-geostrophic (presenting only a consistency argument).

To quantify our discussion, we have defined a measure of geostrophy R, as the ratio of ageostrophic energy to total $(KE + APE)$ energy. The energy partitioning between geostrophic and ageostrophic contributions is defined in Chapter 2 in terms of the normal linear modes of a simple model. The basic model uses an N-layer form of the primitive equations. External gravity waves are excluded, but internal gravity waves are retained. The association of the terms geostrophic and ageostrophic with specific modes depends on their structure (i.e. eigenvectors describing the modes) as well as their time behavior (for all amplitudes in the linear problem, and for large amplitudes in the nonlinear problem).

Both numerical and analytical studies help ascertain which processes are important in determining the function R, and in particular, what processes act to keep R as small as observed. For the numerical studies, Lorenz's (1972) low-order model representing many scales of turbulence is modified so as to apply to our model (Chapter 4).

The analytical study is greatly facilitated by transforming the model equations into a system in which the prognostic variables themselves are the modal amplitudes (Section 6-1). The nonlinear terms are also expressed in terms of the modal amplitudes so that the interactions among modes are described explicitly.

Studies of linear processes that affect R have been reviewed by Blumen (1972). The transformed equations easily yield results similar to those Blumen describes. Most importantly, thermal forcing at large scale and low frequency acts to produce geostrophic energy at a faster rate than ageostrophic energy (Section 6.3). This is a result of the different properties of ageostrophic modes compared with those of geostrophic modes. The ageostrophic modes are nearly inertial at large scale; i.e. their amplitudes are relatively temperature independent. Also their natural frequencies are higher than inertial, and thus low frequency forcing is far from resonance. The geostrophic modes on the other hand are characterized by low frequencies (zero on an f-plane, but more realistically characterized by a frequency of order $L\beta \ll f$). The amplitudes of baroclinic geostrophic modes are strongly temperature dependent at all scales and can be effectively driven by large scale heating.

We have parameterized dissipation by a linear eddy viscosity, linear thermal diffusivity, and Newtonian radiative cooling. The effects of dissipation, in isolation from other processes, have been investigated for both the largest and smallest horizontal scales (Section 6.2). At the former, geostrophic modes tend to be favored. Internal ageostrophic modes

are damped faster than geostrophic modes of the same amplitude. At small horizontal scales all modes are damped at approximately equal rates. However, the generality of these results is in doubt. They are a necessary consequence in the two-layer model with both internal and surface dissipative mechanisms of similar magnitude. The significance of such results is also in doubt since other important interactive processes act on the modes as well. A numerical result suggests that the noted difference in dissipative rates is not critical in affecting the energy partitioning in the non-linear model (Section 9.3). Any further analysis of these processes should incorporate a more detailed vertical structure and a more realistic parameterization scheme.

Our primary purpose has been to investigate the nonlinear advective processes since both the transformed equations and the numerical model are appropriate new tools for that kind of study. Advection acts to exchange energy between modes of various types and scales. In particular, in the absence of forcing and dissipative processes in the model, advection acts to equipartition the available energy among all the scales and modes (Section 5.2). Even under nearly quasi-geostrophic conditions, advective processes involving ageostrophic modes, although small, significantly affect the geostrophic spectra at synoptic scales (Section 8.1).

The stability of small-amplitude, independent geostrophic modes with respect to infinitessimal pertubations in other modes is easily examined with the transformed equations (Chapter 7). The pertubations which grow fastest are quasi-geostrophic. That is, they are characterized by both geostrophic modes and smaller amplitude ageostrophic modes which approximately satisfy the quasi-geostrophic omega equation and a

nonlinear balance condition. However, there are also growing pertubations which are characterized by ageostrophic modes accompanied by smaller amplitude geostrophic modes. Their growth rates are smaller than the former for small enough values of the unperturbed state's Rossby number. As this Rossby number increases towards a value of one, these two types of growing pertubations become indistinguishable. In the model under atmospheric-like conditions, eddy viscosity is sufficiently strong to stabilize the ageostrophic pertubations but not the quasi-geostrophic.

Why the atmosphere does not support ageostrophic modes with energies similar to the geostrophic has not yet been adequately answered. The simple scale analysis of Chapter 3 suggests that solutions with that property can satisfy balance requirements of the model equations. Experiment 4 in Section 5.3 demonstrates the existence of such a solution for small dissipative parameters.

Although solar heating primarily acts to produce geostrophic energy, it is not obvious to us that the advective processes (e.g. energy cascades to smaller scales) should not partition a much greater than observed portion of this energy to ageostrophic modes. And although the stability analysis in Chapter 7 indicates that quasi-geostrophic modes may be favored, the energy exchanges with a spectrum of finite amplitude modes require further examination. In particular, we can ask whether larger portions of ageostrophic energy, if somehow put into the system, can be maintained. If not, why not? In the transformed equations, more than half the terms involve possible exchanges between geostrophic and ageostrophic energies. Yet, their effect on the energy exchange is apparently limited.

The transformed equations facilitate a rather detailed examination of this problem (Section 8.3). In particular, the significance of nonlinear resonant interactions in maintaining the large amplitude modes can be established for small Rossby numbers. The necessary resonance condition is easily satisfied by geostrophic interactions since the natural frequencies of all synoptic-scale geostrophic modes are low.

For ageostrophic modes on the other hand, near-resonance only occurs with other ageostrophic modes of similar scale, since they are dispersive, with relatively high natural frequencies. Therefore, any near-resonant triad interaction between ageostrophic and geostrophic modes requires that the two ageostrophic modes be oriented symmetrically with respect to the geostrophic mode. Neither ageostrophic mode is favored energetically, and the resonant interactions simply exchange energy between the ageostrophic modes. The geostrophic mode acts as a kind of catalytic agent. Therefore, we suggest that no efficient mechanism exists for exchanging geostrophic and ageostrophic energies, except for maintaining those ageostrophic modes approximated by (6-25). We note that a more realistic geometry (e.g. a β -plane) would probably modify this symmetry requirement, but perhaps not to the degree of invalidating our argument.

All the numerical experiments presented have planetary scale, time-independent forcing (except Experiment 3 with no forcing). Given such forcing, the energy partitioning depends on the magnitude of the motion (e.g. the mean enstrophy or a Rossby number), the mean static stability, and the strength of the dissipative processes (Chapter 9). The first is determined by the heating rate in conjunction with the latter factors.

Details of the dissipative mechanisms do not have as large an affect as a linear analysis suggested.

The numerical model can yield solutions very unlike those of the complete spectral system. This has been described in detail for the study of equipartitioning. If ageostrophic resonant interactions were effective at exchanging geostrophic and ageostrophic energies, then the model would likely yield poor results. The choice of vectors in the very-low-order model does not allow near-resonant interactions except at very large scales. Thus, if our assertions in Section 8.3 are to be examined numerically, a different model should be used.

We found that transforming the primitive system of equations into a system in terms of their normal linear modes is useful. Although there was substantial work in actually performing the transformation, our problem became much more tractable once we had done so. We suspect that similar transformations could substantially simplify other problems as well.

Our conclusion is that the atmosphere is quasi-geostrophic for the reasons Charney (1955) suggested. Solar heating generates much more geostrophic energy than ageostrophic energy. We have shown that geostrophic energy is not efficiently transferred to ageostrophic energy. Dissipative processes are effective in removing any large quantity of ageostrophic energy that may be otherwise produced.

Appendix

A1 List of Symbols

A	matrix of coefficients for stability problem; 7.1
A_K	matrix of linear coefficients of spectral equations; 2.2
AE	total ageostrophic energy, 2.3
$A\mathcal{E}_{\underset{\sim}{K}}$	portion of AE contributed by scale $\underset{\sim}{K}$; 2.3
$A\mathcal{E}_m$	portion of AE contributed by band m (4-13)
$\hat{A\mathcal{E}}_m$	power spectra of ageostrophic modes, band m (8-11)
APE	total available potential energy; Ch. 4
BE	total barotropic - geostrophic energy; 2.3
$B\mathcal{E}_{\underset{\sim}{K}}$	portion of BE contributed by scale $\underset{\sim}{K}$; 2.3
$B\mathcal{E}_m$	portion of BE contributed by band m (4-10)
$\hat{B\mathcal{E}}_m$	power spectra of barotropic-geostrophic mode, band m (8-9)
C_K	matrix of eigenvectors of A_K; 2.2
$C_i\ (\underset{\sim}{K},\underset{\sim}{L},\underset{\sim}{M})$	modal-interaction coefficients (6-7 ff)
$C_{i,n}$, $C_{i,n}$	abreviated form of $C_i(\underset{\sim}{K},\underset{\sim}{L},\underset{\sim}{M})$ (following Eq. 7-12)
D	length of horizontal domain; 2.1.1
D_K	diagonal matrix of eigenvalues of A_K ; 2.2
DE	total energy of irrotational wind field; Ch. 4
$D\mathcal{E}_m$	portion of DE contributed by band m (4-6)
$\hat{D\mathcal{E}}_m$	power spectrum of irrotational wind, band m (4-17)
E	total kinetic plus available potential energy (4-17)
E_K	matrix energy operator on $\underset{\sim}{X}_K$; 2.3
E'_K	matrix energy operator on $\underset{\sim}{Y}_K$; 2.3
F_K	dissipation matrix in modal equations; (6-28)
F'_K	dissipation matrix in spectral equations; 6.2
$F_{\zeta n,K}$	parameterized dissipation term in ζ equation (2-84)
$F_{\theta n,K}$	parameterized heating term in θ equation (2-86)
G	forcing term for baroclinic-geostrophic mode; 8.1
G_a	forcing term for ageostrophic mode; 8.1
$\underset{\sim}{G}_K$	vector of forcing functions in modal Eqs.; 6.2
GE	total geostrophic energy; 2.3

$G\mathcal{E}_{\underset{\sim}{K}}$	portion of GE contributed by scale $\underset{\sim}{K}$; 2.3
$G\mathcal{E}_m$	portion of GE contributed by band m (4-12)
H	(subscript) Horizontal
I	multiplicative identity matrix
J(A,B)	Jacobian operator on A and B
$\underset{\sim}{K}$	vector in spectral representation of fields
KE	total kinetic energy; 2.3
L	length scale
N	number of levels at which $\mathcal{S}$ defined; 2.1.2
QE	quasi-geostrophic imbalance pseudo-energy (3-11)
$Q\mathcal{E}_m$	contribution of QE by band m; (4-14)
R	gas constant, or
R	ratio of ageostrophic to total energy
R_Q	measure of quasi-geostrophy (3-13)
T	(superscript) transpose
T_m	low-order representation of θ field; Ch. 4.
$\tilde{T}_m$	low-order representation of heating (θ_{rad}); Ch. 4.
T_o	temperature scale
V	(subscript) vertical
$\underset{\sim}{V}$	horizontal velocity vector
$X_{n,m}$	low-order representation of vorticity field; Ch. 4.
$\underset{\sim}{X}$	vector of pertubation modal amplitudes; 7.1
$\underset{\sim}{X}_{\underset{\sim}{K}}$	vector of prognostic spectral components of scale $\underset{\sim}{K}$; 2.2
Y_m	low-order representation of divergence field; Ch. 4.
$\underset{\sim}{Y}_{\underset{\sim}{K}}$	vector of modal amplitudes of scale $\underset{\sim}{K}$; 2.2
$a_{l,n}$, a	short form of $a_{l\underset{\sim}{K}}$ (following Eq. 7-12)
$a_{l\underset{\sim}{K}}$, $a_{2\underset{\sim}{K}}$	amplitudes of ageostrophic modes (2-68),(2-69)
b_n , b	short form of $b_{\underset{\sim}{K}}$ (following Eq. 7-12)
$b_{\underset{\sim}{K}}$	amplitude of barotropic-geostrophic mode (2-66)
c	coefficient in very-low-order model; Ch.4.
$\underset{\sim}{c}_{iK}$	eigenvector of matrix A_K; 2.2
$d_{\underset{\sim}{K}}$	amplitude of barotropic divergence mode = 0 (2-65)
e_{ij}	element of dissipation matrix F_K; 6.2; 8.1
f	coriolis parameter

f_i	sum of terms that effect a mode; 8.3
f_{ijk}	particular quadratic term of f_i ; (8-12)
g_n , g	short form of $g_{\underset{\sim}{K}}$ (following Eq. 7-12)
$g_{\underset{\sim}{K}}$	amplitude of baroclinic-geostrophic mode (2-67)
$\hat{i}$	unit vector in x-direction
$\hat{j}$	unit vector in y-direction
$\hat{k}$	unit vector = $\hat{i} \times \hat{j}$
m	index usually denoting band number; Ch. 4.
m_f	first band (largest scale) having prognostic terms; Ch. 4.
m_F	band at which heating (forcing) is applied; Ch. 4.
m_l	last band (smallest scale) having prognostic terms; Ch. 4
n	index usually denoting layer; 2.1.2
0( )	means "order of" ; 3.1
p	pressure
$r_{(subscript)}$	denotes nonlinear terms; 2.1.1
s	an arbitrary function of time
t	time
t_o	an initial time
x,y	orthogonal horizontal coordinates
α_n	a pressure dependent quantity (2-33)
γ_i	an arbitrary modal amplitude; 8.3
$\delta, \delta_{n\underset{\sim}{K}}$	divergence (two-dimensional) (2-9)
ε	ordering parameter, generally the Rossby number; 3.1
ε_l	a second ordering parameter; 8.3
ζ, $\zeta_{n\underset{\sim}{K}}$	vorticity (two-dimensional) (2-9)
θ, $\theta_{n\underset{\sim}{K}}$	potential temperature (departure from mean) ; 2.1.1
$\overline{\theta}$	isobaric-mean potential temperature
$\theta_{rad\ \underset{\sim}{K}}$	radiative relaxation temperature of scale $\underset{\sim}{K}$; 2.4
θE	total baroclinic-geostrophic energy; 2.3
$\theta\mathcal{E}_{\underset{\sim}{K}}$	portion of E contributed by scale $\underset{\sim}{K}$; 2.3
$\theta\mathcal{E}_m$	portion of E contributed by band m (4-11)
$\theta\hat{\mathcal{E}}_m$	power spectra of baroclinic-geostrophic mode, band m (8-10)
κ	ratio of gas constants, or eddy diffusion coefficient
λ, λ'	eigenvalue

μ	ratio of length scales; (2-63 ff)
ν	viscosity coefficient; 2.4
σ, σ_n	mean static stability (2-16)
τ	a characteristic time scale
τ_{rad}	radiative relaxation time (2-86)
ϕ	geopotential
χ	velocity potential (2-9)
ψ	stream function (2-9)
ω, $\omega_{\underset{\sim}{K}}$	"vertical wind" component (i.e. dp/dt), 2.1.1
ω_K	inertial-gravitational wave frequency (2-63)
ω_m	inertial-gravitational wave frequency (4-16)
ω_i	denotes natural frequency of mode γ_i
$\hat{\omega}$	(in Fouier transform) frequency; Ch. 8.
$\hat{\omega}$	(in tables) mean frequency of ageostrophic modes (3-14)
$\mathcal{E}_{\underset{\sim}{K}}$	portion of E contributed by scale $\underset{\sim}{K}$; 2.3
$\mathcal{E}_m$	portion of E contributed by band m (4-9)
$\mathcal{L}$	linear operator (3-6)
$\mathcal{N}$	truncation of number of pertubation scales; 7.1
∇	horizontal gradiant operator; Ch. 2.
$\bar{(\ )}$	time-mean, except Chs. 2 and 3 (2-14)

References

Bender, C.M. and S.A. Orszag, 1978 : Advanced Mathematical Methods for Scientists and Engineers. McGraw-Hill: New York, 593 pp.

Blumen, W., 1972: Geostrophic adjustment. Rev. Geophys. & Sp. Phys., 10, 485-528.

Charney, J.G., 1948: On the scale of atmospheric motions. Geofys. Publikasjoner, 17, 17 pp.

——— 1955: The generation of ocean currents by wind. J. Mar. Res., 14, 477-498.

——— 1959: On the theory of the general circulation of the atmosphere. The Atmosphere and the Sea. Oxford University Press: Oxford, 178-193 pp.

———and M.E. Stern, 1962: On the stability of internal baroclinic jets in a rotating atmosphere. J. Atmos. Sci., 19, 159-172.

Chen, T.C. and A.C. Wiin-Nielsen, 1976: On the kinetic energy of the divergent and nondivergent flow in the atmosphere. Tellus, 28, 486-498.

Duffy, D.G., 1974: Resenant interactions of inertial-gravity and Rossby waves. J. Atmos. Sci., 31, 1218-1231.

——— 1975: The barotropic instability of Rossby wave motion: a re-examination. J. Atmos. Sci., 32, 1271-1277.

Eady, E.T., 1949: Long waves and cyclone waves. Tellus, 1, 33-52.

Fjortoft, R., 1953: On the changes in the spectral distribution of kinetic energy for two-dimensional, nondivergent flow. Tellus, 5, 225-237.

Fox, D.G. and S.A. Orszag, 1973: Inviscid dynamics of two-dimensional turbulence. Physics of Fluids, 16, 169-171.

Gierasch, P., R. Goody and P. Stone, 1970: The energy balance of planetary atmospheres. Geophys. Fluid Dyn., 1, 18.

Gill, A.E., 1974: The stability of planetary waves on an infinite Beta-plane. Geophys. Fluid Dyn., 6, 29-47.

Haltiner, 1971: Numerical Weather Prediction. John Wiley and Sons: New York, 317 pp.

Holton, 1972: An Introduction to Dynamic Meteorology. Academic Press: New York, 319 pp.

Kashara, A. and W.N. Washington, 1967: NCAR global circulation model of the atmosphere. Mon. Wea. Rev., 95, 389-402.

Kim, K., 1975: Instability and energetics in a baroclinic ocean. Ph.D. Thesis, M.I.T., 175 pp.

Lin, C.A., 1979: Eddy heat fluxes and stability of planetary waves. Ph.D. Thesis, M.I.T., 146 pp.

Lorenz, E., 1960: Energy and numerical weather prediction. Tellus, 12, 364-373.

——— 1967: The Nature and Theory of the General Circulation of the Atmosphere. World Meteorological Organization: Geneva, 161 pp.

——— 1971: An N-cycle time-differencing scheme for stepwise numerical integration. Mar. Wea. Rev., 99, 644-649.

——— 1972: Barotropic instability of Rossby wave motion. J. Atmos. Sci., 29, 258-264.

——— 1972: Low-order models representing realizations of turbulence. J. Fl. Mech., 55, 545-563.

Peixoto, J. P. and A.H. Oort, 1974: The annual cycle of the energetics of the atmosphere on a planetary scale. J. Geophys. Res., 79, 2705-2719.

Phillips, N.A., 1956: The general circulation of the atmosphere: a numerical experiment. Quart. J. Roy. Meteor. Soc., 82, 123-164.

——— 1963: Geostrophic Motion. Rev. Geophys., 1, 123-176.

Pollard, R.T., 1970: On the generation by winds of inertial waves in the ocean. Deep Sea Res., 17, 795-812.

Rossby, C.G., 1937: On the nutual adjustment of pressure and velocity distributions in certain simple current systems, 1. J. Mar. Res., 1, 15-28.

——— 1938: On the mutual adjustment of pressure and velocity distributions in certain simple current systems, 2. J. Mar. Res., 1, 239-263.

Salman, R., G. Holloway and M.C. Hendershott, 1976: The equilibrium statistical mechanics of simple quasi-geostrophic models. J. Fl. Mech., 75, 691-703.

Stone, P.H., 1972: On non-geostrophic baroclinic stability: Part III. The momentum and heat transports. J. Atmos. Sci., 29, 419-426.

Veronis, G., 1956: Partition of energy between geostrophic and non-geostrophic oceanic motions. Deep Sea Res., 3, 157-177.

——— and H. Stommel, 1956: The action of variable wind stresses on a stratified ocean. J. Mar. Res., 15, 43-75.

Wilkinson, J.H., et.al., 1971: Handbook for Automatic Computations. Spring-Verlag: New York, 439 pp.